



HAL
open science

Synthèse, structure et propriétés de polycyanurates réticulés et de matériaux nanoporeux générés en utilisant des liquides ioniques

Alina Vashchuk

► **To cite this version:**

Alina Vashchuk. Synthèse, structure et propriétés de polycyanurates réticulés et de matériaux nanoporeux générés en utilisant des liquides ioniques. Autre [cond-mat.other]. Université Paris-Est; Institut de la Chimie Macromoléculaire de Kiev (Ukraine), 2019. Français. NNT : 2019PESC0046 . tel-02342195

HAL Id: tel-02342195

<https://theses.hal.science/tel-02342195>

Submitted on 31 Oct 2019

HAL is a multi-disciplinary open access archive for the deposit and dissemination of scientific research documents, whether they are published or not. The documents may come from teaching and research institutions in France or abroad, or from public or private research centers.

L'archive ouverte pluridisciplinaire **HAL**, est destinée au dépôt et à la diffusion de documents scientifiques de niveau recherche, publiés ou non, émanant des établissements d'enseignement et de recherche français ou étrangers, des laboratoires publics ou privés.



Thèse de Doctorat

présentée par :

Alina VASHCHUK

pour obtenir le grade de Docteur de l'Université Paris-Est et de l'Institut de Chimie Macromoléculaire-NASU

Spécialité : Sciences des Matériaux

Synthèse, structure et propriétés de polycyanurates réticulés et de matériaux nanoporeux générés en utilisant des liquides ioniques

Soutenue le 16 Janvier 2019 devant le jury composé de :

Rapporteurs

Eliane ESPUCHE

Professeur, Université Claude Bernard Lyon 1

Victor KRAMARENKO

*Maître de Conférences, Université Technique Nationale
«Institut Polytechnique de Kharkiv»*

Examineurs

Boulos YOUSSEF

Maître de Conférences, INSA de Rouen

Tatyana ZHELTONOZHSKAYA

Professeur, Université Nationale Taras Shevchenko Kiev

Directeurs de thèse

Daniel GRANDE

Directeur de Recherche, CNRS

Alexander FAINLEIB

Professeur, Institut de Chimie Macromoléculaire NASU



Ph.D. Thesis

presented by :

Alina VASHCHUK

to obtain the degree of Doctor of Paris-East University and the Institute of Macromolecular Chemistry-NASU

Speciality: Materials Science

Synthesis, structure and properties of crosslinked polycyanurates and nanoporous materials generated by using ionic liquids

Defended on January 16, 2019 in front of the jury composed of:

Reviewers

Eliane ESPUCHE

Professor, University Claude Bernard Lyon 1

Victor KRAMARENKO

Associate Professor, National Technical University «Polytechnic Institute of Kharkiv»

Examiners

Boulos YOUSSEF

Associate Professor, INSA Rouen

Tatyana ZHELTONOZHSKAYA

Professor, National Taras Shevchenko University of Kiev

Supervisors

Daniel GRANDE

Research Director, CNRS

Alexander FAINLEIB

Professor, Institute of Macromolecular Chemistry, NASU

This PhD thesis was completed in cotutelle between the Institute of Macromolecular Chemistry of the National Academy of Science of Ukraine (IMC, Kiev) and the East-Paris Institute of Chemistry and Materials Science (ICMPE, Thiais) thanks to a NASU scholarship and a ten-month Excellence Eiffel grant from Campus France.



Acknowledgements

I take this opportunity to acknowledge the Paris-East University and the National Academy of Science of Ukraine (NASU) and extend my sincere gratitude for making it possible to realize this PhD thesis. I would like to start with the director of the East-Paris Institute of Chemistry and Materials Science (ICMPE), Dr. Michel LATROCHE, and the acting director of the Institute of Macromolecular Chemistry NASU (IMC), Prof. Yuriy SAVELIEV, for having hosted me in their institutes. I would also like to express my gratitude to Campus France, which has been so helpful and cooperative in giving me its support during my stay in Paris. I extend my sincere thanks to the jury members Prof. Eliane ESPUCHE, Dr. Victor KRAMARENKO, Dr. Boulos YOUSSEF, and Prof. Tatyana ZHELTONOZHSKAYA for their acception to be members of the defense jury.

Special thanks to my Ukrainian supervisor Prof. Alexander FAINLEIB, Corresponding Member of NASU, for providing direction and giving me the keys to organise the PhD work in an efficient way. My next thank will go to my French supervisor Dr. Daniel GRANDE for his tireless research guidance, motivation and support, despite his busy agenda. He allowed this thesis to be my own work, while non-obtrusively steered me in the right direction whenever he thought I needed it.

There is no doubt that the steady progress of my work would not have been possible without the continuous support by the staff of FAINLEIB's lab. I would address my thanks to Dr. Olga GRIGORYEVA for her invaluable help in validation of collected data and useful hints for improving this manuscript. I am deeply grateful to Dr. Olga STAROSTENKO who helped me get my start and taught me how to do research. Without her ideas that helped me sort out the details of my work this thesis would not have been possible. I would like to express my warm thanks to Mrs. Inna DANILENKO for her assistance with the experiments and being there at times when I required motivation.

I express my sincere appreciation to the team of the Complex Polymer Systems laboratory from ICMPE for their remarkable human and scientific environment throughout my staying. I offer my warm thanks to Dr. Agustín RIOS DE ANDA, Dr. Tam NGUYEN, Mr. Laurent MICHELY, Mrs. Sena HAMADI, and Mrs. Marcelle AMMOUR for being available all the time for discussion and help.

I would like to have a special appreciation to the staff at Laboratoire Ingénierie des Matériaux Polymères (Université Claude Bernard Lyon 1), especially Dr. Gisèle BOITEUX and Olivier GAIN, for their assistance and opportunity to learn new things during my staying in April 2017.

I also thanks people who were not part of the previous groups but helped me out, including Rémy PIRES BRAZUNA from ICMPE for his assistance with SEM analyses; Dr. Sergey ROGALSKY for sparing his valuable time whenever I approached him and making things simple; Prof. Valery SHEVCHENKO, Corresponding Member of NASU, for having managed to convince me during our discussions and added his unique vision to this thesis; Dr. Oleksandr BROVKO for his advices, which I have gladly embraced.

Special thanks are going to people who introduced science to me. Big thanks to Dr. Vyacheslav TRACHEVSKY for stimulating me to stay tuned. In his lectures, for the first time I encountered the world of polymers. Especially I should thank Dr. Eleonora PRIVALKO who sparked my interest in polymer chemistry during my student time. She was truly inspirational and the reason why I decided to go to pursue a career in research. Moreover, she has taught me much more than just polymers.

But my both personally and professionally thanks must be reserved for my doctoral colleagues Liubov MATKOVSKA, Sarra MEZHOUD, Romain POUPART, Thibault LEROUGE, Erica Gea RODI, Antoine BENLAHOUES, Azad ERMAN, Etienne DESSAUW, Pierre PUBELLIER, and Vierajitha SRIKANTHAN. I have to thank these people who have in their own ways assisted me as per their abilities, in whatever manner possible. I greatly value their friendship and belief in me. They brighten up my days and I would always cherish the wonderful memories which I shared with all them.

Last but not the least, I would like to thank my friends and my family for their lifelong encouragement in all that I do. Too many to list here, but they know who they are. They will always have a special place in my heart no matter where I go. Most importantly, I wish to thank my parents for giving me liberty to choose what I desired. They were always keen to know what I was doing, although it is probable that sometimes they did not grasp what it was all about. Anyway, they have showing their faith in me and I will always appreciate that.

List of Abbreviations

CER	Cyanate Ester Resin
DCBE	Dicyanate ester of Bisphenol E
DMTA	Dynamic Mechanical Thermal Analysis
DSC	Differential Scanning Calorimetry
FTIR	Fourier Transform Infrared Spectroscopy
SEM	Scanning Electron Microscopy
TGA	Thermogravimetric Analysis
[OMIm][BF₄]	1-octyl-3-methyl imidazolium tetrafluoroborate
[HEAIm][Cl]	2-(hydroxyethylamino) imidazolium chloride
[PHMG][TS]	poly(hexamethylene guanidine) toluene sulfonate
[HPyr][BF₄]	1-heptyl pyridinium tetrafluoroborate

Figure Captions

Figure 1-1: Publications on ILs as determined from the ISI Web of Science® (December 12, 2017).....	6
Figure 1-2: Schematical image of ionic structure of molten salt and IL.....	7
Figure 1-3: Structure of commonly used cations and anions species for ILs	8
Figure 1-4: Schematical image of the structure of thermoplastics, elastomers and thermosets.....	11
Figure 1-5: Potential applications of ionic liquids in thermosetting resins.....	11
Figure 1-6: TEM micrographs of epoxy networks cured with phosphonium dicyanamide IL, wt. %: (a) 5, (b) 9, (c) 23 [66].	16
Figure 1-7: Temperature dependence of ionic conductivity of samples with varying resin contents (wt. %): 1) 30; 2) 50; 3) 40; 4) 50; 5) 50. Samples 1, 3, 5 –based on MVR® 444; 2 – VTM® 57; 4 – VTM® 266 [67].	17
Figure 1-8: Dynamical mechanical properties of DGEBA/IL/MCDEA networks as a function of the IL content, wt. %: (a) 0, (b) 1.0, (c) 1.6, (d) 3.0 [42].	19
Figure 1-9: Surface topography (a) and cross section profiles (b) for the evolution of the wear track on a surface of epoxy resin/[OMIm][BF ₄] (12 wt. %).	21
Figure 1-10: Time dependence of the extracted ionic liquid fraction from films of DGEBA/Tetrad-X/TEPA with [EMIm][TFSI], [HMIm][TFSI] and [BMIm][TFSI] (extraction solvent: acetone) [64].	24
Figure 1-11: SEM micrographs of epoxy samples after extraction of different amounts of electrolyte (EMIm-TFSI + LiTFSI): (a) 60 wt. %; (b) 70 wt. % [67].	24
Figure 2-1: DSC thermograms (a) and temperature dependence of post-curing conversion (b) for CER samples with different [OMIm][BF ₄] contents.....	38
Figure 2-2: FTIR spectra of: DCBE monomer (curve 0) (a) and CER samples with different [OMIm][BF ₄] contents after heating at 150 °C for 6 h (curves 0 ₇ -5.0 ₇ , the number indicating the IL content); uncured DCBE (curve 0) (b) and CER/[OMIm][BF ₄] sample (95/5 wt. %) before	

(curve 5.0) and after (curve 5.0 _T) the same heating stage in the spectral zone of 2370-2200 cm ⁻¹	40
Figure 2-3: Proposed mechanism for the [OMIm][BF ₄]-catalyzed cyclotrimerization of DCBE....	42
Figure 3-1: Reaction scheme of DCBE polycyclotrimerization.	47
Figure 3-2: Typical FTIR spectra in 2320-1290 cm ⁻¹ region during curing procedure for: neat CER (a), CER/[OMIm][BF ₄] (b), CER/[HEAIm][Cl] (c), and CER/[PHMG][TS] (d). The spectra were shifted vertically for the sake of clarity.....	54
Figure 3-3: Kinetic curves at <i>T</i> = 150 °C: time dependence of (a) conversion (α_c) of -OCN groups from DCBE and (b) reaction rate (da/dt). Neat CER (1), CER/[OMIm][BF ₄] (2), CER/[HEAIm][Cl] (3), and DCBE/[PHMG][TS] (4)......	55
Figure 3-4: FTIR spectra in 1780-1350 cm ⁻¹ region for: (1) neat CER, (2) [OMIm][BF ₄], (3) CER/[OMIm][BF ₄] 50/50 wt.%, (4) [HEAIm][Cl], (5) DCBE/[HEAIm][Cl] 50/50 wt.% before curing, (6) CER/[HEAIm][Cl] 50/50 wt.% after curing, (7) [PHMG][TS], (8) DCBE/[PHMG][TS] 50/50 wt.% before curing, (9) CER/[PHMG][TS] 50/50 wt.% after curing. The spectra were shifted vertically for the sake of clarity.	56
Figure 3-5: Proposed mechanism for [OMIm][BF ₄]-catalyzed DCBE polycyclotrimerization.....	57
Figure 3-6: Proposed mechanism for [HEAIm][Cl]-catalyzed DCBE polycyclotrimerization.	58
Figure 3-7: Proposed mechanism for [PHMG][TS]-catalyzed DCBE polycyclotrimerization.....	59
Figure 3-8: Chemical reaction between cyanate groups of DCBE and traces of water or phenol impurity accompanying the DCBE monomer.	60
Figure 3-9: TGA curves for CER-based networks (a) and pure ILs (b): neat CER (-), CER/[OMIm][BF ₄] (-●-), CER/[HEAIm][Cl] (-■-), CER/[PHMG][TS] (-▲-), [OMIm][BF ₄] (-○-), [HEAIm][Cl] (-□-), and [PHMG][TS] (-△-).	60
Figure 3-10: Plot of <i>E'</i> (a) and tan δ (b) as a function of temperature at 1 Hz for: CER (-), CER/[OMIm][BF ₄] (-●-), CER/[HEAIm][Cl] (-■-), and CER/[PHMG][TS] (-▲-).	62
Figure 3-11: Plot of log <i>f</i> vs. 1000/ <i>T</i> for: CER (-), CER/[OMIm][BF ₄] (-●-), CER/[HEAIm][Cl] (-■-), and CER/[PHMG][TS] (-▲-).	64

Figure 4-1: Reaction scheme associated with polycyclotrimerization of DCBE.....	72
Figure 4-2: FTIR spectra in the spectral zone of 2310-2200 cm^{-1} obtained at isothermal curing ($T = 150\text{ }^\circ\text{C}$ for 6 h) of pure DCBE (a) and DCBE/[HPyr][BF ₄] samples: CER ₁ (b), CER ₂₀ (c), and CER ₄₀ (d).....	75
Figure 4-3: FTIR spectra in the spectral zone of 1600-650 cm^{-1} for pure [HPyr][BF ₄] (a), CER ₀ (b), and CER ₄₀ (c).....	76
Figure 4-4: Kinetic plots of (a) -OCN groups fractional conversion, a_c , and (b) reaction rate, $d\alpha_c/dt$, versus curing time: CER ₀ (○), CER ₁ (●), CER ₂₀ (●), CER ₄₀ (■).....	77
Figure 4-5: Proposed mechanism for [HPyr][BF ₄]-catalyzed polycyclotrimerization of DCBE.....	78
Figure 4-6: Scheme for complex formation in CER/[HPyr][BF ₄] networks.	79
Figure 4-7: DSC thermograms for CER/[HPyr][BF ₄] networks: CER ₀ (1), CER ₂₀ (2), CER ₃₀ (3), CER ₄₀ (4).....	80
Figure 4-8: Scheme of CER matrix (a) and agglomerated IL in the CER matrix (b).	82
Figure 4-9: Dependence of storage modulus E' (a) and loss factor $\tan\delta$ (b) on temperature at 1 Hz for CER and CER/[HPyr][BF ₄] networks: CER ₀ (-), CER ₂₀ (●), CER ₃₀ (▲), CER ₄₀ (■).....	84
Figure 4-10: Dependence of E'' on temperature at 1 Hz for CER and CER/[HPyr][BF ₄] networks: CER ₀ (-), CER ₂₀ (●), CER ₃₀ (▲), CER ₄₀ (■). The four observed molecular relaxations in CER ₀ were mathematically deconvoluted and are highlighted (blister lines).....	86
Figure 4-11: 3D spectrum of loss dielectric permittivity as a function of frequency and temperature obtained by BDS measurements for neat CER ₀ with highlighted molecular relaxations.	87
Figure 4-12: Molecular relaxation amplitude for the observed molecular relaxations obtained from BDS measurements for neat CER ₀ : γ (▼), β (●), β' (▲), β'' (■), α (○).....	88
Figure 4-13: Molecular relaxation cartography for the observed molecular relaxations obtained from BDS measurements for neat CER ₀ : γ (▼), β (●), β' (▲), β'' (■), α (○).....	89
Figure 4-14: Secondary transition temperatures of CER/[HPyr][BF ₄] networks as determined by DMTA: T_γ (▼), T_β (●), $T_{\beta'}$ (▲), $T_{\beta''}$ (■).....	91

Figure 4-15: Current-voltage characteristics of In/CER/Ag structure for 900 μm -thick samples at room temperature: in darkness (a) and under white light (b): CER (●), CER ₃₀ (▲) and CER ₄₀ (■) and differential slope of CER ₄₀ in darkness (c) and under white light (d).....	93
Figure 4-16: Evolution of mass loss as a function of temperature, <i>i.e.</i> a) TGA and b) DTG data, of CER networks modified with [HPyr][BF ₄]: CER ₀ (—), CER ₂₀ (●), CER ₃₀ (▲), CER ₄₀ (■), [HPyr][BF ₄] (---).....	95
Figure 5-1: Synthetic route to ionic liquid [HPyr][BF ₄].....	103
Figure 5-2: Scheme of CER network formation.....	103
Figure 5-3: Representative scheme of CER formation in the presence of [HPyr][BF ₄] and subsequent pore formation.....	106
Figure 5-4: Experimental (1) and theoretical (2) values of gel fraction contents after extraction as a function of [HPyr][BF ₄] content.....	107
Figure 5-5: FTIR spectra of ionic liquid [HPyr][BF ₄] and typical CER networks before and after extraction.....	107
Figure 5-6: ¹ H NMR spectra of [HPyr][BF ₄] (a) and sol fraction after CER ₄₀ extraction (b).....	108
Figure 5-7: Typical SEM micrographs of CER-based samples: CER _{ext} (a), CER _{20ext} (b), CER ₄₀ (c), CER _{40ext} (d), and corresponding EDX spectra (e).....	110
Figure 5-8: Pore area distributions derived from SEM data for the nanoporous CER samples.....	111
Figure 5-9: DSC melting thermograms of water confined within the pores of nanoporous CERs (a) and corresponding pore size distribution profiles (b).....	112
Figure 5-10: Mass loss (a) and corresponding derivative (b) curves as determined by TGA for [HPyr][BF ₄] and typical CER-based films.....	113

Table Captions

Table 1-1: Basic types of aprotic and protic ILs	9
Table 1-2: Comparison of ionic liquids with organic solvents [20].....	10
Table 1-3: General overview of IL influence on epoxy resins	25
Table 2-1: Thermal characteristics of CER/[OMIm][BF ₄] samples cured at 150 °C for 6 h as determined by DSC	38
Table 2-2: Conversion values for CER/[OMIm][BF ₄] samples after heating at 150 °C for 6 h.	39
Table 3-1: Chemical structure and basic physico-chemical characteristics of components under investigation.....	51
Table 3-2: Kinetic parameters of DCBE polymerization in the absence and the presence of 1.0 wt.% IL.....	55
Table 3-3: Thermal stability of CER-based networks and pure ILs as investigated by TGA.....	61
Table 3-4: Viscoelastic properties of CER-based networks as investigated by DMTA.	62
Table 4-1: Thermal and mechanical characteristics for CER/[HPyr][BF ₄] nanocomposites	81
Table 4-2: Calculated activation energy E_a for each of the observed molecular relaxations of CER samples	90
Table 5-1: Main porosity characteristics for nanoporous CER-based films	111
Table 5-2: Experimental and theoretical values of element contents in typical CER samples	111
Table 5-3: TGA data obtained for CER-based networks and pure [HPyr][BF ₄]	115

Table of Contents

INTRODUCTION.....	1
CHAPTER 1. APPLICATION OF IONIC LIQUIDS IN THERMOSETTING POLYMERS: EPOXY AND CYANATE ESTER RESINS.....	4
1.1. INTRODUCTION.....	5
1.2. IONIC LIQUIDS	5
1.3. APPLICATIONS OF ILS IN THERMOSETTING POLYMERS	10
1.4. EPOXY RESINS	11
<i>1.4.1. Ionic liquids as catalytic agents</i>	<i>11</i>
<i>1.4.2. Ionic liquids as ionic conducting agents</i>	<i>14</i>
<i>1.4.3. Ionic liquids as plasticizers</i>	<i>18</i>
<i>1.4.4. Ionic liquids as lubricants</i>	<i>19</i>
<i>1.4.5. Ionic liquids as porogens</i>	<i>22</i>
1.5. IONIC LIQUIDS IN CYANATE ESTER RESINS (CERs).....	26
1.6. CONCLUSIONS	26
1.7. REFERENCES.....	28
CHAPTER 2. ACCELERATION EFFECT OF IONIC LIQUIDS ON POLYCYCLOTTRIMERIZATION OF DICYANATE ESTERS	33
2.1. INTRODUCTION.....	34
2.2. EXPERIMENTAL	35
<i>2.2.1. Materials</i>	<i>35</i>
<i>2.2.2. Ionic liquid synthesis.....</i>	<i>35</i>
<i>2.2.3. Preparation of CER/[OMIm][BF₄] samples.....</i>	<i>36</i>
<i>2.2.4. Physico-chemical techniques</i>	<i>36</i>
2.3. RESULTS AND DISCUSSION.....	37
<i>2.3.1. DSC analysis</i>	<i>37</i>
<i>2.3.2. FTIR analysis</i>	<i>40</i>
<i>2.3.3. Proposed mechanism of the [OMIm][BF₄]-catalyzed cyclotrimerization of DCBE</i>	<i>41</i>
2.4. CONCLUSIONS	43
2.5. REFERENCES.....	44

CHAPTER 3. EFFECT OF IONIC LIQUIDS ON KINETIC PECULIARITIES OF DICYANATE ESTER POLYCYCLOTTRIMERIZATION AND ON THERMAL AND VISCOELASTIC PROPERTIES OF RESULTING CYANATE ESTER RESINS..... 46

3.1. INTRODUCTION	47
3.2. EXPERIMENTAL	49
3.2.1. <i>Materials</i>	49
3.2.2. <i>Synthesis of ionic liquids</i>	49
3.2.2.1. <i>Synthesis of 1-octyl-3-methyl imidazolium tetrafluoroborate ([OMIm][BF₄])</i>	49
3.2.2.2. <i>Synthesis of 2-(hydroxyethylamino) imidazolium chloride ([HEAIm][Cl])</i>	50
3.2.2.4. <i>Synthesis of poly(hexamethylene guanidine) toluene sulfonate ([PHMG][TS])</i>	50
3.2.3. <i>Preparation of CER-based networks</i>	51
3.2.4. <i>Physico-chemical techniques</i>	52
3.3. RESULTS AND DISCUSSION.....	54
3.3.1. <i>Kinetic investigation by FTIR</i>	54
3.3.2. <i>CER/IL curing mechanisms</i>	56
3.3.3. <i>Thermal stability of CER-based networks by TGA</i>	60
3.3.4. <i>Viscoelastic properties of CER-based networks by DMTA</i>	62
3.4. CONCLUSIONS	64
3.5. REFERENCES	66

CHAPTER 4. STRUCTURE-PROPERTY RELATIONSHIPS IN NANOCOMPOSITES BASED ON CYANATE ESTER RESINS AND 1-HEPTYL PYRIDINIUM TETRAFLUOROBORATE IONIC LIQUID 69

4.1. INTRODUCTION	70
4.2. EXPERIMENTAL PART	71
4.2.1. <i>Materials</i>	71
4.2.2. <i>Preparation of CER/[HPyr][BF₄] nanocomposites</i>	71
4.2.3. <i>Instrumentation</i>	72
4.3. RESULTS AND DISCUSSION.....	75
4.3.1. <i>Kinetic peculiarities and proposed mechanism for [HPyr][BF₄]-catalyzed polycyclotrimerization of DCBE</i>	75
4.3.2. <i>Molecular mobility and viscoelastic properties of CER/[HPyr][BF₄] nanocomposites</i>	79
4.3.2.1. <i>DSC investigation</i>	79
4.3.2.2. <i>Dynamic Mechanical Thermal Analysis</i>	83

4.3.2.3. Broadband dielectric spectroscopy.....	86
4.3.2.4. Discussion on β' and β'' relaxations	91
4.3.2.5. Tensile testing	92
4.3.3. Photosensitivity of CER/[HPyr][BF ₄] nanocomposites.....	93
4.3.4. Thermal stability of CER/[HPyr][BF ₄] nanocomposites.....	94
4.4. CONCLUSIONS	95
4.5. REFERENCES.....	97
CHAPTER 5. NANOPOROUS POLYMER FILMS OF CYANATE ESTER RESINS DESIGNED BY USING IONIC LIQUIDS AS POROGENS	100
5.1. INTRODUCTION	101
5.2. EXPERIMENTAL	102
5.2.1. Materials	102
5.2.2. Ionic liquid synthesis.....	102
5.2.3. Preparation of CER-based films	103
5.2.4. Physico-chemical techniques	104
5.3. RESULTS AND DISCUSSION	106
5.3.1. Spectroscopic analyses of network structure	107
5.3.2. SEM and EDX analyses of CER-based films	109
5.3.3. Investigation of nanoporous CER-based films by DSC-based thermoporometry.....	112
5.3.4. Thermal stability of CER-based films by TGA	113
5.4. CONCLUSIONS	115
5.5. REFERENCES.....	116
CONCLUSIONS AND PROSPECTS	118

Introduction

Numerous advanced technologies require a combination of properties for polymer films, including high thermal stability, inertness, excellent resistance towards solvents and aggressive media, etc. Cyanate ester resins (CERs), also known as polycyanurates, offer a unique outstanding combination of physical properties which makes them suitable for use in high performance technology ranging from printed circuit boards and radomes to magnet casings for thermonuclear fusion reactors and support structures for interplanetary space probes. The attractive features of CERs are their low dielectric loss characteristics ($\approx 2.6-3.2$), dimensional stability at molten solder temperatures (220-270 °C), high purity, inherent flame-retardancy (giving the potential to eliminate brominated flame retardants), low moisture absorption, and good adhesion to miscellaneous substrates. Though polyimides, such as bismaleimide-derivatized materials, may outmatch CERs in temperature stability, they have a poor shelf-life and are more difficult to process. Phenolics also have similar disadvantages.

Compared to polyepoxides, CERs have much improved hydro/thermal stability. Moreover, CERs offer several advantages over aforementioned thermosets, including their processability, shelf-life, and compatibility with a variety of reinforcements. Despite these qualities, they are rather brittle due to aromatic content and expensive, which limits their potential for high-performance applications. The choice of monomer also plays a critical role for processing operations. Most monomers meant for the synthesis of highly thermostable thermosets require high temperatures to achieve low viscosities and therefore are less processible. Though, dicyanate ester of bisphenol E (DCBE) is particularly unique due to its low melting point and low ambient viscosity (0.09-0.12 Pa·s) caused by the rotational flexibility of the structure. It is known, that DCBE outperformed an epoxy (Epon 828) in all mechanical tests, even at high temperatures (200 °C). This monomer being liquid at room temperature can undergo a thermally initiated polycyclotrimerization reaction to generate densely packed cross-linked thermosets with high glass transition temperature, without releasing volatile products. However, the rate of non-catalyzed thermal polycyclotrimerization is generally slow, and it depends on the concentration of impurities (traces of phenols and other residues from synthesis). Using a catalyst is necessary to achieve a controlled polycyclotrimerization process, which is a key factor for producing materials with excellent properties. This reaction is generally catalyzed by a combination of salts of transition metals, like acetyl acetonates of Cu, Co, Zn, Fe, Mn, Cr, etc. and an active hydrogen containing initiator like nonylphenol. Because

of the well-known toxicity of phenolic compounds, attempts to find new effective catalysts for dicyante ester polycyclotrimerization are of scientific and practical interest.

Ionic liquids (ILs) are the subject of widespread interest as alternatives to conventional catalysts, due to their peculiar properties. Being composed entirely of ions, these novel multifunctional agents, so called as «designer solvents», have extremely low vapour pressure and low volatility, are non-flammable, and exhibit a wide temperature range of liquid state up to about 300 °C in some instances, thus providing the opportunity to carry out high-temperature reactions. As a result of one or more of these characteristic properties, ILs have already been exploited in polymer chemistry for diverse applications. Nevertheless, the investigation of the design and synthesis of CERs in the presence of ILs is fairly limited in the literature, and only a few reports have been published so far (mainly by the French-Ukrainian consortium involved in this PhD thesis). Certainly, the addition of ionic liquids can be a challenging and facile way to tune the properties of CER-based materials and eventually to widen their applications.

The first chapter focuses on a general overview on the existing literature about using ILs as catalysts, curing agents, electroconductive components, plasticizers, lubricants or porogens for a wide range of applications in thermosetting polymers, and more particularly epoxy and cyanate ester resins. This review emphasizes the urgent need for understanding the role, efficiency, and perspectives of ILs with the potential to impact across many areas of thermosetting polymers.

As a starting point for our investigation of the catalytic behaviour of ILs in CER systems, the second chapter is dedicated to a thorough kinetic and mechanistic study on the polycyclotrimerization reaction of DCBE in the presence of varying concentrations (from 0.5 to 5 wt%) of an aprotic IL. The third chapter then extends this investigation to the comparison of the catalytic behaviour associated with three ILs with contrasted reactivity, namely an imidazolium-based aprotic IL, an imidazolium-containing protic one, and a protic polymeric one. It is expected that using ionic liquids can give rise to combinations of properties not possible with conventional catalysts. In this way, such properties can be tuned by the selection of IL type. A comprehensive study of their effect on kinetic peculiarities (induction time, reaction time, monomer conversion degree, etc) of DCBE polycyclotrimerization as well as on thermal stability and viscoelastic properties of the resulting CERs is addressed. Plausible mechanisms for all the DCBE/IL systems are also proposed to explain the acceleration effect of ILs.

In the fourth chapter, the effects of a pyridinium-based aprotic IL on the formation peculiarities and properties of CER nanocomposites are investigated in view of the scarcity on this type of IL-based networks. To the best of our knowledge, it is the first trial to investigate the influence of pyridinium-based ILs on the CER curing process and to examine the thermal behavior and viscoelastic properties, as well as the photosensitivity of related nanocomposite materials. Moreover, inert ILs can be easily recovered and recycled from the CER-based composites that could be applied as precursors to designing porous materials.

Accordingly, the last chapter focuses on the engineering of novel nanoporous CER-based films by quantitative extraction of pyridinium-based aprotic IL from nanocomposites synthesized in the previous chapter. The effect of porogen content on the structure and properties of resulting porous CERs is examined. To the best of our knowledge, ILs have not been used as porogens to generate porous thermosets so far.

CHAPTER 1

Application of Ionic Liquids in Thermosetting Polymers: Epoxy and Cyanate Ester Resins

Abstract: Thermosetting polymers are widely used as industrial materials due to good heat resistance, dimensional stability and chemical resistance. There is a longstanding and widespread interest in designing novel polymer networks, and utilization of ionic liquids (ILs) opens up new frontiers to meet this challenge by creating new materials. For thermosetting polymers, ILs offer many advantages, either as catalytic agents, plasticizers, conducting additives, or porogens. Furthermore, ILs show rich structural diversity and can be incorporated into a polymer matrix to achieve better final properties. This review emphasizes the urgent need for understanding the role, efficiency and perspectives of an innovative class of components, namely ILs with the potential to impact across many areas of thermosetting polymers. To avoid ambiguity and make the review self-reading, basic ideas about the application of ILs in thermosetting polymers are first outlined.

A.Vashchuk, A. Fainleib, O. Starostenko, D. Grande: Application of ionic liquids in thermosetting polymers: epoxy and cyanate ester resins. *eXPRESS Polymer Letters*, **12**, 898-917 (2018).

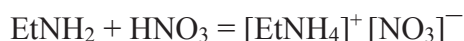
1.1. Introduction

Ionic liquids (ILs) are the subject of widespread interest as alternatives to conventional organic solvents due to their very special properties, including recycling ability. Many known ILs are commercially available from several suppliers. Ideally, ILs are non-flammable, optically clear and are relatively inexpensive to manufacture [1]. Many ILs exhibit a wide temperature range of liquid state up to about 300 °C, providing the opportunity to carry out high-temperature reactions. Being composed entirely of ions, these novel multifunctional agents so called as «designer solvents» have extremely low vapour pressure and low volatility. As a result of one or more of these characteristic properties, ILs have already been found useful in the polymer chemistry for diverse applications [2-5]. ILs make an increasing impact in the field of cross-linked polymers, in particular on the development of thermosetting polymers and composite materials with various interesting properties [6-12]. All these applications require a strong confinement of the ionic liquid within the polymer network with no exudation of the ILs.

In this way, herein, we are going to review the using of ILs for a wide range of applications in thermoset materials that could be important hosts for ILs. The application of ILs in thermosets has quickly advanced from using them as a reaction media to application as functional additives. Certainly, innovation in this field requires the control of their structure at nanoscale and addition of ILs can be a new and facile method to manage the morphology and properties of thermoset polymers as well as to widen their application.

1.2. Ionic liquids

ILs may be considered as a class of salts with a melting temperature below 100 °C. The story of ILs begins with the first report on the preparation of ethylammonium nitrate salt using the reaction of ethylamine with nitric acid having melting point of 12 °C in 1914 [13]:



Despite this pioneering work, the interest in ILs has developed after the discovery of binary ILs made from mixtures of aluminum (III) chlorides and N-alkylpyridinium [14] or 1,3-dialkylimidazolium chlorides [15]. Nevertheless, a major drawback of all chloroaluminate (III) ILs, their moisture sensitivity remained unresolved. In particular, Wilkes

and Zawarotko [16] prepared and characterized the air and water stable 1-ethyl-3-methylimidazolium ILs with different anions.

Over the last two decades a large variety of ILs have been investigated marked by an exponential growth in a number of publications represented by the yearly increase starting from near 10 in 1990 to more than 7000 papers published last year (**Figure 1-1**). The first publications on using ILs in polymers have appeared in 2002 and then increased quickly in the last two decades and a summary on their applications and properties may be found in a number of review articles [17-23] and book [24]. There is no doubt that this area of research has been an important point of polymer chemistry as well.

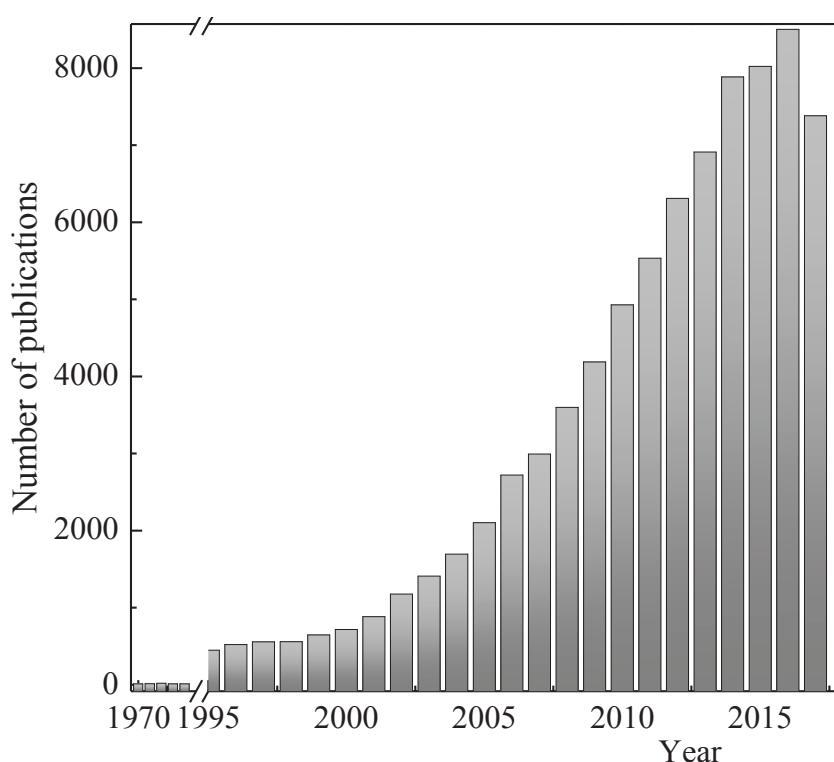


Figure 1-1: Publications on ILs as determined from the ISI Web of Science® (December 12, 2017).

ILs are self-dissociated and do not need a solvent to dissociate into cations and anions that uniquely distinguish them from classical salts like NaCl, KBr. What is the difference between a molten salt and an IL? Both molten salts and ILs are liquid salts containing only ions (**Figure 1-2**). However, in molten salts, there are symmetric cations and anions making the lattice well packed and hence it requires a large energy to break the lattice. Contrary to molten

salts, IL cations have irregular shape preventing crystal packing [25-27]. Therefore, molten salts melt above 100 °C ($T_{\text{melt NaCl}} = 801 \text{ °C}$, $T_{\text{melt KCl}} = 770 \text{ °C}$), and ILs melt much below that temperature (in particular, Room temperature ILs (RTIL) are liquid already at an ambient temperature).

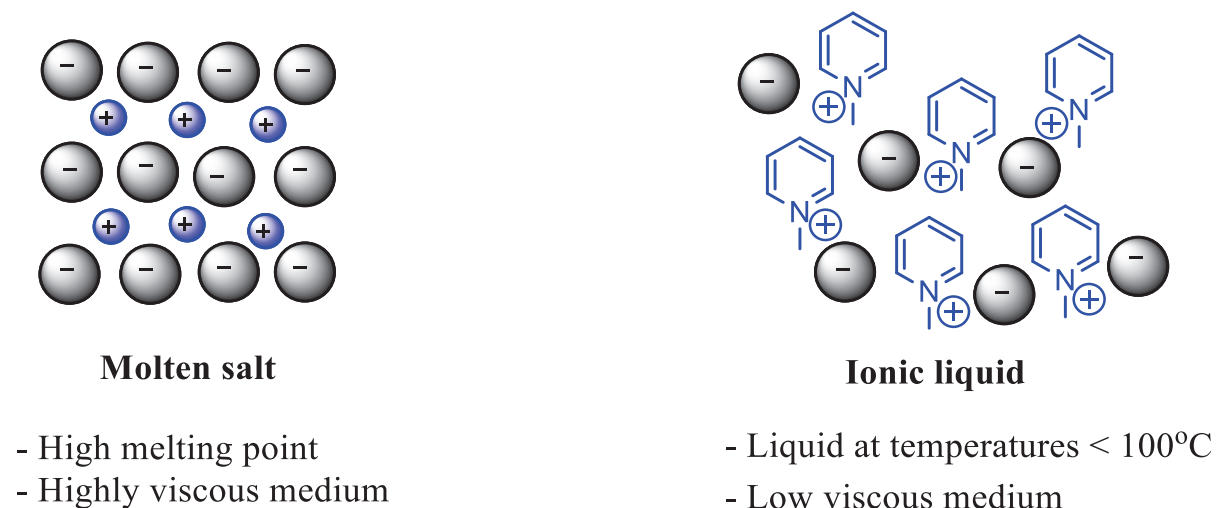
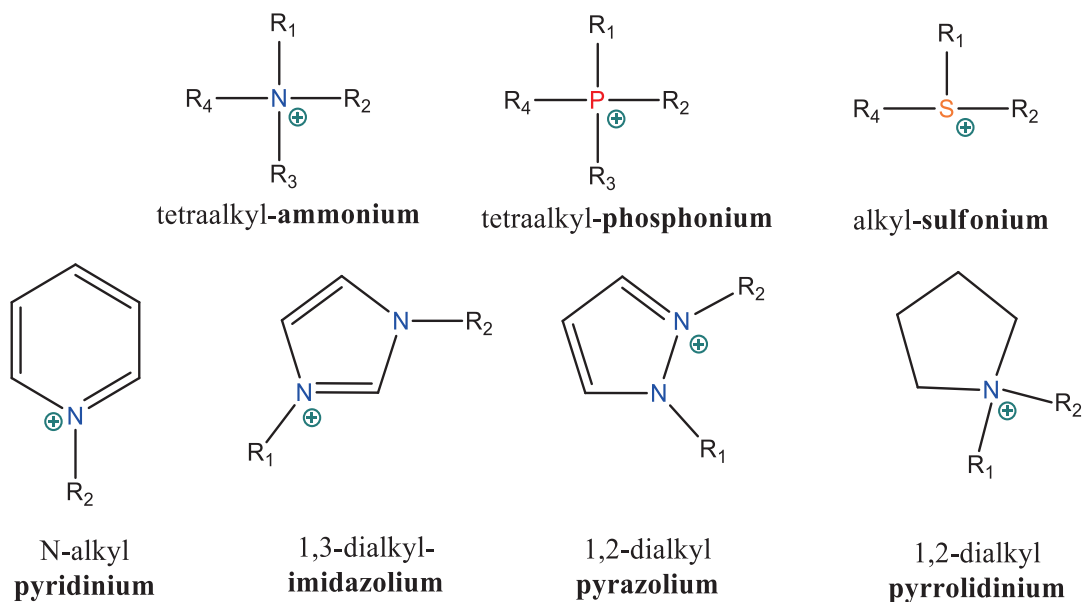


Figure 1-2: Schematical image of ionic structure of molten salt and IL.

The most common classes of cations and anions are illustrated in **Figure 1-3**. The structural design of ILs is playing a very important role as the major properties may be easily controlled by changing the combinations of cation and anion types (10^{18} potential structures [28]). In this way, their properties can be varied dramatically by the creation of unique combinations of cations, anions and chains lengths. The change of anion can drastically affect physical properties of ILs such as hydrophilicity, viscosity and melting point as well as thermal stability. On the basis of reported data, the relative thermal stability (T_{onset} , °C) of imidazolium IL, *i.e.* $[\text{C}_2\text{MIm}]$ containing some common anions decreases in the following order: $[\text{C}(\text{CN})_3]^- \approx [\text{BF}_4]^- (450 \text{ °C}) > [\text{I}]^- (303 \text{ °C}) > [\text{Cl}]^- (285 \text{ °C}) > [\text{N}(\text{CN})_2]^- (275 \text{ °C}) \gg [\text{SCN}]^- (226 \text{ °C})$ [29-32]. The purity of ILs is a very important issue and the influence of major contaminants such as water and chlorine ion on some of their physical properties has been discussed by Seddon *et al.* [33]. It is noteworthy that ILs are often determined as green solvents, but such character is disputable. Typical ILs consisting of halogen-containing anions may cause serious concerns if the hydrolytic stability of the anion is poor *e.g.* for $[\text{AlCl}_4]^-$ and $[\text{PF}_6]^-$ or if a thermal treatment of ILs used is required [29]. In both cases, additional effort is needed to avoid the liberation of toxic and corrosive HF or HCl into the environment.

Possible cations



Possible anions

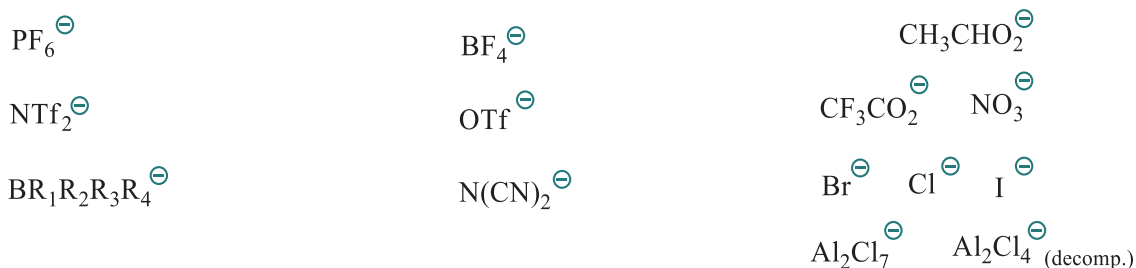
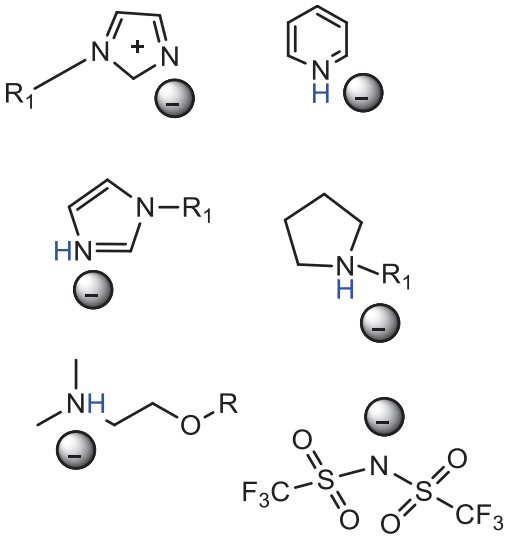
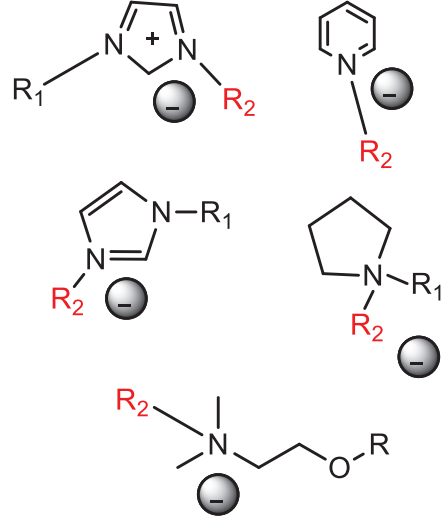


Figure 1-3: Structure of commonly used cations and anions species for ILs.

ILs can be divided into two broad categories, namely protic ILs (PILs) and aprotic ILs (AILs) [34-37]. PILs are formed in general by the transfer of a proton between an equimolar amount of Brønsted acid and base. Due to the «free» available proton, they are capable of hydrogen bonding, including proton acceptance and proton donation. AILs contain no acidic protons and exhibit characteristics significantly different from those of PILs (**Table 1-1**). It should be noted that AILs are more thermally and electrochemically stable than the corresponding PILs [38].

Table 1-1: Basic types of aprotic and protic ILs

Protic ILs	Aprotic ILs
 <p data-bbox="375 1041 662 1075">R_1 – different alkyl groups</p> <ul data-bbox="207 1142 790 1400" style="list-style-type: none">• simpler and cheaper to synthesize (no by-products)• high fluidity and conductivity• low melting points• suitable for fuel cells	 <p data-bbox="901 1086 1236 1120">R_1, R_2 – different alkyl groups</p> <ul data-bbox="821 1198 1284 1444" style="list-style-type: none">• more expensive and complicated (multistep reactions)• low fluidity and conductivity• high melting points• suitable for lithium batteries

Due to their ability to be reused/recycled, most ILs could replace toxic industrial volatile organic compounds (VOCs) [39], and solve the following problems: (i) loss of solvent by uncontrolled evaporation, and (ii) traces of solvent in final product. In addition to the interactions existing in VOCs (hydrogen bonding, dipole–dipole and van der Waals interactions), ILs have ionic interactions (mutual electrostatic attractions or repulsion of charged particles), which make them very miscible with polar substances. Generally speaking, ILs have properties that are quite different from those of organic solvents (cf. **Table 1-2**).

Table 1-2: Comparison of ionic liquids with organic solvents [20]

Property	Organic Solvents	Ionic Liquids
Number of solvents	>1,000	> 1,000,000
Applicability	Single function	Multifunction
Catalytic ability	Rare	Common and tunable
Chirality	Rare	Common and tunable
Vapour pressure	Obeys the Clausius-Clapeyron Equation	Negligible under normal conditions
Flammability	Usually flammable	Usually nonflammable
Solvation	Weakly solvating	Strongly solvating
Tunability	Limited range of solvents available	Unlimited range means «designer solvents»
Polarity	Conventional polarity concepts apply	Polarity concept questionable
Cost	Normally inexpensive	2 to 100 times the cost of organic solvents
Recyclability	Green imperative	Economic imperative
Viscosity/cP	0.2-100	22-40,000
Density/g cm ⁻³	0.6-1.7	0.8-3.3
Refractive index	1.3-1.6	1.5-2.2

1.3. Applications of ILs in thermosetting polymers

Numerous advanced technologies require polymers possessing high thermal stability, inertness, excellent resistance towards solvents and aggressive media, etc. It is well known that highly crosslinked structures *via* covalent bonds are directly responsible for the high mechanical strength and high thermal stability, but at the same time provides a poor elasticity or elongation compared with thermoplastics or elastomers (**Figure 1-4**). Unlike thermoplastics, thermosets retain their strength and shape even when heated. In this context, the generation of high-performance thermosetting polymers in the presence of ILs may thus constitute an interesting challenge.

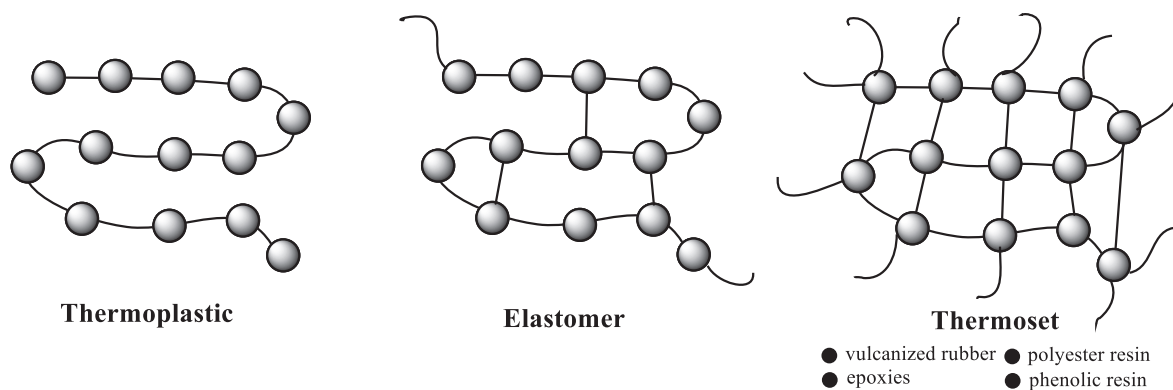


Figure 1-4: Schematical image of the structure of thermoplastics, elastomers and thermosets.

In the next sections the application of ILs in epoxy based thermosets as catalysts, curing agents, electroconductive components, plasticizers, lubricants and porogens is presented (**Figure 1-5**). Additionally, using ILs in high-performance Cyanate Ester Resins (CERs) will be discussed as well.

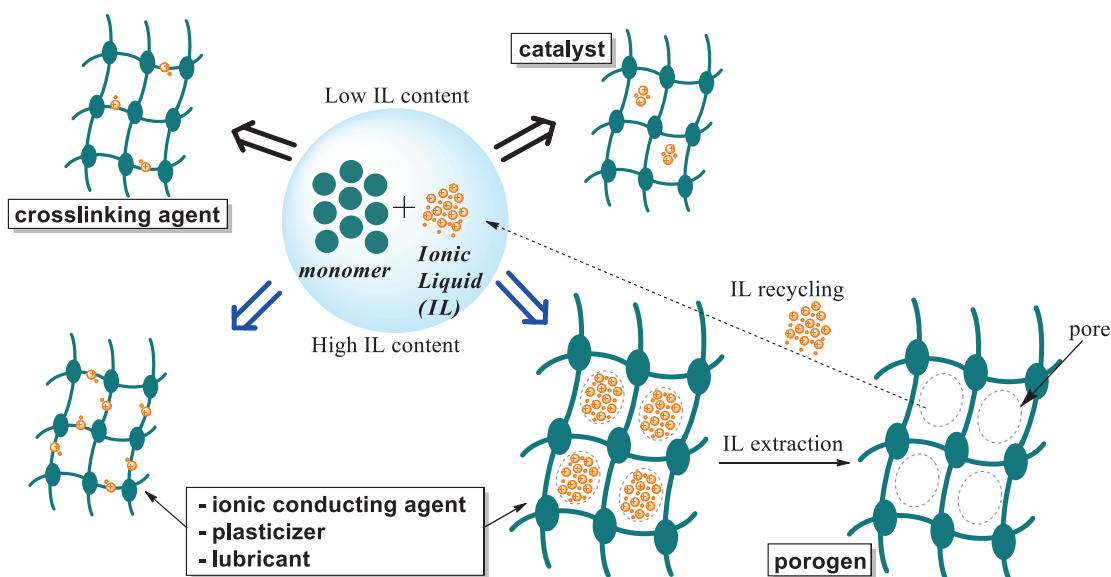


Figure 1-5: Potential applications of ionic liquids in thermosetting resins.

1.4. Epoxy resins

1.4.1. Ionic liquids as catalytic agents

ILs represent an exciting new class of catalytic or/and crosslinking agents for thermosetting polymers, especially for epoxy resins [40-50]. The first trial of using

1-butyl-3-methylimidazolium tetrafluoroborate [BMIm][BF₄] IL for cross-linking of epoxy resin was described by Kowalczyk and Spychaj in 2003 [41]. Palmese's team for the first time [47] used 1-ethyl-3-methylimidazolium dicyanamide [EMIm][N(CN)₂] in a range of 3-20 wt.% and found a lower cross-linking temperature than that reported by Kowalczyk and Spychaj for [BMIm][BF₄].

As discussed in the literature [40-41], imidazolium-based ILs act as curing agents for the epoxy systems at high temperature. Liebner *et al.* [51] suggested that such ILs may undergo a thermal decomposition leading to formation of imidazole and other decomposition products. In an early study, Farkas and Strohm, reported about the high catalytic activity of imidazoles for curing of epoxy resins, proving that the imidazole became permanently attached to the polymer chain [52]. The curing kinetics and mechanisms of diglycidyl ether of bisphenol A (DGEBA) using imidazole and 1-methyl imidazole as curing agents were studied by Ghaemy and Sadjady [53]. Soares *et al.* [42] synthesized epoxy crosslinked materials containing *N,N'*-dioctadecylimidazolium iodide (1-12 wt.%) by curing a mixture of DGEBA with 4,4'-methylene-bis 3-chloro-2,6-diethylaniline (MCDEA) as a hardener. It was found that the high temperature used for curing might favour some degradation of the IL, generating new species, which also took part in the curing process.

Maka *et al.* [46] also reported that reaction activity of ILs towards epoxy resins was connected with its thermal decomposition characteristics. They prepared and investigated the epoxy compositions with ILs possessing the imidazolium cation with alkyl chains of different length (butyl or decyl), and different anion type ([N(CN)₂]⁻, [BF₄]⁻, [Cl]⁻), the ILs concentration was varied as well (1, 3, or 8 wt.%). On the basis of the results, the authors concluded that *i*) the curing process started at lower temperature (120→150 °C) when ILs with [N(CN)₂]⁻ anion were applied, in comparison with those containing [BF₄]⁻ anions (200→240 °C); *ii*) the alkyl chain length of imidazolium cation influenced slightly the onset temperature curing range: for decyl substituent, 200→240 °C, and butyl, 210→230 °C; *iii*) as a rule bimodal exotherms appeared on DSC thermograms, the first was placed at a lower temperature range above 110 °C (compositions with ILs and basic [N(CN)₂]⁻ anion) and the second was placed above 250 °C (compositions with ILs bearing [BF₄]⁻ anion). The observed bimodal exotherms and FTIR absorption bands at 1740-1750 cm⁻¹ were explained by the proposed mechanism of epoxy resin anionic polymerization initiated by thermal decomposition products of 1,3-dialkylimidazolium liquids. In 2015, the same group [49] performed comparison of two dicyanamide ILs with various cation types: imidazolium, *i.e.* 1-ethyl-3-

methylimidazolium dicyanamide ([EMIm][N(CN)₂]) and phosphonium, *i.e.* (trihexyltetradecyl phosphonium dicyanamide ([THTDP][N(CN)₂])). The composition of neat epoxy resin with IL exhibited prolonged storage times, namely > 45 days and > 70 days, when [EMIm][N(CN)₂] and [THTDP][N(CN)₂] was applied, respectively. Increasing the IL amount in epoxy composition resulted in shortening the pot life, and this influence was more pronounced in the case of [EMIm][N(CN)₂]. It was also shown that DSC thermograms for compositions with [EMIm][N(CN)₂] were bimodal with the first maximum (T_{\max}) in a temperature range from 136 to 133 °C and the second one from 180 to 164 °C. Epoxy compositions with [THTDP][N(CN)₂] exhibited unimodal thermograms with T_{\max} from 180 to 170 °C. A simple relationship between IL thermal stability and its activity as epoxy resin curing agent was found: the observed T_{\max} values for the second exothermal peaks of investigated epoxy curing process correlated qualitatively with the thermal degradation of IL. It should be noted that epoxy compositions cured with 6 wt.% [THTDP][N(CN)₂] showed higher transparency ($\approx 85\%$) in comparison to that with 3 wt.% [EMIm][N(CN)₂] (black opaque) [49].

Gérard *et al.* [43] has fulfilled a comparative study on the effects exerted by different ILs (imidazolium, pyridinium and phosphonium) with long alkyl chains on DGEBA curing at high temperature. The hardener used for the curing process was MCDEA. The results clearly demonstrated once again that imidazolium- and pyridinium-based ILs may decompose at high temperature used for the curing process, and the resulting decomposition products (imidazole or pyridine [54-56], respectively) could act as additional curing agents for epoxy systems. In contrast, phosphonium-based IL did not participate in the curing process and/or displayed the highest thermal stability or if they decomposed, the products formed did not react with the epoxy prepolymer. However, there has been some discrepancy concerning the catalytic activity of phosphonium-based IL on epoxy resins curing. Nguyen *et al.* [57] substantiate the use of different amounts (9, 17, 23 wt.%) of tributyl (ethyl) phosphonium diethyl phosphate (CYPHOS[®] IL169) and trihexyl (tetradecyl) phosphonium bis 2,4,4-(trimethyl pentyl)-phosphinate (CYPHOS[®] IL104) for DGEBA curing. In both cases, all the samples were homogeneous except the mixtures containing 17 and 23 wt.% IL104, in which some exudation was observed. The results clearly showed that 9 wt.% IL104 was an excellent alternative to a large amount of amines (40 wt.% Jeffamine D400) required for crosslinking of epoxy resins. The lower reactivity of phosphate anion was explained by its lower basicity compared to phosphinate anion (higher pK_a): phosphinate anion possessing two alkyl groups exerts an inductive donor effect, which leads to enrichment of electrons for the -OH bond and makes very

difficult the rupture of the -OH bond. Soares *et al.* [58] highlighted the double role of CYPHOS[®] IL104 as a curing agent for the epoxy prepolymer and an excellent dispersant aid for the multiwalled carbon nanotubes (MWCNTs), giving rise to materials which combine excellent electrical conductivity and high thermal properties. Maka *et al.* [50] reported that phosphonium ionic liquid trihexyltetradecylphosphonium bis(2,4,4-trimethylpentyl) phosphinate played a triple function: carbon nanofiller dispersing medium, catalytic curing agent, and anti-flammability additive. With increasing IL content (3→8 wt.%) in epoxy resin, the curing reaction started at lower temperature as determined by rheometry (145→125 °C) and DSC (133→118 °C). Only slight influence of carbon nanotubes or graphene (0.25-1.0 wt.%) on curing characteristics of epoxy systems was observed.

Nguyen *et al.* [59] reported a new way to synthesize epoxy networks using 9-23 wt.% of phosphonium-based ILs combined with phosphinate, carboxylate, and phosphate counter-anions. In all the cases, ILs displayed a high reactivity towards epoxy prepolymer and led to the formation of epoxy networks with high epoxy group conversion (up to 90 %). The authors have demonstrated that the reactivity of ILs is controlled by their basicity and is ranked in the following order: carboxylate > phosphinate > phosphate [59]. The findings of this study indicated that ILs were excellent alternatives to conventional amines as lower amounts of the former are required for crosslinking reaction: 9 wt.% for phosphinate and carboxylate, 23 wt.% for phosphate compared to 25 wt.% for Jeffamine D230 and 35 wt.% for MCDEA.

So far imidazolium-based ILs have been more often applied in epoxy resin systems as curing agents than phosphonium ones [50]. However, the reasons why one might be interested in phosphonium ILs, even in industrial processes, include their availability and cost.

1.4.2. Ionic liquids as ionic conducting agents

ILs are promising candidates for novel high-performance electrolytes for electrochemical devices such as lithium-ion batteries and electronic double layer capacitors. ILs have low viscosity and excellent ionic conductivity up to their decomposition temperature. Nevertheless, a drawback for practical application is that IL fluidity may cause liquid electrolyte leakage. Ohno and co-workers attempted to polymerize ILs composed of imidazolium substituted methacrylates [60-62]. However, polymerization of ionic compounds often reduces the molecular motion and provides low ionic conductivity. To solve this problem, polymers which

have three-dimensionally highly crosslinked structures and possess excellent physicochemical properties could be used. DGEBA/Jeffamine D400 system was modified with 2.5 and 5.0 wt.% of ILs based on imidazolium and phosphonium cations with long alkyl chains, such as *N,N'*-dioctadecyl-imidazolium iodide, or octadecyl-triphenylphosphonium iodide ([ODTPP][I]) [63]. These results clearly demonstrated the higher conductivity of DGEBA/D400/[ODTPP][I] system compared to the others although the conductivity values were not high enough for a solid electrolyte, probably because of the low amount of IL used.

Polymer networks confining an 1-ethyl-3-methylimidazolium bis(trifluoromethane sulfonyl) imide ([EMIm][TFSI]), were prepared [64] by curing a mixture of DGEBA and tetrafunctional epoxy resins with tetraethylenepentamine (TEPA) in the presence of ionic liquid. The ionic liquid confinement, ionic conductivity, mechanical strength, and morphology of the materials strongly depended on the ionic liquid content. At a low [EMIm][TFSI] content (< 40 wt.%), the material tightly confined the ionic liquid and showed little ionic conductivity with a high Young's modulus. This seems reasonable because there are no freely mobile ions in the samples, in which rigid and glassy polymer network locally confine ions. At a high IL content (> 40 wt.%), the material did not tightly confine the IL showing higher ionic conductivity. The microphase separation between the [EMIm][TFSI] and the epoxy networked polymer was observed by scanning electron microscopy (SEM). The ionic conductivity of the DGEBA/TetradX/TEPA/(50 wt.%) [EMIm][TFSI] was equal to $1.0\text{-}12.0 \times 10^{-2}$ S/m in the frequency range from 1 to 100 KHz, which is quite high and corresponds to about 1/8 of the reported bulk [EMIm][TFSI] conductivity (84.0×10^{-2} S/m). Subsequently, Matsumoto *et al.* [65] synthesized the highly flexible ion conductive films of an epoxy-based crosslinked polymer containing an ionic liquid having a quaternary ammonium salt structure. The polymers having trimethylammonium bis(trifluoromethanesulfonyl)imide groups were synthesized by heating a mixture of diepoxide, glycidyl trimethylammonium bis(trifluoromethanesulfonyl)imide (GTMATFSI), and diamine curing reagent. Ethylene glycol diglycidyl ether (EGGE), poly(ethylene glycol) diglycidyl ether (PEGGE), and poly(propylene glycol) diglycidyl ether (PPOGE) were used as diepoxides, and ethylene glycol bis(3-aminopropyl) ether (EGBA), poly(ethylene glycol) diglycidyl ether bis(3-aminopropyl ether) (PEGBA), and polypropylene glycol bis(2-aminopropyl ether) (PPOBA) were used as diamine curing reagents. The obtained networks having quaternary ammonium structure showed high thermal stability (temperature of 5 wt.% decomposition above 270 °C), low crystallinity, low glass transition temperature, and good ionic conductivity. In particular, the crosslinked polymers consisting of poly(ethylene

glycol) segments showed high ionic conductivity ($> 0.1 \times 10^{-2}$ S/m) at room temperature and reached 5.8×10^{-2} S/m for EGGE-GTMATFSI-1.2/PEGBA and 4.1×10^{-2} S/m for PEGGE/GTMATFSI-1.2/PEGBA at 90 °C, which is also quite high for a solid polymeric material. These networks were mechanically strong and tough enough to produce self-standing thin films and will be useful materials for application as ionic conductive membranes in electrochemical devices.

Livi *et al.* designed IL-containing polymer networks, which could be employed as new polymer electrolytes [66]. They used trihexyl(tetradecyl)phosphonium IL with dicyanamide counteranion as functional additives to synthesize nanostructured epoxy networks with very high mechanical properties and thermal stability (> 400 °C). In addition, TEM micrographs (**Figure 1-6**) showed the formation of ionic clusters of the size of 20-30 nm with excellent distribution (characterized by the white spots) for the epoxy network loaded with the highest concentration (23 wt.%) of this IL. These results are promising and open new perspectives in the field of energy where the IL can be used as ionic channels for lithium salts to ensure suitable conduction properties [66].

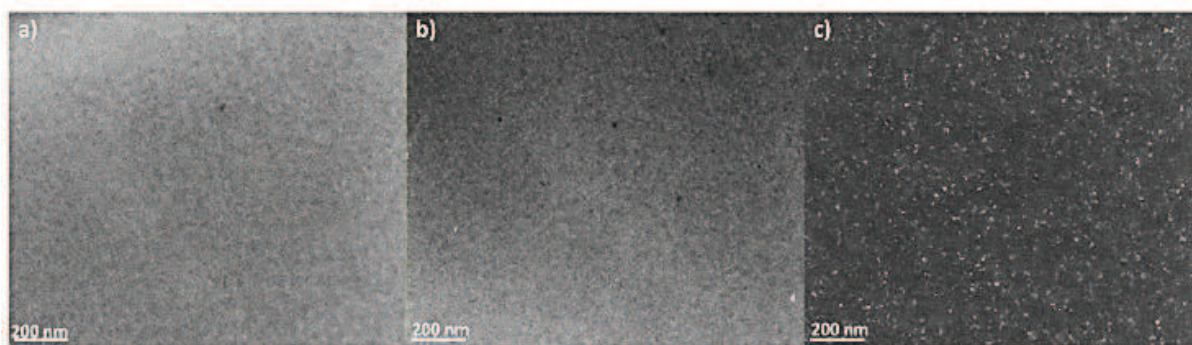


Figure 1-6: TEM micrographs of epoxy networks cured with phosphonium dicyanamide IL, wt.%: (a) 5, (b) 9, (c) 23 [66].

Shirshova *et al.* [67] prepared a series of epoxy resin-ionic liquid composites to identify the optimum system microstructure required to achieve a high level of multifunctionality. Structural electrolytes based on fully formulated commercially available epoxy resins (pure one with trademark MVR[®] 444 and toughened ones, MTM[®] 57 and VTM[®] 266) were obtained by adding the mixture of bis(trifluoromethane) sulfonimide lithium salt (LiTFSI) and ethyl-3-methylimidazolium bis(trifluoromethylsulfonyl)imide ([EMIM][TFSI]) ionic liquid. Detailed

temperature-dependent ionic conductivity measurements were carried out using dielectric spectroscopy in a temperature range of -30 °C to 60 °C. The ionic conductivity was extracted from the plateau region of each dielectric spectrum (**Figure 1-7**). At only 30 wt.% of structural resin (MVR[®]444) and 70 wt.% of IL-based mixture, containing 17 wt.% of the Li salt, stiff monolithic plaques with thicknesses of 2-3 mm possessing room temperature ionic conductivity of 8.0×10^{-2} S/m (0.5×10^{-2} S/m at -20 °C) and Young's modulus of 0.2 GPa were obtained. The authors concluded that the room temperature conductivity close to 8.0×10^{-2} S/m was not only a desirable value for supercapacitor applications, but was also high enough to potentially consider thin films of MVR[®] 444/30 as separation membranes for Li-ion batteries [67].

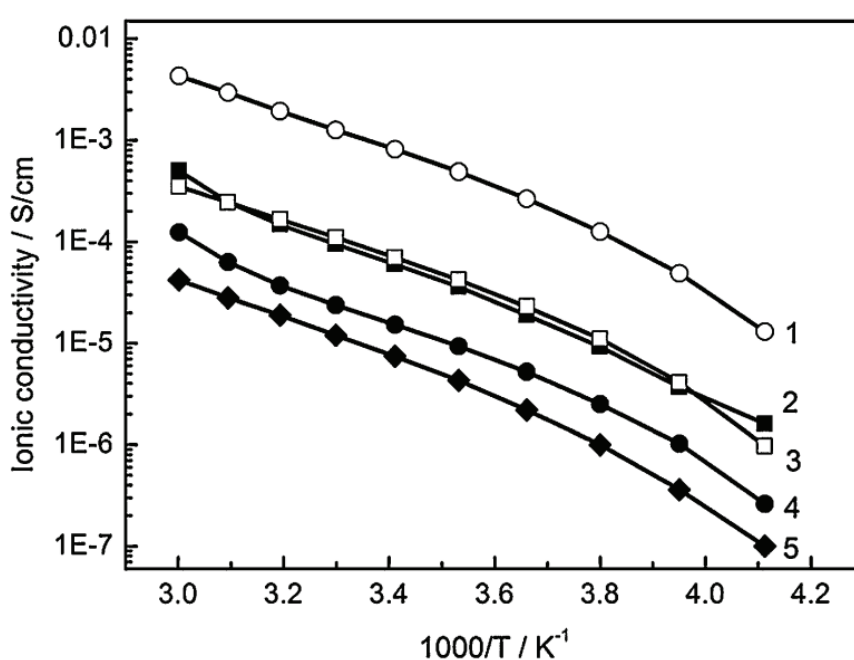


Figure 1-7: Temperature dependence of ionic conductivity of samples with varying resin contents (wt.%): 1) 30; 2) 50; 3) 40; 4) 50; 5) 50. Samples 1, 3, 5 –based on MVR[®] 444; 2 – VTM[®] 57; 4 – VTM[®] 266 [67].

Soares *et al.* [68] investigated the influence of different ILs based on tetraalkylphosphonium cations containing different counter-anions, such as dicyanamide, bis(trifluoro-methanesulfonyl)imide and dodecylbenzene sulfonate on the ionic conductivity of epoxy resin based on DGEBA cured with poly(propylene glycol) bis(2-aminopropyl ether). A significant increase in the ionic conductivity (0.01×10^{-2} S/m at 110 °C) was observed with the presence of 13 wt.% of CYPHOS 105, mainly at a temperature higher than T_g , when the ion

mobility increased. Other epoxy-IL systems reported in the literature possess higher conductivity values, but with the higher IL content (60-80 wt.%) [67]. The incorporation of a 1-decyl-3-methylimidazolium bromide ([DMIm][Br]) content as high as 50 wt.% within the epoxy matrix resulted in solid and flexible electrolyte with high thermal stability and ionic conductivity of around 0.1×10^{-2} S/m at room temperature, which increased up to 10×10^{-2} S/m at 170 °C [69]. It was concluded that this electrolyte presented a prodigious potential for applications at high temperature in electrochemical devices like batteries and supercapacitors, and the flexibility of this solid electrolyte persisted at low temperature because of its low glass transition temperature. Furthermore, leakage problems were not observed.

1.4.3. Ionic liquids as plasticizers

A plasticizer is a substance incorporated into a polymer to increase its flexibility, workability or distensibility. Normally, plasticizers have a large influence on physical, chemical, and electrochemical properties of modified polymers: for instance, they reduce melt viscosity, temperature of a second order glass transition (T_g) or elastic modulus of a polymer. The plasticizers used in the industry are mostly derivatives of phthalates, which represent approximately 70 percent of the market. However, due to their toxicity, academic and industrial researchers have been looking for new plasticizers. In fact, RTILs have the necessary qualities of a good plasticizer: *i*) excellent melting properties, *ii*) minimal interaction with resins at room temperature and *iii*) non-volatility at ambient conditions. As one can conclude, RTILs can be utilized as efficient plasticizers to manage mechanical properties of thermosetting polymers, at that the chemical nature of organic cations and anions plays a significant role in the distribution of ionic domains in the polymer matrix. According to the literature, imidazolium and pyridinium ILs lead to the formation of aggregates of ionic clusters, while phosphonium ILs generate a structuration at a nanoscale denoted as «spider-web» morphology [52]. Thus, it is possible to control the plasticization effect of thermosets by varying IL molar mass and chemical structure.

Lu *et al.* reported [3] a significant decrease in the T_g , of epoxy networks by using several types of ILs, and this effect was more pronounced in the systems modified with imidazolium-based ILs, than that in the systems containing phosphonium-based ILs. Duchet-Rumeau and Gérard's group successfully used *N,N'*-dioctadecylimidazolium iodide with long alkyl chains as a new additive for epoxy networks [42]. The T_g value as determined at the maximum of the

$\tan\delta$ peak decreased as the amount of the IL increased. This behaviour suggested a plasticizing effect of the IL imparted by the presence of the two long alkyl chains in its structure. The authors noted that the storage moduli at temperatures below T_g were higher in the thermosets containing IL probably because of the good interactions between the components (**Figure 1-8**) [42]. At temperatures above T_g , the modulus of the system containing 1 wt.% of IL was higher than that of the pure epoxy network, indicating high interactions between the blend components. However, when increasing the amount of IL, the moduli in this region decreased, suggesting that the plasticizing effect imparted by the long alkyl groups in the IL molecules contributed more for this property than the interactions between the components. The T_g tendency found in DSC experiments was similar to that detected by DMA analysis and also confirmed the plasticizing effect of the IL.

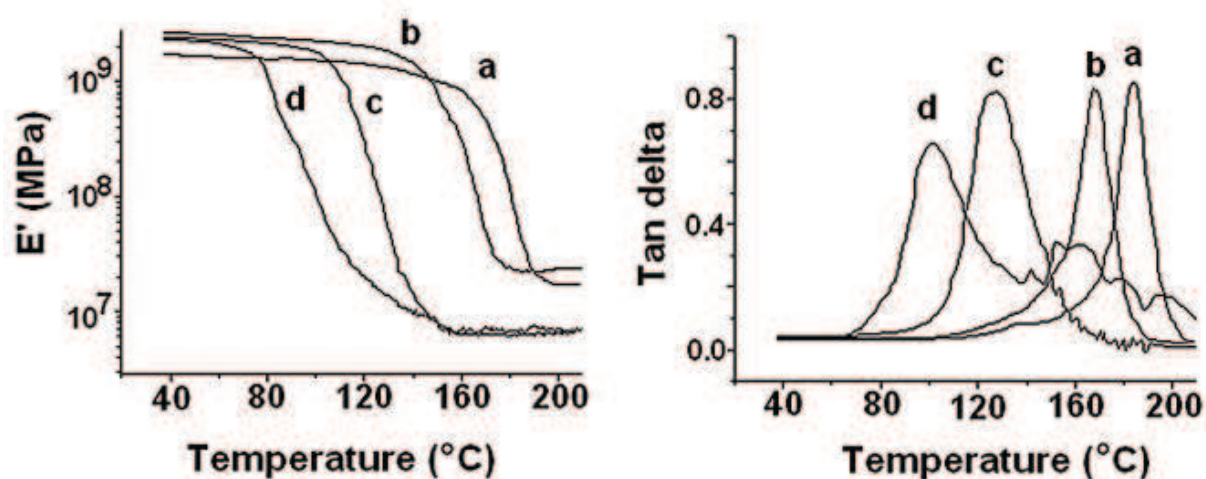


Figure 1-8: Dynamical mechanical properties of DGEBA/IL/MCDEA networks as a function of the IL content, wt.%: (a) 0, (b) 1.0, (c) 1.6, (d) 3.0 [42].

Sanes *et al.* [70-76] also reported that addition of IL to epoxy resins enhanced chain mobility and provided a plasticizing effect as well as reduced friction coefficient and wear rate of the final materials.

1.4.4. Ionic liquids as lubricants

It is known that the poor tribological performance of epoxy resins is a major limitation in many applications. The main strategy which has been followed in order to improve their

resistance consists in using internal lubricants. The first IL used as an inner lubricant of epoxy resin was the short alkyl chain 1-ethyl-3-methylimidazolium tetrafluoroborate ([EMIm][BF₄]) added in a concentration range between 0.5 and 3.3 wt.% [70]. It was found that dry friction coefficients decreased exponentially from 0.73 to 0.29 as the IL proportion increased and wear resistance was improved in several orders of magnitude for a critical IL concentration of 2.7 wt.%.

Hameed *et al.* [77] described the controlled mechanical behaviour of epoxy resin from brittle to ductile and even to elastomeric behaviour, when high amounts (10-60 wt.%) of the 1-butyl-3-methylimidazolium chloride IL were added. The authors proposed the formation of electron donor-electron acceptor complexes between the hydroxyl groups of the epoxy chains and bulky IL ions, resulting in high modulus and toughness. At the elevated temperatures, these complex bonds break and the presence of detached bulky ions leads to flexible networks and reduced glass transition region.

Saurín *et al.* [71-72] claimed a good tribological performance and even self-healing effect of abrasion surface damage on an epoxy resin material with the addition of a relatively high (7-12 wt.%) amount of the 1-octyl-3-methylimidazolium tetrafluoroborate ([OMIm][BF₄]). It was the first paper describing a self-healing process induced by an IL additive [71]. From the results, it was concluded that the addition of IL (*i*) reduced hardness and tensile strength, (*ii*) increased elongation at break by a 42 %, (*iii*) showed an area reduction of approximately 55 % after 5 h, (*iv*) induced a self-healing process with a 41 % recovery after 30 min and a total self-repair of the abrasion damage under multiple scratching after 22 h at room temperature, and (*v*) reduced the surface damage by 88 % with respect to individual network, after 24 h at room temperature (single scratches under the maximum load of 20 N). Further investigation [72] emphasized that material with 7 wt.% IL content demonstrated a lower friction coefficient than the neat epoxy, due to its lower instantaneous surface damage. In contrast, the self-healing ability over time increased with increasing IL concentration with maximum obtained for the 9 wt.% IL proportion (96.2 % reduction after 22 h at room temperature). The surface topography and cross-section profiles with time after the scratch tests on epoxy resin containing 12 wt.% of [OMIm][BF₄] are shown in **Figure 1-9** [72]. Authors concluded that interactions between the cation-anion pairs of the [OMIm][BF₄] and the polar groups of the polymer chains reduced the brittle behaviour of the resin and the permanent damage produced by crack propagation under load and could be responsible for the observed self-healing behaviour.

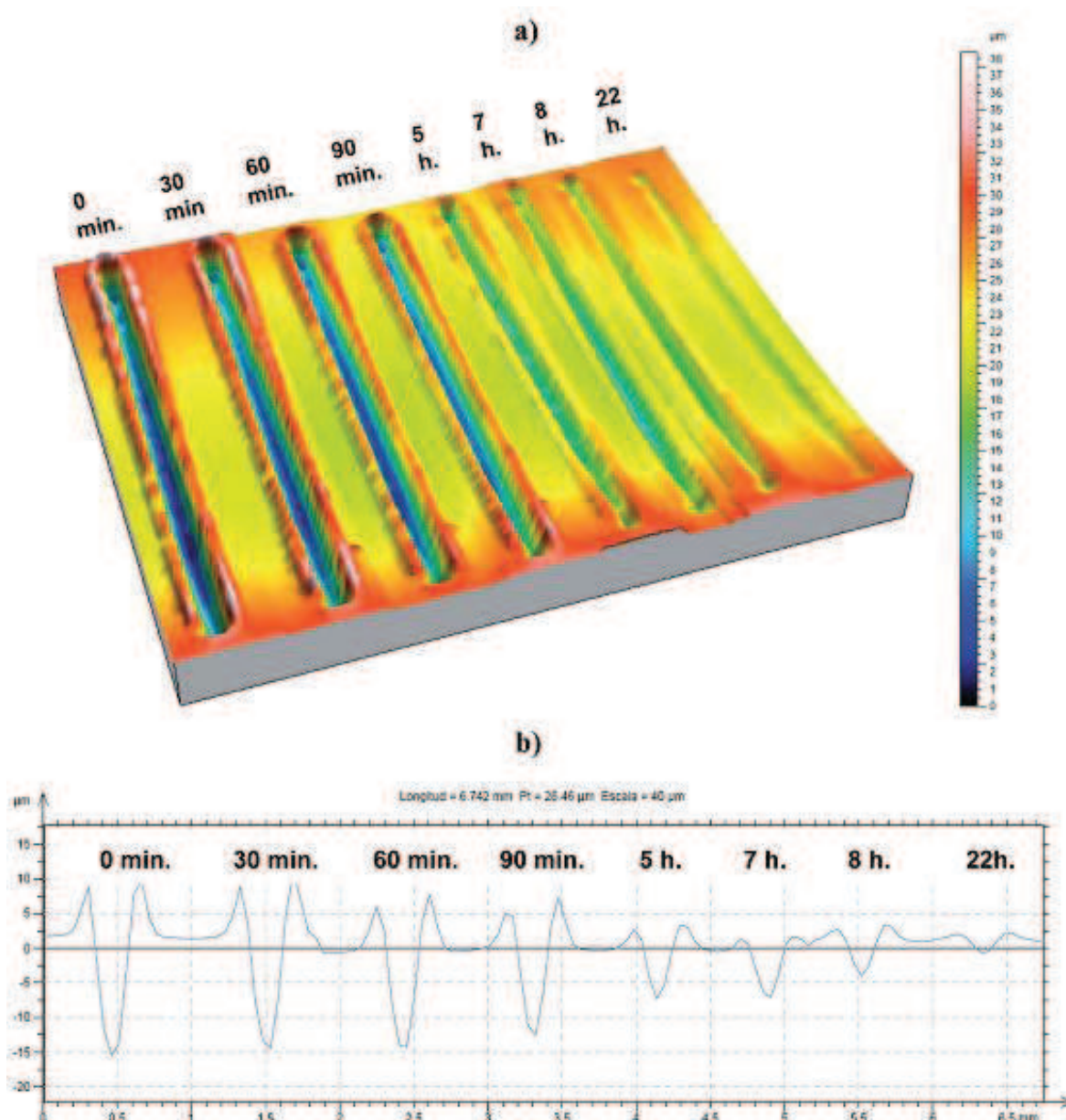


Figure 1-9: Surface topography (a) and cross section profiles (b) for the evolution of the wear track on a surface of epoxy resin/[OMIm][BF₄] (12 wt.%).

It was found that [OMIm][BF₄] showed an outstanding friction-reducing and anti-wear performance for the epoxy resin-stainless steel contact, which was further improved by addition of ZnO nanoparticles [73], graphene [74] or single walled carbon nanotubes (SWCNTs) [75]. The reinforcement effect of graphene responsible for the good tribological performance, while IL acts as a plasticizing agent, increasing chain mobility, reducing T_g and shifting the storage modulus onset, the loss modulus and $\tan \delta$ peaks to lower temperatures [74]. SWCNTs and the IL show a synergistic effect when are added to an epoxy resin matrix, being able to reduce both

friction coefficient, in a 53 %, and wear rate, in a 86 %, with respect to neat epoxy resin under pin-on-disc sliding contact against stainless steel [75]. Very similar effects can be achieved with SWCNTs pre-modified by ILs.

Recently, Avilés [76] *et al.* synthesized and characterized a new self-lubricating, wear resistant epoxy polymer by addition of 9 wt.% of the room-temperature protic ionic liquid – tri-[bis(2-hydroxyethyl)ammonium)] citrate (DCi). It was shown more than 50 % reduction of the friction coefficient with respect to neat epoxy resin, and a polished surface, in contrast with the severe wear that takes place in the case of neat epoxy resin. The high polarity of the protic ionic liquid molecules produced low miscibility of the liquid phase within the epoxy matrix and reduces the wettability of the resin surface.

1.4.5. Ionic liquids as porogens

The novel peculiarity of ILs as «designer solvents» is the possibility to design porous thermosets with the necessary properties for the specific applications. The basic requirements to porogens are as follows: (i) boiling point higher than the temperature of polymer synthesis; (ii) inertness towards basic components of polymer synthesis; (iii) predetermined ratio of polarity and solubility parameters of monomer, polymer, and porogen. The solubility parameter (δ , (J/cm³)^{1/2}) of the polymer is defined as the square root of the cohesive energy density in the amorphous state at room temperature [78], which provides a numerical estimation of the degree of interaction between materials:

$$\delta = \left(\frac{E_{coh}}{V} \right)^{1/2}$$

The solubility parameter is crucial for a porogen selection, and it is used to compare the solvation, miscibility, and swelling properties of the components used. The consideration of nature and possible interactions of porogen-polymer, porogen-monomer (s), and porogen-initiator is also an important issue during synthesis of porous materials. Mohamed *et al.* [79] reported that the closer the solubility parameters of a porogen, reactants (monomer/crosslinker/polymer), the greater the surface area and the smaller the pore volume, while the smaller surface area and the higher pore volume in porous polymers could be reached at higher difference in solubility parameters of the components used. The uni-modal (micro, meso, or macroporous) polymer can be obtained by varying the type and amount of a porogen.

In addition to this, bi-modal (micro-meso, meso-macro, or micro-macro) porosity can be generated using a porogen mixture or varying the porogen ratio. A low molar mass porogen is generally preferred to obtain the smaller pore size, which results into a greater surface area and vice-versa for a high molar mass porogen [80]. However, increasing the molar mass of a porogen increases the viscosity of the polymerization reaction composition, and it is recommended to use high molar mass porogens in combination with a porogen of low molar mass [81]. Therefore, the use of RTILs as porogens for the preparation of porous polymers [82-86] has some distinct advantages: (i) ILs are thermally stable and nonvolatile and can be easily recycled; (ii) the morphology and porous structure can be easily changed through a proper selection of the structural features of the IL used; (iii) pore diameter can be managed by varying the amount of IL used; (iv) due to extremely low viscosity, ILs can be used as porogens without using any additional solvent.

Nowadays, several researchers have studied the extraction of ILs from epoxy polymer networks, however no-one has reported on the characterization of porous thermosets obtained thereof. Matsumoto and Endo [64] extracted the IL from polymer/IL composites in order to examine the morphologies of the cross-linked materials. **Figure 1-10** shows the results of acetone extraction of various ILs from DGEBA/TEPA/IL epoxy network systems. The IL confinement was in the order [EMIm][TFSI] > [HMIm][TFSI] > [BMIm][TFSI], which was the opposite order of the steric hindrance of the cations. The reason for this remained unknown, but the authors assumed that the hexyl or benzyl groups in the cationic part may increase the compatibility of the IL with the epoxy network that provides the enhanced segmental motion of the network, so the IL can easily escape from the network. Materials confining IL were insulating with a high Young's modulus, while those not confining IL were ion conducting with a low Young's modulus. SEM observation revealed that the drastic change of the fundamental properties of the epoxy materials could be due to the morphology transition of the materials, in which the IL transformed discrete phases to continuous phases in the epoxy-based networks. These results suggest that the addition of IL can be a new and facile method to control the morphology of polymer networks.

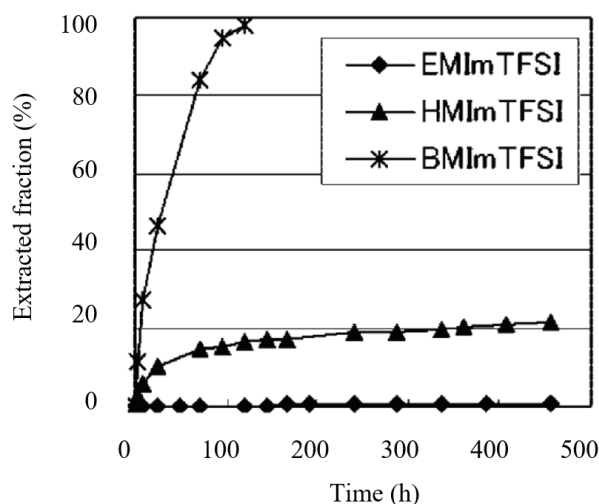


Figure 1-10: Time dependence of the extracted ionic liquid fraction from films of DGEBA/Tetrad-X/TEPA with [EMIm][TFSI], [HMIm][TFSI] and [BMIm][TFSI] (extraction solvent: acetone) [64].

Shirshova *et al.* [67] reported that there were no dimensional changes observed as a result of electrolyte ([EMIM][TFSI] + LiTFSI) extraction removing more than > 95 wt.% of the original IL-based electrolyte content from an epoxy network (MVR[®] 444). The SEM images of all the samples showed a bicontinuous morphology (**Figure 1-11**). It seemed likely that MVR[®]444 formed a fully miscible one-phase system at the cure temperature, but that phase separation occurred at an earlier stage during the polymerization as a result of its lower miscibility with the ionic liquid. The authors concluded that this system based on commercial components could be readily applied to the development of structural electrical energy storage composite devices.

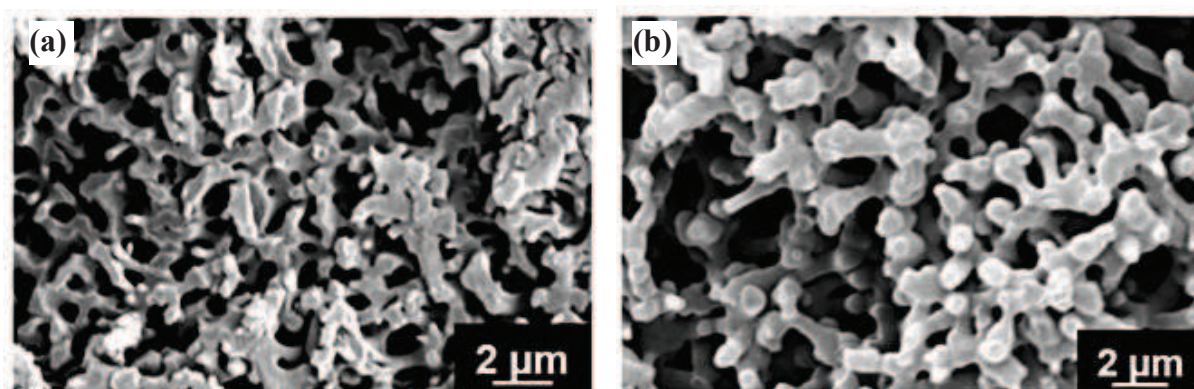


Figure 1-11: SEM micrographs of epoxy samples after extraction of different amounts of electrolyte (EMIm-TFSI + LiTFSI): (a) 60 wt.%; (b) 70 wt.% [67]

In conclusion, ILs constitute excellent multifunctional agents that are sustainable for developing new high-performance epoxy materials (**Table 1-3**).

Table 1-3: General overview of IL influence on epoxy resins

Base polymer	Ionic liquid	Results	Ref.
DGEBA	[DiOIm][I]	crosslinking promotion, plasticizing effect	[42]
	[apbIm][NTf ₂] [N4444][Leu]	catalytic effect, conductivity improvement	[40]
	[DodIm][I] [OdPyr][I] [OdTPP][I] [OdTPP][PF ₆]	accelerating effect, plasticizing effect, stiffness improvement	[43]
	CYPHOS [®] IL104	catalytic effect, thermal stability improvement	[44]
	[BMIm][N(CN) ₂] [BMIm][BF ₄] [DMIm][N(CN) ₂] [DMIm][BF ₄] [DMIm][Cl]	catalytic effect	[46]
	[EMIm][N(CN) ₂]	thermally latent curing agent	[47]
	CYPHOS [®] IL104 CYPHOS [®] IL169	homopolymerization promotion, hydrophobicity and thermal stability improvement	[57]
	CYPHOS [®] IL104	curing agent for the epoxy prepolymer, excellent dispersant aid for the MWCNT	[58]
	[OdTPP][I] [DodIm][I]	accelerating effect, phase separation, tensile properties and conductivity improvement	[63]
	CYPHOS [®] IL105	catalytic effect, phase separation generation	[66]
	[DMIm][Br]	solid and flexible electrolyte with good thermal stability below 180°C	[69]
	[OMIm][BF ₄]	accelerating effect, lower hardness, viscoelastic recovery and healing ability of damaged surface with time	[70] [72] [74]
	DGEBA, TEPA	[EMIm][TFSI] [HMIm][TFSI] [BMIm][TFSI]	microphase separation, morphology and properties dependence on IL content
Bisphenol A epichlorhydrin	[OMIm][BF ₄]	self-healing under ambient conditions	[71]
EGGE PPOGE PEGGE PPOBA PEGBA	[GTMA][TFSI]	high thermal stability, flexibility and good ionic conductivity	[65]
Bisphenol A- based Epidian 6 (E6)	[BMIm][SCN]	catalytic activity	[48]
	[EMIm][N(CN) ₂] [THTDP][N(CN) ₂]	catalytic effect	[49]
MVR [®] 444 MTM [®] 57 VTM [®] 266	[EMIm][TFSI]	ionic conductivity improvement	[67]

1.5. Ionic liquids in Cyanate Ester Resins (CERs)

To the best of our knowledge, only a few reports on the IL utilization for designing CER systems have been published so far [87-89]. Throckmorton and Palmese in 2016 firstly reported [87] a new way to accelerate CER polycyclotrimerization by using dicyanamide-containing RTILs ($[\text{DCNA}]^-$) as a new catalytic system alternative to conventional catalysts normally based on metal acetylacetonates and nonyl phenol. Novel ionic thermosetting polymers, *i.e.* polycyanurates containing the ILs incorporated chemically directly into the triazine network, were thus synthesized. The catalytic effect was found in a number of dicyanamide-containing ILs with diverse cations, namely 1-ethyl-3-methyl imidazolium, 1-(3-cyanopropyl)-3-methyl imidazolium, 1-(2-hydroxyethyl)-3-methylimidazolium, 1-butyl-1-methyl-pyrrolidinium, and 1-butyl-3-methyl pyridinium. For comparison, the non-dicyanamide RTIL, 1-ethyl-3-methyl imidazolium tetrafluoroborate ($[\text{BMIm}][\text{BF}_4]$) was checked as a catalyst for CER polycyclotrimerization. It was found that the reaction kick off temperature in CER/ $[\text{BMIm}][\text{BF}_4]$ system was significantly higher than that for the $[\text{DCNA}]^-$ containing ILs. The following conclusions could be done on the basis of these results: (i) RTILs of varying structures and concentrations accelerated curing of CERs; (ii) $[\text{DCNA}]^-$ ILs were incorporated directly into the triazine network; (iii) plasticization effect was fixed depending on RTIL content (0.5-10 wt.%) due to decrease in cross-linking density (nearly 100 °C decrease in T_g at 10 wt.% IL loading). Finally, the ionic thermoset structure presented a cured resin with ionically bound species that provided an excellent subject for future research in ionomers and nanocomposites.

Although the reaction mechanism of CER curing in the presence of $[\text{DCNA}]^-$ -based ILs was investigated thoroughly, the mechanism of catalysis by non-dicyanamide RTILs was not discussed. Based on the studies mentioned above, one can conclude that in order to develop novel CER-based materials with new properties, research on the application of other ILs should be continued.

1.6. Conclusions

According to the best of our knowledge, up to now, no systematic study on the application of ionic liquids in thermosetting polymers, especially epoxy and cyanate ester resins have been reported. The present review aims at defining a new generation of thermally stable materials based on thermosets modified by ionic liquids (ILs). Among the wide range of potential

applications of ILs, their use in the development of new thermoset-IL hybrid materials has been limited by modification of epoxy and cyanate ester resins. In fact, the studies on epoxy resin systems with ILs are quite extensive. In the reviewed studies, we have found that ILs can be effectively used for epoxy resins as catalytic or/and crosslinking agents, plasticizers, lubricants, electrolytes or porogens thus providing a new route to the design of advanced materials. So far, imidazolium ILs have been more often applied in epoxy resin systems than other ones, however the reasons why one might be interested in a phosphonium ILs, even in industrial processes, include its availability and cost. It seems that epoxy resin systems could be improved by the selection of IL type and concentration as well as by the introduction of additives, *e.g.* nanoparticles, graphene or carbon nanotubes, in low loading to obtain high-performance materials. On the other side, the investigation of cyanate ester resins (CERs) is fairly limited in the literature and only few researchers have developed the use of ILs as catalysts and porogens. Despite these successes, using ILs still remains an exciting and emerging field of research. The influence of IL on the ductility, abrasion resistance, and self-repairing ability of epoxy resins has been well understood, however, self-healing ability of IL-based CER materials remains to be studied. It appears reasonable to expect (i) comprehension of IL organization within the polymer network; (ii) network-IL interactions; (iii) suitable functionalization of the ILs for reactive modification of thermosets; (iv) molecular mechanisms of IL lubrication; (v) separation/sorption properties of IL-based thermosetting networks before and after extraction for membrane technologies; (vi) compatibilizing effect of ILs in the hydrophobic polymer networks filled with hydrophilic fillers. Through numerous attempts made so far, the prospect of ILs as electrolyte salts for engineering of highly conducting polymer electrolytes and characterizing their ion transport behaviour left out of consideration and further studies are still needed. The IL-based thermosetting materials could be good candidates for use in any application, in which high conductivity combined with high thermal stability and non-volatility are required.

1.7. References

1. Huddleston J. G., Visser A. E., Reichert W. M., Willauer H. D., Broker G. A., Rogers R. D.: Characterization and comparison of hydrophilic and hydrophobic room temperature ionic liquids incorporating the imidazolium cation. *Green Chemistry*, **3**, 156-164 (2001).
2. Li Y., Zhang C., Zhou Y., Chen Y. D. W.: Novel multi-responsive polymer materials: When ionic liquids step in. *European Polymer Journal*, **69**, 441-448 (2015).
3. Lu J., Yan F., Texter J.: Advanced applications of ionic liquids in polymer science. *Progress in Polymer Science*, **34**, 431-448 (2009).
4. Welton T.: Ionic liquids in catalysis. *Coordination Chemistry Reviews*, **248**, 2459-2477 (2004).
5. Winterton N.: Solubilization of polymers by ionic liquid. *Journal of Materials Chemistry*, **16**, 4281-4293 (2006).
6. Snedden P., Cooper A. I., Scott K., Winterton, N.: Cross-linked polymer-ionic liquid composite materials. *Macromolecules*, **36**, 4549-4556 (2003).
7. Klingshirn M. A., Spear S. K., Subramanian R., Holbrey J. D., Huddleston J. G., Rogers R. D. J.: Gelation of ionic liquids using a cross-linked poly(ethylene glycol) gel matrix. *Chemistry of Materials*, **16**, 3091-3097 (2004).
8. Susan M. A. B. H., Kaneko T., Noda A., Watanabe M. J.: Ion gels prepared by *in situ* radical polymerization of vinyl monomers in an ionic liquid and their characterization as polymer electrolytes. *Journal of the American Chemistry Society*, **127**, 4976-4983 (2005).
9. Nakajima H., Ohno H.: Preparation of thermally stable polymer electrolytes from imidazolium-type ionic liquid derivatives. *Polymer*, **46**, 11499-11504 (2005).
10. Neouze M. A., Bideau J. L., Gaveau P., Bellayer S., Vioux A.: Ionogels, new materials arising from the confinement of ionic liquids within silica-derived networks. *Chemistry of Materials*, **18**, 3931-3936 (2006).
11. Tigelaar D. M., Meador M. A. B., Bennett W. R.: Composite electrolytes for lithium batteries: Ionic liquids in APTES cross-linked polymers. *Macromolecules*, **40**, 4159-4164 (2007).
12. Xie Y., Zhang Z., Jian T., He J., Han B., Wu T., Ding K.: CO₂ cycloaddition reactions catalyzed by an ionic liquid grafted onto a highly cross-linked polymer matrix. *Angewandte Chemie International Edition*, **46**, 7255-7258 (2007).
13. Walden P.: Molecular weights and electrical conductivity of several fused salts. *Bulletin of the Imperial Academy of Sciences (Saint Petersburg)*, **1800**, 405-422 (1914).
14. Chum H. L., Koch V. R., Miller L. L., Osteryoung R. A.: Electrochemical scrutiny of organometallic iron complexes and hexamethylbenzene in a room temperature molten salt. *Journal of the American Chemistry Society*, **97**, 3264-3267 (1975).
15. Wilkes J. S., Levisky J. A., Wilson R. A., Hussey C. L.: Dialkylimidazolium chloroaluminate melts: a new class of room-temperature ionic liquids for electrochemistry, spectroscopy, and synthesis. *Inorganic Chemistry*, **21**, 1263-1264 (1982).
16. Wilkes J. S., Zaworotko M. J.: Air and water stable 1-ethyl-3-methylimidazolium based ionic liquids. *Journal of the Chemical Society, Chemical Communications*, 965-967 (1992).
17. Welton T.: Room-temperature ionic liquids. Solvents for synthesis and catalysis. *Chemical Reviews*, **99**, 2071-2083 (1999).
18. Hallett J. P., Welton T.: Room-temperature ionic liquids: solvents for synthesis and catalysis. 2. *Chemical Reviews*, **111**, 3508-3576 (2011).
19. Marsh K. N., Boxall J. A., Lichtenthaler R.: Room temperature ionic liquids and their mixtures – a review. *Fluid Phase Equilibria*, **219**, 93-98 (2004).

20. Plechkova N. V., Seddon K. R.: Applications of ionic liquids in the chemical industry. *Chemical Society Reviews*, **37**, 123-150 (2008).
21. Rogers R. D., Seddon K. R.: Ionic liquids – Solvents of the future? *Science*, **302**, 792-793 (2003).
22. Armand M., Endres F., MacFarlane D. R., Ohno H., Scrosati B.: Ionic-liquid materials for the electrochemical challenges of the future. *Nature materials*, **8**, 621-629 (2009).
23. Livi S., Duchet-Rumeau J., Gérard J. F., Pham T. N.: Polymers and ionic liquids: a successful wedding. *Macromolecular Chemistry and Physics*, **216**, 359-368 (2015).
24. Mecerreyes D.: Applications of ionic liquids in polymer science and technology. Berlin: Springer-Verlag (2015).
25. Gaune-Escard M., Seddon K. R.: Molten salts and ionic liquids: never the twain? Hoboken: WILEY (2010).
26. Wilkes J.S.: A short history of ionic liquids - From molten salts to neoteric solvents. *Green Chemistry*, **4**, 73-80 (2002).
27. Dupont J.: From molten salts to ionic liquids: a «nano» journey. *Accounts of Chemical Research*, **44**, 1223-1231 (2011).
28. Gore R. G., Rohitkumar N. G.: Safer and greener catalysts – design of high performance, biodegradable and low toxicity ionic liquids. Chapter 19. In book: *Ionic liquids – new aspects for the future*. Ed. Kadokawa J. InTech, 2013.
29. Sowmiah S., Srinivasadesikan V., Tseng M. C., Chu Y. H.: On the chemical stabilities of ionic liquids. *Molecules*, **14**, 3780-3813 (2009).
30. Pringle J. M., Golding J., Forsyth C. M., Deacon G. B., Forsyth M., MacFarlane D. R. J.: Physical trends and structural features in organic salts of the thiocyanate anion. *Journal of Materials Chemistry*, **12**, 3475-3480 (2002).
31. Kulkarni P. S., Branco L. C., Crespo J. G., Nunes M. C., Raymondo A., Alfonso C. A. M.: Comparison of physicochemical properties of new ionic liquids based on imidazolium, quaternary ammonium, and guanidinium cations. *Chemistry a European Journal*, **13**, 8478-8488 (2007).
32. Maton C., De Vos N., Stevens C. V.: Ionic liquid thermal stabilities: decomposition mechanisms and analysis tools. *Chemical Society Reviews*, **42**, 5963-5977 (2013).
33. Seddon K. R., Stark A., Torres M. J.: Influence of chloride, water, and organic solvents on the physical properties of ionic liquids. *Pure and Applied Chemistry*, **72**, 2275-2287 (2000).
34. Angell C. A., Byrne N., Belieres A. P.: Parallel developments in aprotic and protic ionic liquids: physical chemistry and applications. *Accounts of Chemical Research*, **40**, 1228-1236 (2007).
35. Tsuzuki S., Shinoda W., Miran M. S., Kinoshita H., Yasuda T., Watanabe M.: Interactions in ion pairs of protic ionic liquids: Comparison with aprotic ionic liquids. *Journal of Chemical Physics*, **139**, 174504/1-174504/9 (2013).
36. Greaves T. L., Drummond C. J.: Protic ionic liquids: properties and applications. *Chemical Reviews*, **108**, 206-237 (2008).
37. Belieres J. P., Angell A. C.: Protic ionic liquids: preparation, characterization, and proton free energy level representation. *The Journal of Physical Chemistry B*, **111**, 4926-4937 (2007).
38. Luo H., Huang J. F., Dai S.: Studies on thermal properties of selected aprotic and protic ionic liquids. *Separation Science and Technology*, **43**, 2473-248 (2008).
39. Hong K., Zhang H., Mays J. W., Visser A. E., Brazel C. S., Holbrey J. D., Reichert W. M., Rogers R. D.: Conventional free radical polymerization in room temperature ionic liquids: a green approach to commodity polymers with practical advantages. *Chemical Communications*, **13**, 1368-1369 (2002).
40. Maksym P., Tarnacka M., Dzienia A., Matuszek K., Chrobok A., Kaminski K., Paluch M.: Enhanced polymerization rate and conductivity of ionic liquid-based epoxy resin *Macromolecules*, **50**, 3262-3272 (2017).

41. Kowalczyk K., Spychaj T.: Ionic liquids as convenient latent hardeners of epoxy resins. *Polimery (Warsaw)*, **48**, 833-835 (2003).
42. Soares B. G., Livi S., Duchet-Rumeau J., Gérard J. F.: Synthesis and characterization of epoxy/MCDEA networks modified with imidazolium-based ionic liquids. *Macromolecular Materials and Engineering*, **296**, 826-834 (2011).
43. Soares B. G., Livi S., Duchet-Rumeau J., Gérard J. F.: Preparation of epoxy/MCDEA networks modified with ionic liquids. *Polymer*, **53**, 60-66 (2012).
44. Silva A. A., Livi S., Netto D. B., Soares B. G., Duchet J., Gérard J. F.: New epoxy systems based on ionic liquid. *Polymer*, **54**, 2123-2129 (2013).
45. Pat. WO 2011142855 A2, PCT/US2011/023739. Room temperature ionic liquids and ionic liquid epoxy adducts as initiators for epoxy systems. Palmese G.R., Rahmathullah M.A.M., Jeyarajasingam A. Publ. 17.11.11.
46. Maka H., Spychaj T., Pilawka R.: Epoxy resin/ionic liquid systems: the influence of imidazolium cation size and anion type on reactivity and thermomechanical properties. *Industrial & Engineering Chemistry Research*, **51**, 5197-5206 (2012).
47. Rahmathullah A. M., Jeyarajasingam A., Merritt B., VanLandingham M., McKnight S. H., Palmese G. R.: Room temperature ionic liquids as thermally latent initiators for polymerization of epoxy resins. *Macromolecules*, **42**, 3219-3221 (2009).
48. Maka H., Spychaj T., Kowalczyk K.: Imidazolium and deep eutectic ionic liquids as epoxy resin crosslinkers and graphite nanoplatelets dispersants. *Journal of Applied Polymer Science*, **131**, 40401/1-40401/7 (2014).
49. Maka H., Spychaj T., Zenker M.: High performance epoxy composites cured with ionic liquids. *Journal of Industrial and Engineering Chemistry*, **31**, 192-198 (2015).
50. Maka H., Spychaj T., Pilawka R.: Epoxy resin/phosphonium ionic liquid/carbon nanofiller systems: chemorheology and properties. *eXPRESS Polymer Letters*, **8**, 723-732 (2014).
51. Liebner F., Patel I., Ebner G., Becker E., Horix M., Potthast A., Rosenau T.: Thermal aging of 1-alkyl-3-methylimidazolium ionic liquids and its effect on dissolved cellulose. *Holzforschung*, **64**, 161-166 (2010).
52. Farkas A., Strohm P. F.: Imidazole catalysis in the curing of epoxy resins. *Journal of Applied Polymer Science*, **12**, 159-168 (1968).
53. Ghaemy M., Sadjady S.: Kinetic analysis of curing behavior of diglycidyl ether of bisphenol A with imidazoles using differential scanning calorimetry techniques. *Journal of Applied Polymer Science*, **100**, 2634-2641 (2006).
54. Meng F., Zhang W., Zheng S.: Epoxy resin cured with poly(4-vinyl pyridine). *Journal of Materials Science*, **40**, 6367-6373 (2005).
55. Ricciardi F., Joullie M. M.: Mechanism of imidazole catalysis in the curing of epoxy resins. *Journal of Polymer Science: Polymer Letters Edition*, **20**, 127-133 (1982).
56. Xue G., Ishida H., Konig J. L.: Polymerization of styrene oxide with pyridine. *Macromolecular Rapid Communications*, **7**, 37-41 (1986).
57. Nguyen T. K. L., Livi S., Pruvost S., Soares B. G., Duchet-Rumeau J.: Ionic liquids as reactive additives for the preparation and modification of epoxy networks. *Journal of Polymer Science, Part A: Polymer Chemistry*, **52**, 3463-3471 (2014).
58. Soares B. G., Riany N., Silva A. A., Barra G. M. O., Livi S.: Dual-role of phosphonium-based ionic liquid in epoxy/MWCNT systems: electric, rheological behavior and electromagnetic interference shielding effectiveness. *European Polymer Journal*, **84**, 77-88 (2016).
59. Nguyen T. K. L., Livi S., Soares B. G., Pruvost S., Duchet-Rumeau J., Gérard J.-F.: Ionic liquids: a new route for the design of epoxy networks. *ACS Sustainable Chemistry & Engineering*, **4**, 481-490 (2016).

60. Ogihara W., Washiro S., Nakajima H., Ohno H.: Effect of cation structure on the electrochemical and thermal properties of ion conductive polymers obtained from polymerizable ionic liquids. *Electrochimical Acta*, **51**, 2614-2649 (2006).
61. Nakajima H., Ohno H.: Preparation of thermally stable polymer electrolytes from imidazolium-type ionic liquid derivatives. *Polymer*, **46**, 11499-11504 (2005).
62. Washiro S., Yoshizawa M., Nakajima H., Ohno H.: Highly ion conductive flexible films composed of network polymers based on polymerizable ionic liquids. *Polymer*, **45**, 1577-1582 (2004).
63. Soares B. G., Silva A. A., Livi S., Duchet-Rumeau J., Gerard J.-F.: New epoxy/Jeffamine networks modified with ionic liquids. *Journal of Applied Polymer Science*, **131**, 39834/1-39834/6 (2014).
64. Matsumoto K., Endo T.: Confinement of ionic liquid by networked polymers based on multifunctional epoxy resins. *Macromolecules*, **41**, 6981-6986 (2008).
65. Matsumoto K., Endo T.: Synthesis of ion conductive networked polymers based on an ionic liquid epoxide having a quaternary ammonium salt structure. *Macromolecules*, **42**, 4580-4584 (2009).
66. Livi S., Silva A. A., Thimont Y., Nguyen T. K. L., Soares B. G., Gérard J. F., Duchet-Rumeau J.: Nanostructured thermosets from ionic liquid building block/epoxy prepolymer mixtures. *RSC Advances*, **4**, 28099-28106 (2014).
67. Shirshova N., Bismarck A., Carreyette S., Fontana Q. P. V., Greenhalgh E. S., Jacobsson P., Johansson P., Marczewski M. J., Kalinka G., Kucernak A. R. J., Scheers J., Shaffer M. S. P., Steinkef J. H. G., Wienriche M.: Structural supercapacitor electrolytes based on bicontinuous ionic liquid-epoxy resin systems. *Journal of Materials Chemistry A*, **1**, 15300-15309 (2013).
68. Soares B. G., Silva A. A., Pereira J., Livi S.: Preparation of epoxy/Jeffamine networks modified with phosphonium based ionic liquids. *Macromolecular Materials and Engineering*, **300**, 312-319 (2015).
69. Silva L. C. O., Soares B. G.: New all solid-state polymer electrolyte based on epoxy resin and ionic liquid for high temperature applications. *Journal of Applied Polymer Science*, **135**, 45838/1-45838/8 (2017).
70. Sanes J., Carrión-Vilches F. J., Bermúdez M. D.: New epoxy-ionic liquid dispersions. Room temperature ionic liquid as lubricant of epoxy resin-stainless steel contacts. *e-Polymers*, 005/1-005/12 (2007).
71. Saurín N., Sanes J., Bermúdez M. D.: Self-healing of abrasion damage in epoxy resin-ionic liquid nanocomposites. *Tribology Letters*, **58**, 4/1-4/9 (2015).
72. Saurín N., Sanes J., Carrion F. J., Bermúdez M. D.: Self-healing of abrasion damage on epoxy resin controlled by ionic liquid. *RSC Advances*, **6**, 37258-37264 (2016).
73. Sanes J., Carrión F. J., Bermúdez M. D.: Effect of the addition of room temperature ionic liquid and ZnO nanoparticles on the wear and scratch resistance of epoxy resin. *Wear*, **268**, 1295-1302 (2010).
74. Saurín N., Sanes J., Bermúdez M. D.: Effect of graphene and ionic liquid additives on the tribological performance of epoxy resin. *Tribology Letters*, **56**, 133-142 (2014).
75. Sanes J., Saurín N., Carrion F. J., Ojados G., Bermúdez M. D.: Synergy between single-walled carbon nanotubes and ionic liquid in epoxy resin nanocomposites. *Composites Part B*, **105**, 149-159 (2016).
76. Avilés M. D., Saurín N., Espinosa T., Sanes J., Arias-Pardilla J., Carrión F. J., Bermúdez M. D.: Self-lubricating, wear resistant protic ionic liquid-epoxy resin. *eXPRESS Polymer Letters*, **11**, 219-229 (2017).
77. Hameed N., Salim N. V., Walsh T. R., Wiggins J. S., Ajayan P. M., Fox B. L.: Ductile thermoset polymers via controlling network flexibility. *Chemical Communications*, **51**, 9903-9906 (2015).

78. Van Krevelen D.W.: Properties of polymers: their correlation with chemical structure: their numerical estimation and prediction from additive group contributions. Amsterdam: Elsevier (2009).
79. Mohamed M. H., Wilson L. D.: Porous copolymer resins: tuning pore structure and surface area with non reactive porogens. *Nanomaterials*, **2**, 163-186 (2012).
80. Okay O.: Macroporous copolymer networks. *Progress in Polymer Science*, **25**, 711-779 (2000).
81. Mane S.: Effect of porogens (type and amount) on polymer porosity: a review. *Canadian Chemical Transactions*, **4**, 210-225 (2016).
82. Kubisa P.: Ionic liquids in the synthesis and modification of polymers. *Journal of Polymer Science Part A: Polymer Chemistry*, **43**, 4675-4683 (2005).
83. Snedden P., Cooper A. I., Khimyak Y. Z., Scott K., Winterton N.: Cross-linked polymers in ionic liquids: ionic liquids as porogens. In book: *Ionic liquids in polymer systems. Solvents, additives, and novel applications*. Ed.: Brazell C. S., Rogers R. D. American Chemical Society, Chapter 9 (2005).
84. Booker K., Holdsworth C. I., Doherty C. M., Hill A. J., Bowyer M. C., McCluskey A.: Ionic liquids as porogens for molecularly imprinted polymers: propranolol, a model study. *Organic & Biomolecular Chemistry*, **12**, 7201-7210 (2014).
85. Singco B., Lin C. L., Cheng Y. J., Shih Y. H., Huang H. Y.: Ionic liquids as porogens in the microwave-assisted synthesis of methacrylate monoliths for chromatographic application. *Analytica Chimica Acta*, **746**, 123-133 (2012).
86. Hasegawa G., Kanamori K., Nakanishi K., Yamago S.: Fabrication of highly crosslinked methacrylate-based polymer monoliths with well-defined macropores via living radical polymerization. *Polymer*, **52**, 4644-4647 (2011).
87. Throckmorton J., Palmese G.: Acceleration of cyanate ester trimerization by dicyanamide RTILs. *Polymer*, **91**, 7-13 (2016).

CHAPTER 2

Acceleration Effect of Ionic Liquids on Polycyclotrimerization of Dicyanate Esters

Abstract: The polycyclotrimerization reaction of dicyanate ester of bisphenol E (DCBE) in the presence of varying amounts (from 0.5 to 5 wt%) of 1-octyl-3-methylimidazolium tetrafluoroborate ([OMIm][BF₄]) ionic liquid has been investigated using differential scanning calorimetry (DSC) and Fourier transform infrared spectroscopy (FTIR) techniques, after a curing stage at 150 °C for 6 h. It is noteworthy that an amount of [OMIm][BF₄] as low as 0.5 wt% accelerates dramatically the thermal curing process leading to the formation of a polycyanurate network. The conversion of DCBE increased with increasing [OMIm][BF₄] content in the temperature range studied. A reaction mechanism associated with the ionic liquid-catalyzed DCBE polycyclotrimerization is newly proposed *via* the involvement of a $\sigma^+[\text{CN}] \cdots [\text{OMIm}]^{\sigma-}$ complex as a key intermediate.

A. Fainleib, O. Grigoryeva, O. Starostenko, A. Vashchuk, S. Rogalsky, D. Grande: Acceleration effect of ionic liquids on polycyclotrimerization of dicyanate esters. *eXPRESS Polymer Letters*, **10**, 722-729 (2016).

2.1. Introduction

Cyanate ester resins (CERs) – also known as polycyanurates (PCNs) – are commonly used in aerospace applications and electronic devices as high temperature polymer matrices. The specific interest in these high performance polymers arises from their unique combination of intrinsic properties, including thermal, fire, radiation and chemical resistance, high tensile moduli (3.1-3.4 GPa) and glass transition temperatures ($T_g > 250$ °C), low dielectric constants ($\epsilon \sim 2.5$ -3.2), high adhesion to conductor metals and composites as well as low water/moisture adsorption [1, 2].

Ionic liquids (ILs) have attracted widespread interest in polymer science, due to their unique properties, such as low melting temperature, incombustibility, electrochemical, and high-temperature stability. They have progressively been used as solvents and substances with catalytic properties [3, 4] as well as conductive fillers [5]. Miscellaneous reports on using ILs in polymerization processes have been published [6-12]. For instance, Wu et al. [12] have recently investigated the cationic polymerization of isobutyl vinyl ether in 1-octyl-3-methylimidazolium tetrafluoroborate ([OMIm][BF₄]). It was noticed that the cationic process led to higher monomer conversions in the presence of [OMIm][BF₄]. Although the polymerization reaction in [OMIm][BF₄] could not be controlled, due to the presence of β proton elimination, the monomer addition experiments confirmed the existence of long-lived species. The results showed that introducing a small amount of 2,6-di-*tert*-butyl pyridine into the system might lead to a controlled polymerization. In contrast, reports on ILs involved in crosslinking processes are much scarcer [13].

The curing kinetics of neat CERs has extensively been reported in the literature [14-21]. It is of common knowledge that the polycyclotrimerization of dicyanate esters is rather slow, and it generally requires the presence of a curing catalyst which may be either a Lewis acids or acetylacetonates of Cu²⁺, Co³⁺, Zn²⁺ and Mn²⁺ [22], or a chelate in the presence of an active hydrogen-containing co-catalyst (such as nonylphenol), acting as a source of proton. Recently, Throckmorton [23] has examined the effect of ILs on curing of cyanate esters in IL-modified thermosets and their nanocomposites, and interestingly, he concluded that the ionic liquids accelerated the CER curing.

In the present work, we have highlighted the acceleration effect occurring in the polymerization of a dicyanate monomer in the presence of a specific ionic liquid, namely [OMIm][BF₄], and for the first time suggested the mechanism of the polycyclotrimerization of

cyanate ester in the presence of imidazolium IL. It is worth noting that ILs are thermally stable compounds that is important for the polycyclotrimerization, which is usually carried out at high temperatures up to 230-280 °C [1, 2]. The structure of such catalyst systems allows for easier separation, recovery, and recycling from the reaction mixtures [24].

Additionally, introducing ILs into CER frameworks may impart conductivity to the CER-based nanocomposites. ILs could be extracted and potentially used repeatedly; therefore, CER/IL composites could be applied as precursors to porous materials as well.

2.2. Experimental

2.2.1. Materials

1,1'-Bis(4-cyanatophenyl)ethane (dicyanate ester of bisphenol E, DCBE) under the trade name Primaset™ LECy, was kindly supplied by Lonza Ltd., Switzerland, and was used as received. The following chemicals were used for the synthesis of the 1-octyl-3-methylimidazolium tetrafluoroborate ([OMIm][BF₄]): 1-methylimidazole, 1-bromooctane, tetrafluoroboric acid (50 % in H₂O), ethyl acetate, hexane, methylene chloride, and sodium sulfate. The chemicals were provided by Fluka and were used as received.

2.2.2. Ionic liquid synthesis

1-octyl-3-methylimidazolium tetrafluoroborate [OMIm][BF₄] was synthesized using the approaches described elsewhere [25, 26]. The mixture of 1-bromooctane (27 g, 0.14 mol) and 1-methylimidazole (10 g, 0.12 mol) was heated at 140 °C for 2 h under stirring and argon atmosphere. The viscous liquid of light brown color obtained was cooled to room temperature and washed with ethyl acetate-hexane mixture (3:1 (v/v), 3×100 mL). Residual solvents were removed under reduced pressure, and the obtained product was dissolved in 150 mL of water. Tetrafluoroboric acid (25 mL) was added to the solution, followed by stirring for 1 h. The water immiscible layer formed was extracted with methylene chloride (2×100 mL), and dried overnight with sodium sulfate. The solvent was distilled off, and the resulting ionic liquid was dried under a reduced pressure of 1 mbar at 80 °C for 12 h. The product yield was equal to 72%. The onset temperature of thermal degradation (T_d) was equal 343 °C as determined by thermogravimetric analysis (TGA) under air. ¹H NMR (300 MHz, DMSO-D₆): δ = 0.86 (t, 3H,

CH₃, J= 7.2 Hz), 1.25 (m, 10H, CH₃(CH₂)₅), 1.78 (m, 2H, NCH₂CH₂), 3.85 (s, 3H, NCH₃), 4.16 (t, 2H, NCH₂, J= 7.2 Hz), 7.67 (br s, 1H, C₄-H), 7.74 (brs, 1H, C₅-H), 9.06 (s, 1H, C₂-H).
¹⁹F NMR (188 MHz, DMSO-D₆): δ = -148.8 (s, 4F, BF₄).

2.2.3. Preparation of CER/[OMIm][BF₄] samples

The blends of DCBE monomer with 0.5, 1.0, 2.0, 3.0, 4.0, and 5.0 wt% [OMIm][BF₄] were stirred at $T \approx 20$ °C for 3 min to obtain homogeneous mixtures, followed by a heating step at 150 °C for 6 h.

2.2.4. Physico-chemical techniques

¹H NMR and ¹⁹F NMR techniques were used to characterize the ionic liquid. The spectra were recorded with a Varian (300 MHz) NMR spectrometer at 23 °C using DMSO-D₆ as the deuterated solvent.

The thermal stability of the ionic liquid was assessed by TGA under air atmosphere using a TA Instruments TGA Q-50 thermobalance over a temperature range from 25 to 700 °C at a heating rate of 10 °C·min⁻¹.

Differential scanning calorimetry (DSC) measurements were performed using a Perkin-Elmer DSC-7 under nitrogen atmosphere, in a temperature range from 150 to 340 °C at a heating rate of 10 °C·min⁻¹. The samples mass was about 6-9 mg. The post-curing conversion (α_{post}) of cyanate (O-C≡N) groups from DCBE was calculated from **Equation 2-1** [27]:

$$\alpha_{post} = \left(\alpha_c + \frac{\Delta H_t}{\Delta H_{tot}} \right) \times 100 \quad (2-1)$$

where $\alpha_c \left(\frac{\Delta H_{tot} - \Delta H_{post}}{\Delta H_{tot}} \right)$ [28] is the conversion after heating at 150 °C for 6 h, ΔH_t is the reaction enthalpy at time t , ΔH_{tot} is the total enthalpy of polycyclotrimerization of DCBE monomer ($\Delta H_{tot} = 770$ J g⁻¹ [29]), and ΔH_{post} is the post-curing enthalpy, which was calculated from the exotherm area of cured sample divided by its mass.

Fourier transform infrared (FTIR) spectra were recorded between 4000 and 600 cm^{-1} using a Bruker Tensor 37 spectrometer. For each spectrum, 16 consecutive scans with a resolution of 0.6 cm^{-1} were averaged. All spectra were recorded at room temperature.

The mono mer conversion was determined from the absorbance variation of the bands with maxima at 2266 and 2235 cm^{-1} , corresponding to the stretching vibrations of the cyanate groups. The stretching band of benzene ring at 1501 cm^{-1} was used as an internal standard. The conversion (α_c) of cyanate groups after heating at 150 °C for 6 h was calculated from **Equation 2-2**:

$$\alpha_c = 1 - \frac{A_{(t)2266-2235}/A_{(0)2266-2235}}{A_{(t)1501}/A_{(0)1501}} \times 100 \quad (2-2)$$

where $A_{(t)2266-2235}$ is the area under absorption bands of O–C≡N groups at time t , $A_{(t)1501}$ is the area under absorption band of benzene ring at time (t), and $A_{(0)}$ is the area under absorption bands of the corresponding groups in initial DCBE monomer.

2.3. Results and discussion

In the first stage the mixtures of DCBE monomer with different amounts of ionic liquid [OMIm][BF₄] were heated at 150 °C for 6 h. In the presence of a catalyst, one such curing step permitted to attain a gel point [30].

2.3.1. DSC analysis

Figure 2-1a exhibits the DSC thermograms for neat CER and CER/[OMIm][BF₄] samples of different compositions cured at 150 °C for 6 h, and their main thermal characteristics are summarized in **Table 2-1**. For the neat CER sample, the exotherm maximum is associated with a temperature of post-curing (T_{p1}) equal to 294 °C with some weak shoulder at $T \sim 239$ °C. The shoulder may be attributed to the formation of the intermediate linear CER dimers, trimers and potentially other higher even-mers [31]. The CER/[OMIm][BF₄] samples display bimodal curing profiles with distinct exothermic peaks corresponding to CER post-curing process at the selected heating rate (10 °C·min⁻¹). For the CER/[OMIm][BF₄] specimens, T_{p1} was shifted toward much lower temperatures, *i.e.* 218-221 °C (**Table 2-1**). This fact attested that, in the presence of [OMIm][BF₄], the polycyclotrimerization of DCBE mostly occurred at lower

temperatures. Yet, in the latter case, it should be noted that weak peaks (T_{p2}) appeared around 279-282 °C, namely at a temperature similar to that of pure DCBE polymerization. One could suppose that the first exotherm maximum corresponded to the curing reaction catalyzed by [OMIm][BF₄], while the second peak was attributed to a higher temperature thermal curing without catalyst participation.

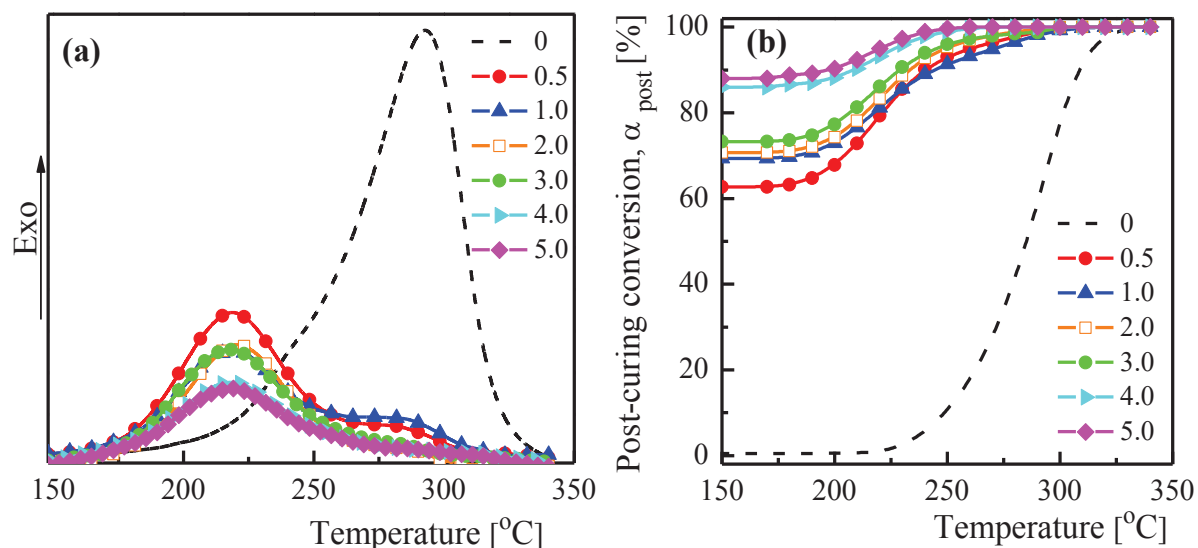


Figure 2-1: DSC thermograms (a) and temperature dependence of post-curing conversion (b) for CER samples with different [OMIm][BF₄] contents.

Table 2-1: Thermal characteristics of CER/[OMIm][BF₄] samples cured at 150 °C for 6 h as determined by DSC

[OMIm][BF ₄] content [wt. %]	Post-curing interval [°C]			T_{p1}^b [°C]	T_{p2}^c [°C]	ΔH_{post}^d [J g ⁻¹]	ΔH_c^e [J g ⁻¹]
	T_{onset}	T_{end}	ΔT^a				
0.0	208	340	132	294	-	755	15
0.5	160	318	158	219	280	296	474
1.0	162	317	155	218	279	233	537
2.0	166	309	143	221	280	223	544
3.0	167	300	133	218	281	203	567
4.0	171	268	97	220	282	120	650
5.0	174	262	88	218	282	114	656

^a Post-curing temperature interval: $\Delta T = T_{end} - T_{onset}$; ^b Peak temperature of post-curing associated with first endotherm maximum; ^c Peak temperature of post-curing associated with second endotherm maximum; ^d Post-curing enthalpy under selected conditions (from 150 °C to 340 °C at 10 °C min⁻¹); ^e Curing enthalpy after heating at 150 °C for 6 h: $\Delta H_c = \Delta H_{tot} - \Delta H_{post}$, $\Delta H_{tot} = 770 \text{ J g}^{-1}$ [29].

Table 2-1 clearly shows that the reaction rate of CER curing was enhanced by the presence of [OMIm][BF₄]. It is noteworthy that loading of [OMIm][BF₄] was associated with a substantial narrowing the post-curing temperature interval from 179 °C for neat CER to 163-168 °C for CER/[OMIm][BF₄] samples. Moreover, the enthalpy of post-curing process (ΔH_{post}) for pure DCDE was equal to 755 J·g⁻¹. According to literature [29], the total enthalpy of polycyclotrimerization of DCBE monomer (ΔH_{tot}) was equal to 770 J·g⁻¹. Therefore, one could conclude that the polymerization of neat DCBE practically did not occur after the 6 h-curing stage at 150 °C. In sharp contrast, ΔH_{post} for DCBE post-polycyclotrimerization in the IL-containing samples dramatically decreased with increasing [OMIm][BF₄] contents, so in turn the curing enthalpy after the curing stage at 150 °C for 6 h (ΔH_c) increased accordingly. **Figure 2-1b** displays the temperature dependence of post-curing conversion values (α_{post}) for neat CER and CER/[OMIm][BF₄] samples. As stated above, the polymerization of DCBE monomer hardly occurred during thermal heating at 150 °C for 6 h, thus the corresponding curve started around 2 % conversion. When pure DCBE was post-cured from 150 to 340 °C with a heating rate of 10 °C min⁻¹, an induction period was found to last around 7.5 min before reaching 225 °C, i.e. the temperature from which α_{post} appeared to sharply increase up to 100 % conversion. Contrarily, the O–C≡N conversion (α_c) in the CER/[OMIm][BF₄] samples after heating at 150 °C for 6 h reached values as high as 62-85 %, depending on the [OMIm][BF₄] content (**Table 2-2**).

Table 2-2: Conversion values (α_c) for CER/[OMIm][BF₄] samples after heating at 150 °C for 6 h.

[OMIm][BF ₄] content [wt. %]	α_c [%]	
	DSC ^a	FTIR ^b
0.0	2	1
0.5	62	59
1.0	69	65
2.0	71	76
3.0	74	77
4.0	84	86
5.0	85	87

^a The experimental error on values determined by DSC was estimated to be equal to 1 %.

^b The experimental error on values determined by FTIR was estimated to be equal to 2 %.

Notably, complete conversion was not reached because of the low curing temperature (150 °C) as far as the final curing temperature should be equal to 230-270 °C, and even higher [1, 2]. When heating from 150 to 340 °C, the DCBE conversion values (α_{post}) further increased gradually to attain completion. In summary, the higher the [OMIm][BF₄] content, the higher the O–C≡N conversion (α_c) reached after heating at 150 °C for 6 h, and the shorter the time to reach complete conversion during post-curing process.

2.3.2. FTIR analysis

The peculiarities of DCBE polycyclotrimerization in the absence and in the presence of [OMIm][BF₄] were also investigated using FTIR. **Figure 2-2** shows the FTIR absorption spectra for uncured DCBE monomer (curve **0**), neat CER (curve **0_T**), and CER/[OMIm][BF₄] samples (curves **0.5_T**–**5.0_T**) after heating at 150 °C for 6 h.

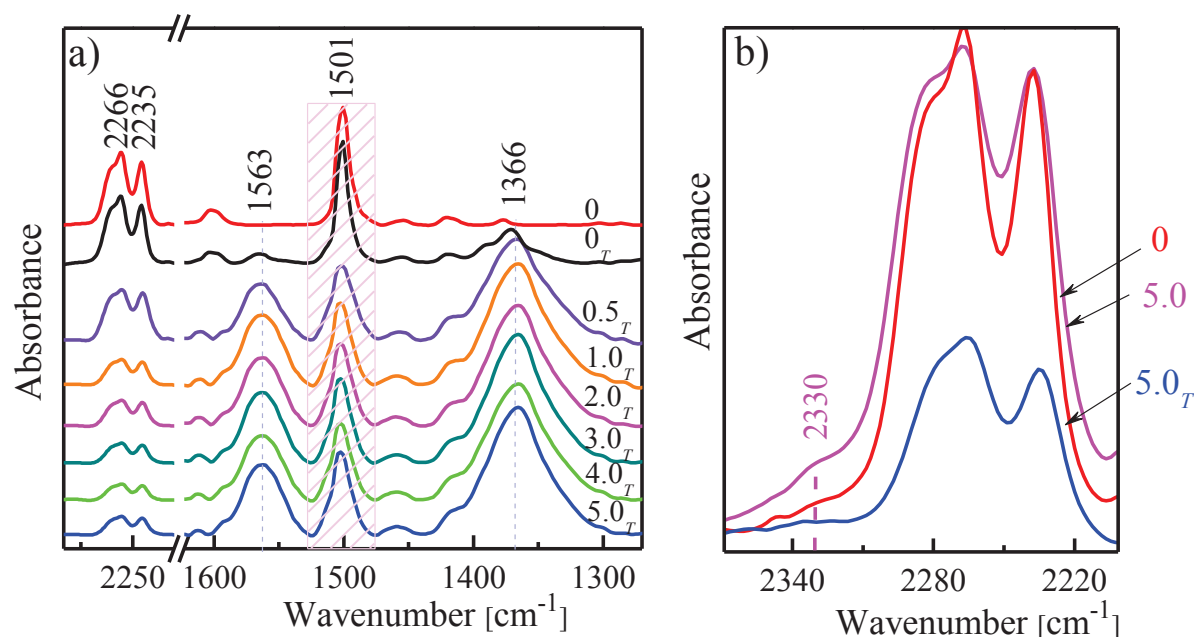


Figure 2-2: FTIR spectra of: DCBE monomer (curve **0**) (a) and CER samples with different [OMIm][BF₄] contents after heating at 150 °C for 6 h (curves **0_T**–**5.0_T**, the number indicating the IL content); uncured DCBE (curve **0**) (b) and CER/[OMIm][BF₄] sample (95/5 wt.%) before (curve **5.0**) and after (curve **5.0_T**) the same heating stage in the spectral zone of 2370-2200 cm⁻¹.

For neat CER, no visible changes in the intensity of the bands of cyanate groups at 2266-2235 cm^{-1} were observed, and a very low conversion of DCBE could be suggested on the basis of the appearance of small bands at 1563 and 1366 cm^{-1} , corresponding to C=N–C groups and N–C–O groups of cyanurate cycles, respectively. In contrast, concerning CER/[OMIm][BF₄] samples, the intensity of the bands at 2266-2235 cm^{-1} decreased, and bands clearly appeared at 1563 and 1366 cm^{-1} , thus evidencing the formation of polycyanurate crosslinked structures. This conclusion was in a good agreement with the DSC data discussed above. The conversion values (α_c) of O–C≡N groups associated with the different [OMIm][BF₄] contents was calculated using FTIR data, and both sets of values obtained from FTIR and DSC data matched pretty well (see **Table 2-2**).

Both FTIR and DSC results clearly evidenced an acceleration effect of [OMIm][BF₄] on the CER formation during curing process at 150 °C for 6 h. Interestingly, the catalytic effect was already noticeable at the lowest content of [OMIm][BF₄] investigated, *i.e.* 0.5 wt.%. This could be attributed to the presence of an acid center in the ring of the [OMIm] cation, which might accelerate the polycyclotrimerization of the dicyanate monomer.

2.3.3. Proposed mechanism of the [OMIm][BF₄]-catalyzed cyclotrimerization of DCBE

It has been well investigated that Lewis acids, such as TiCl₄, could be used as catalysts for polycyclotrimerization of dicyanate esters [32]. Martin and coworkers [33, 34] reported the appearance of bands around 2300 cm^{-1} when dicyanates were treated with an excess of Lewis acid. A strong band at 2320 cm^{-1} indeed appeared upon addition of 1-5 equiv. of TiCl₄ to bisphenol A dicyanate ester; no ‘free’ cyanate was detectable in these cases [32]. The band at 2320 cm^{-1} , attributed to a cyanate-catalyst complex, was formed rapidly on mixing before gradually disappearing at the end of the reaction. Therefore, the band around 2300-2320 cm^{-1} was ascribed to a simple cyanate-Lewis acid complex [32-34].

Likewise, in our investigation, we proposed a mechanism involving a cyanate-ionic liquid complex. Indeed, the appearance of a shoulder at 2330 cm^{-1} in the FTIR spectra after mixing DCBE with 5 wt% of [OMIm][BF₄] was observed in **Figure 2-2b** (curve **5.0**). After heating the mixture at 150 °C for 6 h and reaching high conversion of cyanate groups, this shoulder disappeared (curve **5.0t**). We proposed a possible mechanism for the DCBE/[OMIm][BF₄] system in **Figure 2-3**. First, a pseudo-nitrillium ion **2** was formed when mixing dicyanate with

[OMIm][BF₄] via the involvement of a [CN]^{δ+}-[OMIm]^{δ-} complex whose characteristic FTIR absorption band could be assigned to the shoulder at 2330 cm⁻¹. This cyanate ionic liquid complex was then attacked by a ‘free’ cyanate monomer **1**, thus leading to the formation of a nitrillium ion **3**. The latter was attacked by a ‘free’ dicyanate molecule **1** with formation of a nitrillium ion **4**, which was transformed into an acyclic trimer **5** with [OMIm][BF₄] release, and finally into a cyclotrimer (cyanurate) **6**. Taking in account the existence of an acid center in the ring of 1-octyl-3-methylimidazolium cation (*i.e.*, C–H bond in position **2** imparts slight acidity); we could suppose that this center indeed catalyzed the cyclotrimerization reaction of DCBE. It has to be noted here that a small shoulder at 2330 cm⁻¹ is also observed in the FTIR spectrum of the DCBE. It is known that phenolic groups catalyze polycyclotrimerization of CER and it occurs also through formation of the intermediate structure, which disappear after formation of triazine cycle and reclaiming phenol [1]. So the traces of bisphenol E, left after DCBE synthesis, could form the dimer structures with cyanate ester and this complex may be also characterized by the shoulder at 2330 cm⁻¹ in FTIR spectrum of neat cyanate ester.

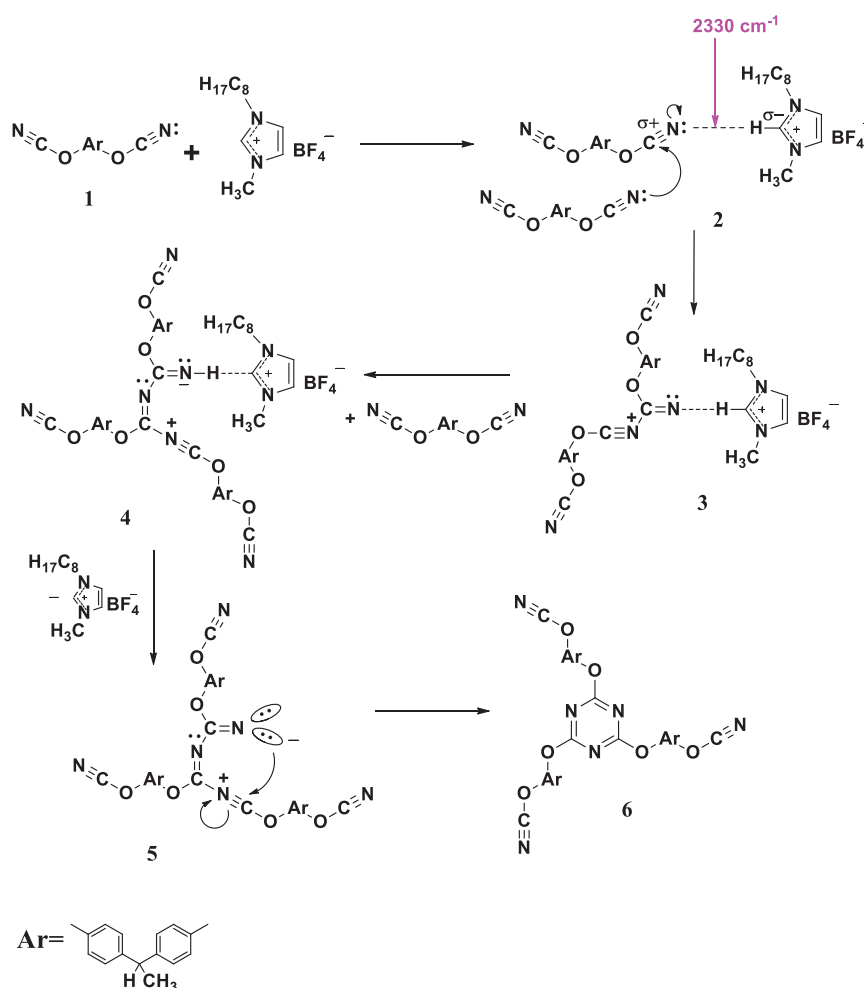


Figure 2-3: Proposed mechanism for the [OMIm][BF₄]-catalyzed cyclotrimerization of DCBE.

2.4. Conclusions

The [OMIm][BF₄]-catalyzed polycyclotrimerization of DCBE was investigated through DSC and FTIR analyses. A dramatic influence of the ionic liquid on CER curing was demonstrated. For samples containing [OMIm][BF₄], polycyclotrimerization of DCBE took place even at the heating stage at 150 °C, while for pure DCBE polycyclotrimerization practically did not occur. The conversion of DCBE increased with increasing [OMIm][BF₄] contents in the temperature range studied. A plausible mechanism based on the formation of a [CN]^{δ+}-[OMIm]^{δ-} complex was proposed to account for the acceleration effect of the ionic liquid on the curing process associated with CERs. We assume that one such catalytic effect of imidazoliumbased ILs will take place for any dicyanate mono-mer. The effect of other IL types on kinetics of polycyclotrimerization of dicyanate esters has to be further studied.

It should be emphasized that [OMIm][BF₄] displayed a catalytic activity in the absence of any additional organic solvent or co-catalyst. Interestingly, the ionic liquid is not destroyed during the CER synthesis.

2.5. References

1. Hamerton I. ed.: Chemistry and technology of cyanate ester resins. Chapman & Hall, Glasgow (1994).
2. Fainleib A. ed.: Thermostable polycyanurates: synthesis, modification, structure and properties. Nova Science Publishers, New York (2010).
3. Wang Y., Li H., Wang C., Jiang H.: Ionic liquids as catalytic green solvents for cracking reactions. *Chemical Communications*, **17**, 1938-1939 (2004).
4. Olivier-Bourbigou H., Magna L., Morvan D.: Ionic liquids and catalysis: recent progress from knowledge to applications. *Applied Catalysis A: General*, **373**, 1-56 (2010).
5. Ohno H., Yoshizawa M., Ogihara W.: Development of new class of ion conductive polymers based on ionic liquids. *Electrochimica Acta*, **50**, 255-261 (2004).
6. Wasserscheid P., Welton T. ed(s): Ionic liquids in synthesis. VCH-Wiley, Weinheim (2002).
7. Holbrey J. D., Chen J., Turner M. B., Swatloski R. P., Spear S. K., Rogers R. D.: Applying ionic liquids for controlled processing of polymer materials. in "Ionic liquids in polymer systems. Solvents, additives, and novel applications" (ed(s): Brazel C. S., Rogers R. D.) ACS Symposium Series, Washington, DC, 71-87 (2005).
8. Vasile I. P., Hardacre C.: Catalysis in ionic liquids. *Chemical Reviews*, **107**, 2615-2665 (2007).
9. Strehmel V., Berdzinski S., Ehrentraut L., Faßbender C., Horst J., Leeb E., Liepert J., Ruby M. P., Senkowski V., Straßburg P., Wenda A., Strehmel C.: Application of ionic liquids in synthesis of polymeric binders for coatings. *Progress in Organic Coatings*, **89**, 297-313 (2015).
10. Stejskal J., Dybal J., Trchová M.: The material combining conducting polymer and ionic liquid: Hydrogen bonding interactions between polyaniline and imidazolium salt. *Synthetic Metals*, **197**, 168-174 (2014).
11. Trchova M., Sedenkova I., Moravkova Z., Stejskal J.: Conducting polymer and ionic liquid: improved thermal stability of the material – a spectroscopic study. *Polymer Degradation and Stability*, **109**, 27-32 (2014).
12. Wu Y., Han L., Zhang X., Mao J., Gong L., Guo W., Guab K., Li S.: Cationic polymerization of isobutyl vinyl ether in an imidazole-based ionic liquid: characteristics and mechanism. *Polymer Chemistry*, **6**, 2560-2568 (2015).
13. Snedden P., Cooper A. I., Khimyak Y. Z., Scott K., Winterton N.: Cross-linked polymers in ionic liquids: ionic liquids as porogens. "Ionic liquids in polymer systems. Solvents, additives, and novel applications" (ed(s): Brazel C. S., Rogers R. D.) ACS Symposium Series, Washington, DC, 133-147 (2005).
14. Owusu A. O., Martin G. C., Gotro J. T.: Analysis of the curing behavior of cyanate ester resin systems. *Polymer Engineering & Science*, **31**, 1604-1609 (1991).
15. Owusu A. O., Martin G. C., Gotro J. T.: Catalysis and kinetics of cyclotrimerization of cyanate ester resin systems. *Polymer Engineering & Science*, **32**, 535-541 (1992).
16. Wu S. J., Mi F. L.: Cure kinetics of a cyanate ester blended with poly(phenylene oxide). *Polymer International*, **55**, 1296-1303 (2006).
17. Gomez C. M., Recalde I. B., Mondragon I.: Kinetic parameters of a cyanate ester resin catalyzed with different proportions of nonylphenol and cobalt acetylacetonate catalyst. *European Polymer Journal*, **41**, 2734-2741 (2005).
18. Simon S. L., Gillham K. J.: Cure kinetics of a thermosetting liquid dicyanate ester monomer/high- T_g polycyanurate material. *Journal of Applied Polymer Science*, **47**, 461-485 (1993).
19. Li W., Liang G., Xin W.: Triazine reaction of cyanate ester resin systems catalyzed by organic tin compound: kinetics and mechanism. *Polymer International*, **53**, 869-876 (2004).

20. Fainleib A., Bardash L., Boiteux G.: Catalytic effect of carbon nanotubes on polymerization of cyanate ester resins. *eXPRESS Polymer Letters*, **3**, 477-482 (2009).
21. Bershtein V. A., Fainleib A. M., Pissis P., Bei I. M., Dalmas F., Egorova L. M., Gomza Yu. P., Kriptou S., Maroulos P., Yakushev P. N.: Polycyanurate – organically modified montmorillonite nanocomposites: structure-dynamics-properties relationships. *Journal of Polymer Science Part B Polymer Physics*, **47**, 555-575 (2008).
22. Li Q. F., Lu K., Yang Q. Q., Jin R.: The effect of different metallic catalysts on the coreaction of cyanate/epoxy. *Journal of Applied Polymer Science*, **100**, 2293-2302 (2006).
23. Throckmorton J. A.: Ionic liquid-modified thermosets and their nanocomposites: Dispersion, exfoliation, degradation, and cure. PhD dissertation, Drexel University (2015).
24. Valkenberg M. H., de Casto C., Holderich W. F.: Immobilisation of ionic liquids on solid supports. *Green Chemistry*, **4**, 88-93 (2004).
25. Dzyuba S. V., Bartsch R. A.: Efficient synthesis of 1-alkyl(aralkyl)-3 methyl(ethyl)imidazolium halides: precursors for room-temperature ionic liquids. *Journal of Heterocyclic Chemistry*, **38**, 265-268 (2001).
26. Ennis E., Handy T. S.: Facile route to C₂-substituted imidazolium ionic liquids. *Molecules*, **14**, 2235-2245 (2009).
27. Li J., Chen P., Ma Z., Ma K., Wang B.: Reaction kinetics and thermal properties of cyanate ester-cured epoxy resin with phenolphthalein poly(ether ketone). *Journal of Applied Polymer Science*, **111**, 2590-2596 (2009).
28. Zhao L., Hu X.: A variable reaction order model for prediction of curing kinetics of thermosetting polymers. *Polymer Journal*, **48**, 6125-6133 (2007).
29. Reams J. T., Guenther A. J., Lamison K. R., Vij V., Lubin L. M., Mabry J. M.: Effect of chemical structure and network formation on physical properties of di(cyanate ester) thermosets. *ACS Applied Materials & Interfaces*, **4**, 527-535 (2012).
30. Fainleib A., Gusakova K., Grigoryeva O., Starostenko O., Grande D.: Synthesis, morphology, and thermal stability of nanoporous cyanate ester resins obtained upon controlled monomer conversion. *European Polymer Journal*, **73**, 94-104 (2015).
31. Kasehagen L. J., Macosko C. W.: Structure development in cyanate ester polymerization. *Polymer International*, **44**, 237-247 (1997).
32. Cunningham I. D., Brownhill A., Hamerton I., Howlin B.: Kinetics and mechanism of the titanium tetrachloride-catalysed cyclotrimerisation of aryl cyanates. *Journal of the Chemical Society, Perkin Transactions 2*, **9**, 1937-1943 (1994).
33. Martin D., Weise A.: Cyansäureester, XIV. Komplexe von cyansäure-arylestern mit lewis-säuren und ihre alkylierung. *Chemische Berichte*, **100**, 3747-3755 (1967).
34. Martin D., Bauerand M., Pankratov V. A.: Cyclotrimerisation of cyano-compounds into 1,3,5-triazines. *Russian Chemical Reviews*, **47**, 975-990 (1978).

CHAPTER 3

Effect of Ionic Liquids on Kinetic Peculiarities of Dicyanate Ester Polycyclotrimerization and on Thermal and Viscoelastic Properties of Resulting Cyanate Ester Resins

Abstract: A strong catalytic effect of 1.0 wt.% ionic liquids (ILs) on kinetic peculiarities of dicyanate ester of bisphenol E (DCBE) polycyclotrimerization was evidenced, and structure-property relationships of resulting densely cross-linked cyanate ester resins (CERs) were investigated. Three different ILs with contrasted reactivity were employed as a catalysts: an aprotic IL, *i.e.* 1-octyl-3-methyl imidazolium tetrafluoroborate ([OMIm][BF₄]), a protic IL, *i.e.* 2-(hydroxyethylamino) imidazolium chloride ([HEAIm][Cl]), and a protic polymeric IL, *i.e.* poly(hexamethylene guanidine) toluene sulfonate ([PHMG][TS]). Both [HEAIm][Cl] and [PHMG][TS] were reactive towards DCBE monomer, whereas [OMIm][BF₄] was chemically inert, as confirmed by FTIR spectroscopy. Noticeably, the conversion (α_c) of cyanate groups in the presence of ILs dramatically increased, and a significant dependence of α_c values on IL chemical structure was found. The corresponding mechanisms of DCBE polycyclotrimerization in the presence of different ILs were proposed. All the CER/IL networks exhibited a high thermal stability inherent to neat CER, as shown by TGA, whereas unexpected significant changes of the viscoelastic characteristics for CER/IL networks compared to pure CER analogue was observed using DMTA.

A. Fainleib, O. Grigoryeva, A.Vashchuk, O. Starostenko, S. Rogalsky, A. Rios de Anda, T-Th-T. Nguyen, D. Grande: Effect of ionic liquids on kinetic peculiarities of dicyanate ester polycyclotrimerization and on thermal and viscoelastic properties of resulting cyanate ester resins. EXPRESS Polymer Letters, submitted.

3.1. Introduction

Cyanate ester resins (CERs) represent a family of thermosetting polymers possessing attractive intrinsic features, such as excellent dimensional stability, high glass transition temperature ($T_g > 250$ °C), low dielectric constants (2.5-3.2), flame-retardancy, and high adhesion to conductor metals and composites. Therefore, they are promising materials for aerospace and microelectronic applications, especially as polymer matrices for structural composites, adhesives, potting resins, and coatings that work under severe conditions (high temperature, humidity, corrosive media, etc) [1-6]. Dicyanate ester monomers undergo thermal polycyclotrimerization to generate high T_g polycyanurate networks (PCNs), *i.e.* cyanate ester resins (CERs), without releasing volatile products. **Figure 3-1** describes the reaction scheme of polycyclotrimerization of one of the widely used monomers, *i.e.* dicyanate ester of bisphenol E (DCBE).

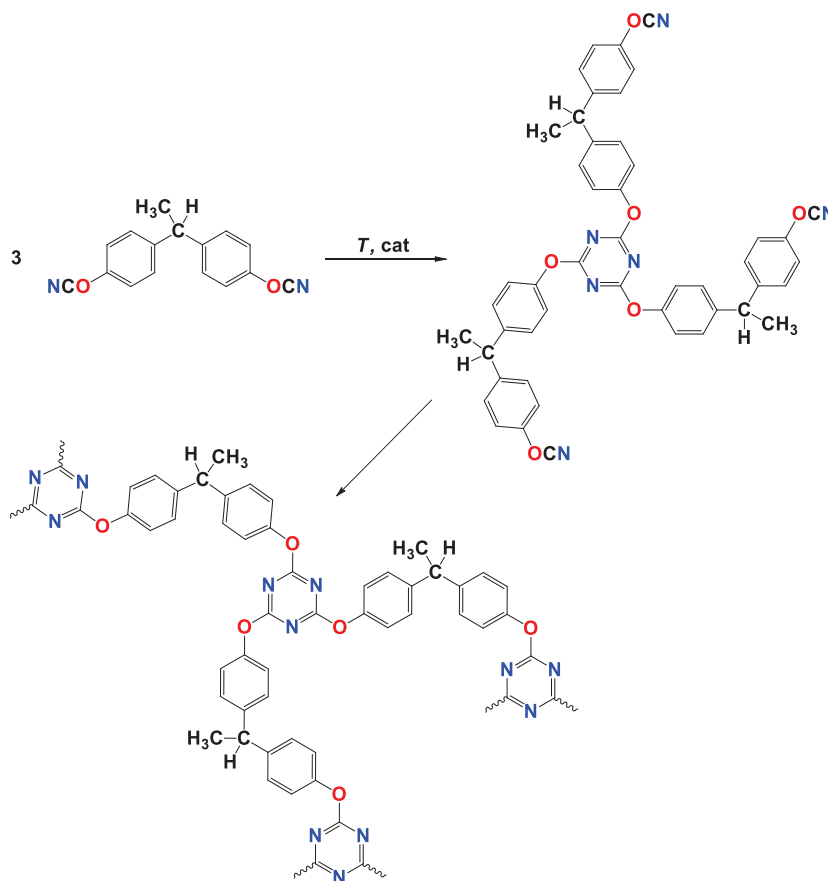


Figure 3-1: Reaction scheme of DCBE polycyclotrimerization.

Dicyanate ester homopolymerization occurs at high temperature in the presence or the absence of a specific catalyst. The rate of non-catalyzed polycyclotrimerization is generally

slow, and it depends on the concentration of impurities (traces of phenols and other residues from synthesis) [1]. Using a catalyst is necessary to achieve a controlled polycyclotrimerization process, which is a key factor for producing materials with excellent properties. This reaction is generally catalyzed by a combination of salts of transition metals, like acetyl acetonates of Cu, Co, Zn, Fe, Mn, Cr, etc. and an active hydrogen containing initiator like nonylphenol. Because of the well-known toxicity of phenolic compounds, attempts to find new effective catalysts for dicyante ester polycyclotrimerization are of scientific and practical interest. In this regard, Throckmorton and Palmese [7] have found an acceleration of cyanate ester trimerization by dicyanamide-containing ionic liquids (ILs).

ILs are salts with melting points at temperatures below 100 °C. They have attracted much attention due to their interesting properties, including negligible vapour pressure, large choice of salts liquid at room temperature, tunable physico-chemical characteristics, excellent thermal and chemical stability, selective solubility, ease of synthesis and good stability to oxidative and reductive conditions [8]. Since they are non-flammable, non-volatile and recyclable, they are greener alternatives to conventional organic solvents. Furthermore, they may be used as effective and reusable catalysts in some polymerization reactions [9-13] and as initiators of free-radical [14, 15] or cationic [16, 17] polymerization processes. Thus, ILs have attracted widespread interest in polymer chemistry, due to their versatile properties [18, 19]. In addition, ILs can also be suitable as porogens for producing nanoporous films and membranes, due to their high thermal stability and chemical inertness. In this regard, our teams have indeed successfully used 1-heptyl pyridinium tetrafluoroborate [HPyr][BF₄] as inert porogenic agent to produce nanoporous thermostable CER films [20].

Recently, our consortium has also found that an addition as small as 1.0 wt.% of the latter aprotic IL significantly accelerated the kinetics of DCBE polycyclotrimerization, which was explained by the formation of a [CN]^{δ+}[HPyr]^{δ-} complex as a key intermediate [21].

In the present paper, we thoroughly investigate the catalytic behaviour of three ILs with contrasted reactivity, namely an aprotic IL, *i.e.* [OMIm][BF₄], a protic IL, *i.e.* 2-(hydroxyethylamino) imidazolium chloride ([HEAIm][Cl]), and a protic polymeric IL, *i.e.* poly(hexamethylene guanidine) toluene sulfonate ([PHMG][TS]). A comprehensive investigation of their effect on kinetic peculiarities (induction time, reaction time, monomer conversion degree, etc) of DCBE polycyclotrimerization as well as on thermal stability and viscoelastic properties of the resulting CERs is addressed.

3.2. Experimental

3.2.1. Materials

1,1-bis(4-cyanatophenyl) ethane (dicyanate ester of bisphenol E, DCBE), under the trade name PRIMASET™ LECy was kindly supplied by Lonza (Switzerland), and was used as received. The following chemicals (Fluka) were used as received for the synthesis of ILs: 1-methylimidazole, 1-bromooctane, 2-ethanolamine, tetrafluoroboric acid (50 % in H₂O), ethyl acetate, hexane, methylene chloride, sodium sulfate, isopropanol, potassium hydroxide, guanidine hydrochloride, hexamethylenediamine, 0.1 N sodium chloride, sodium toluenesulphonate, and ethanol.

3.2.2. Synthesis of ionic liquids

3.2.2.1. Synthesis of 1-octyl-3-methyl imidazolium tetrafluoroborate ([OMIm][BF₄])

[OMIm][BF₄] ionic liquid was synthesized using literature methods previously described [22,23]. The stirred mixture of 1-bromooctane (27 g, 0.14 mol) and 1-methylimidazole (10 g, 0.12 mol) was heated at 140 °C for 2 h under argon atmosphere. The viscous liquid of light brown color obtained was cooled to room temperature and washed with ethyl acetate-hexane mixture (3:1 (v/v), 3×100 mL). Residual solvents were removed at reduced pressure and the obtained product was dissolved in 150 mL of water. Tetrafluoroboric acid (25 mL) was added to the solution followed by stirring for 1 h. The immiscible aqueous layer formed was extracted with methylene chloride (2×100 mL), and dried overnight with sodium sulfate. The solvent was distilled off, and the resulting ionic liquid was dried under reduced pressure of 1 mbar at 80 °C for 12 h. The product yield was equal to 72 %. ¹H NMR (300 MHz, CDCl₃): δ (ppm): 0.86 (t, 3H, CH₃, J=7.2 Hz), 1.25-1.31 (m, 9H, CH₂), 1.86 (m, 3H, CH₂), 3.94 (s, 3H, NCH₃), 4.16 (t, 2H, NCH₂, J=7.2 Hz), 7.27-7.38 (m, 2H, NC(H)C(H)N), 8.78 (s, 1H, NC(H)N). ¹⁹F NMR (188 MHz, CDCl₃): δ (ppm): -151.4. ¹H NMR (300 MHz, DMSO-*d*₆, TMS): δ (ppm): 0.85 (t, 3H, CH₃), 1.25 (m, 10H, CH₃(CH₂)₅), 1.78 (m, 2H, NCH₂CH₂), 3.85 (s, 3H, NCH₃), 4.16 (t, 2H, NCH₂), 7.67 (br s, 1H, C₄-H), 7.74 (br s, 1H, C₅-H), 9.06 (s, 1H, C₂-H). ¹⁹F NMR (188 MHz, DMSO-*d*₆, CFCl₃): δ (ppm): -148.8 (s, 4F, BF₄).

3.2.2.2. Synthesis of 2-(hydroxyethylamino) imidazolinium chloride ([HEAIm][Cl])

2-methylmercaptoimidazoline-2-chlorohydrate was obtained according to a literature method [24]. ¹H NMR (300 MHz, DMSO-*d*₆): δ (ppm): 2.71 (s, 3H, CH₃), 3.84 (s, 4H, CH₂), 10.64 (2H, br s, NH).

The stirred mixture of 2-methylmercaptoimidazoline-2-chlorohydrate (5 g, 0.032 mol) and 2-ethanolamine (2.1 g, 0.035 mol) in 50 mL of isopropanol was heated to boiling for 6 h. Methylmercaptane formed as by-product was absorbed by 20 % water solution of potassium hydroxide. The solvent was removed at reduced pressure and the obtained solid residue of [HEAIm][Cl] was purified by double recrystallization from isopropanol. Yield: 85 %. ¹H NMR (300 MHz, DMSO-*d*₆): δ (ppm): 3.25 (m, 2H, CH₂OH), 3.56 (m, 6H, NHCH₂CH₂OH), 7.64 (4H, br s, NH, OH)

3.2.2.3. Synthesis of poly(hexamethylene guanidine) toluene sulfonate ([PHMG][TS])

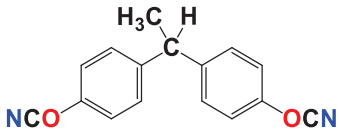
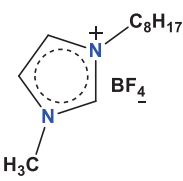
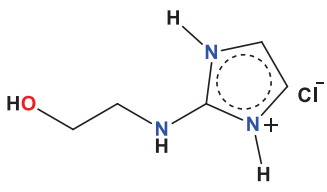
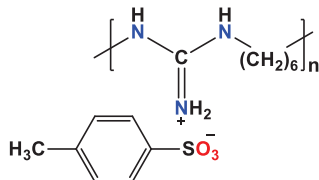
The mixture of guanidine hydrochloride (10 g, 0.104 mol) and hexamethylene diamine (11.7 g, 0.1 mol) was heated at 100 °C for 4 h under constant stirring. Further, the reaction was carried out for 4 h at 140 °C, 4 h at 180 °C and 3 h at 200 °C to obtain a highly viscous liquid. After cooling the reaction mixture to room temperature, the vitreous solid of poly(hexamethylene guanidine) hydrochloride obtained ([PHMG][Cl]) was dissolved in water (150 mL), filtered and precipitated by addition of saturated water solution of sodium chloride (50 mL). The polymer was isolated by decantation of water solution, dried at 140 °C for 24 h and ground in a porcelain mortar. The intrinsic viscosity was equal to 7 cm³/g for [PHMG][Cl] solution in 0.1 M sodium chloride at 25 °C. ¹H NMR (300 MHz, DMSO-*d*₆): δ (ppm): 1.3-1.44 (m, 8H, (CH₂)₄), 3.14 (m, 4H, (N-CH₂)₂), 7.15-7.8 (br s, 4H, C-NH, C=NH₂⁺). Elemental analysis: (C₇H₁₆N₃Cl)_x (177.5)_x: calculated (%): C 47.3, H 9.0, N 23.6, Cl 20.0; found (%): C 46.7, H 8.6, N 24.1, Cl 20.6.

Sodium toluene sulfonate (11.4 g, or 0.058 mol) was added to a solution of [PHMG][Cl] (10 g, 0.056 mol) in 100 mL of ethanol, and the mixture was stirred for 20 h at room temperature. The resulting sodium chloride precipitate was filtered off, and the filtrate was poured into water (300 mL). The white slurry was separated by decantation, followed by washing with water. It was dried at 120-130 °C for 24 h and ground to obtain [PHMG][TS] as a powder. ¹H NMR (300 MHz, DMSO-*d*₆): δ (ppm): 1.24 (m, 4H, (CH₂)₂), 1.42 (m, 4H,

NCH₂CH₂), 2.29 (s, 3H, TsO-CH₃), 3.14 (m, 4H, (NCH₂), 7.14 (d, 2H, H-3, H-5), 7.3-7.35 (br s, 4H, C-NH, C=NH₂⁺), 7.53 (d, 2H, H-2, H-6). Elemental analysis: (C₁₄H₂₃N₃O₃S)_x (313)_x: calculated: C 53.6, H 7.3, N 13.4, S 10.2; found: C 53.1, H 7.0, N 13.8, S 10.5.

The chemical structure and some physico-chemical characteristics of individual components used in this study are summarized in **Table 3-1**. The solubility parameters (δ) of DCBE and ILs were calculated according to Fedor's Group Contribution Method [25].

Table 3-1: Chemical structure and basic physico-chemical characteristics of components under investigation

Component	Structure	Characteristics
<i>1,1-bis(4-cyanatophenyl) ethane</i> DCBE		$M = 264 \text{ g/mol}$ $T_m \approx 29 \text{ }^\circ\text{C}$ $T_d \approx 434 \text{ }^\circ\text{C}$ $\delta = 24.5 \text{ (J/cm}^3\text{)}^{1/2}$
<i>1-octyl-3-methylimidazolium tetrafluoroborate</i> [OMIm][BF ₄]		$M = 282 \text{ g/mol}$ $T_m \approx -88 \text{ }^\circ\text{C}$ $T_d \approx 401 \text{ }^\circ\text{C}$ $\delta = 18.8 \text{ (J/cm}^3\text{)}^{1/2}$
<i>2-(hydroxyethylamino) imidazolium chloride</i> [HEAIm][Cl]		$M = 164 \text{ g/mol}$ $T_m \approx 97-98 \text{ }^\circ\text{C}$ $T_d \approx 244 \text{ }^\circ\text{C}$ $\delta = 28.9 \text{ (J/cm}^3\text{)}^{1/2}$
<i>Polyhexamethylene guanidine toluene sulfonate</i> [PHMG][TS]		$M_n = 12,520 \text{ g/mol (n } \sim 40-50)$ $T_m \approx 110-115 \text{ }^\circ\text{C}$ $T_d \approx 371 \text{ }^\circ\text{C}$ $\delta = 25.6 \text{ (J/cm}^3\text{)}^{1/2}$

3.2.3. Preparation of CER-based networks

Mixtures of DCBE with 1.0 wt.% IL were first stirred until homogeneous state as follows. DCBE monomer was mixed with [OMIm][BF₄], [HEAIm][Cl] or [PHMG][TS] at $T \sim 150 \text{ }^\circ\text{C}$

for ~3 min, then the homogeneous DCBE/IL mixtures were polymerized by a step-by-step curing procedure with the following successive heating conditions: 150 °C/8 h, 180 °C/3h, 210 °C/3 h, 230 °C/1 h.

The effect of IL chemical structure on the resulting CER/[OMIm][BF4], CER/[HEAIm][Cl] or CER/[PHMG][TS] networks was studied by FTIR to detect possible chemical reactions between OCN groups of DCBE and functional groups of ILs. A model composition for DCBE/IL equal to 50/50 wt.% was used at 150 °C for 3 min to obtain homogeneous mixtures, followed by a step-by-step curing procedure with the following heating conditions: 150 °C/8 h, 180 °C/3 h, 210 °C/3 h, 230 °C/1 h.

3.2.4. Physico-chemical techniques

¹H NMR and ¹⁹F NMR techniques were used to characterize the ionic liquids synthesized. The spectra were recorded with a Varian (300 MHz) NMR spectrometer at 23 °C using DMSO-*d*₆ as the deuterated solvent.

Elemental analysis of the ionic liquids synthesized was performed using classical approaches described elsewhere [24].

For kinetic measurements by FTIR, neat DCBE or DCBE/IL mixtures of 99/1 wt.% compositions were poured directly onto NaCl windows, followed by their isothermal heating in a temperature-controlled oven at 150 °C for 8 h with periodic sampling out (every 30 min). FTIR spectra were recorded at room temperature between 4000 and 600 cm⁻¹ using a Bruker Tensor 37 spectrometer. For each spectrum, 32 consecutive scans with a resolution of 4 cm⁻¹ were averaged.

The IR band at 1500 cm⁻¹ of benzene ring vibrations was used as an internal standard. DCBE conversion was determined by monitoring the disappearance of –O–C≡N stretching band at 2266 cm⁻¹. The conversion (α_c) of cyanate groups was calculated using **Equation 3-1**:

$$\alpha_c = \left(1 - \frac{I_{(t)2266} / I_{(0)2266}}{I_{(t)1500} / I_{(0)1500}}\right) \times 100 \quad (3-1)$$

where $I_{(t)2266}$ is the intensity of C≡N vibration band in –O–C≡N at 2266 cm⁻¹ at time t ; $I_{(t)1500}$ is the intensity of carbon-carbon stretching vibrations in aromatic ring band at 1500 cm⁻¹ at time

t ; $I_{(0)}$ is the intensity of corresponding vibration bands in the initial DCBE-containing mixture.

Thermogravimetric analysis (TGA) measurements were performed using a Setaram SETSYS evolution 1750 thermobalance. Samples were heated in a platinum crucible from 20 to 700 °C at a heating rate of 10 °C·min⁻¹ under argon atmosphere. The sample mass was about 10 mg.

Dynamic mechanical thermal analysis (DMTA) was carried out using a DMA-Q800 equipment (TA Instruments) in a temperature range from 20 to 350 °C at a heating rate of 4 °C/min and frequency values of 1, 3, 5, 10, 15 and 20 Hz using single cantilever bending mode. Rectangular samples of size 40×5×1 mm were tested.

The apparent activation energy (ΔE_a) for α relaxation was determined by applying the Vogel-Fulcher-Tammann (VFT) equation as follows (**Equation 3-2**) [26-29]:

$$f = f_0 \exp\left(-\frac{\Delta E_a}{R(T - T_{VFT})}\right) \quad (3-2)$$

where f represents the frequency, f_0 is analogous to the rate constant and pre-exponential factor of Arrhenius Equation, R is the gas constant ($R = 8.314 \cdot 10^{-3} \text{ kJ} \cdot \text{mol}^{-1} \cdot \text{K}^{-1}$), T stands for absolute temperature, T_{VFT} is about 50 °C lower than the α transition temperature T_α .

The shift of α relaxation temperatures ($T_{\alpha 1}$ and $T_{\alpha 2}$) due to changes in the test frequencies (f_1 and f_2) allows for the determination of ΔE_a values by using **Equations 3-3, 3-4 and 3-5** [30]:

$$\frac{f_1}{f_2} = \frac{\exp\left(\frac{-\Delta E_a}{R(T_{a1} - T_{VFT})}\right)}{\exp\left(\frac{-\Delta E_a}{R(T_{a2} - T_{VFT})}\right)} \quad (3-3)$$

$$\log\left(\frac{f_1}{f_2}\right) = \log a_T = \frac{\Delta E_a}{R} \left(\frac{1}{(T_{a2} - T_{VFT})} - \frac{1}{(T_{a1} - T_{VFT})} \right) \log e \quad (3-4)$$

$$\Delta E_a = -R \left(\frac{d(\ln f)}{d(1/(T_a - T_{VFT}))} \right) \quad (3-5)$$

3.3. Results and discussion

3.3.1. Kinetic investigation by FTIR

Kinetics of neat CER formation and DCBE polymerization in the presence of [OMIm][BF₄], [HEAIm][Cl] or [PHMG][TS] was investigated by FTIR. The normalized FTIR spectra of corresponding networks during their isothermal curing at 150 °C are shown in **Figure 3-2**.

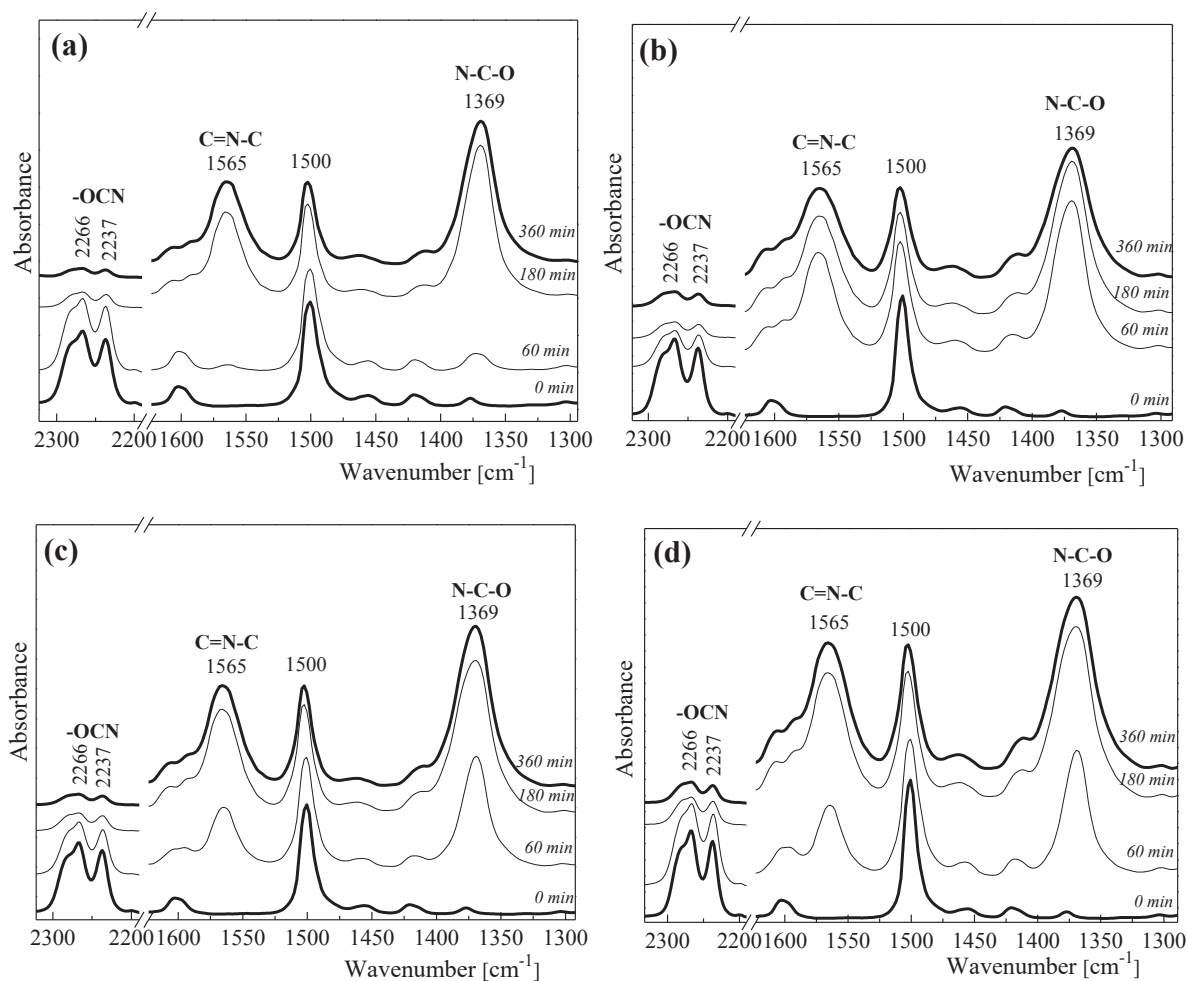


Figure 3-2: Typical FTIR spectra in 2320-1290 cm⁻¹ region during curing procedure for: neat CER (a), CER/[OMIm][BF₄] (b), CER/[HEAIm][Cl] (c), and CER/[PHMG][TS] (d). The spectra were shifted vertically for the sake of clarity.

The absorption doublet at 2266-2237 cm⁻¹ corresponding to -O-C≡N group stretching vibrations diminished with the curing time for pure CER as well as for all the CER/IL networks, while the bands at 1565 and 1369 cm⁻¹, respectively corresponding to valence vibrations of C=N bonds ($\nu_{C=N}$) in C=N-C groups and N-C bonds (ν_{N-C}) in N-C-O groups of cyanurate cycles, appeared [1, 2]. The time dependence of cyanate group conversion (α_c) and reaction

rate ($W = d\alpha/dt$) for neat CER and CER/IL networks is shown in **Figure 3-3**. For pure CER, the induction period of DCBE polycyclotrimerization was equal to about 60 min, whereas for CER/[OMIm][BF₄], CER/[HEAIm][Cl] and CER/[PHMG][TS], the induction period was by 1.5-3.0 times shorter, depending on IL structure (**Table 3-2**).

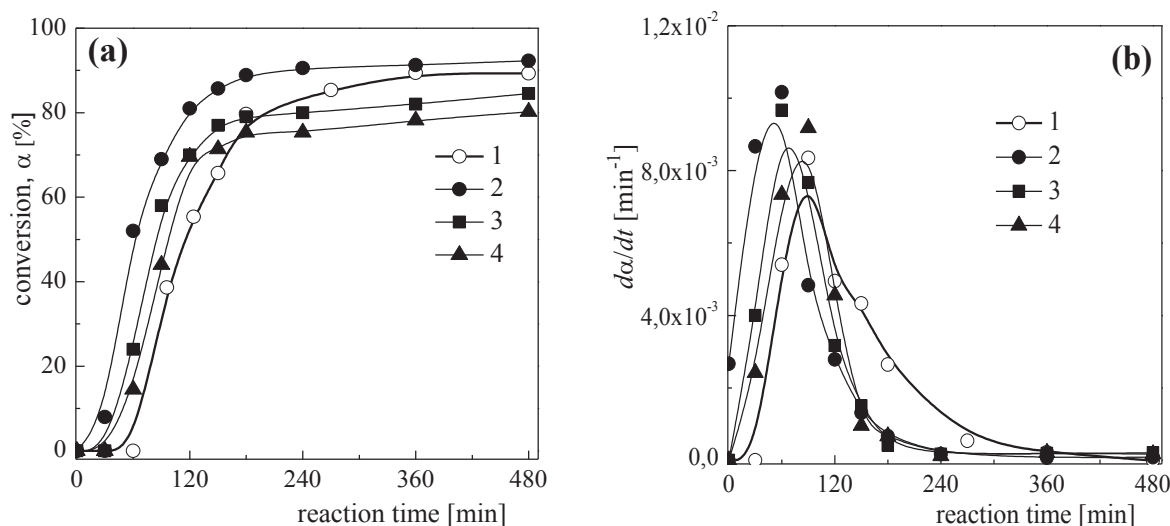


Figure 3-3: Kinetic curves at $T = 150\text{ }^{\circ}\text{C}$: time dependence of (a) conversion (α_c) of $-\text{OCN}$ groups from DCBE and (b) reaction rate ($d\alpha/dt$). Neat CER (1), CER/[OMIm][BF₄] (2), CER/[HEAIm][Cl] (3), and DCBE/[PHMG][TS] (4).

Table 3-2: Kinetic parameters of DCBE polymerization in the absence and the presence of 1.0 wt.% IL

Network	t_i [min]	$W_{\max} \cdot 10^3$ [min ⁻¹]	t_{\max} [min]	α_c [%]
Neat CER	60	8.4	89	89
CER/[OMIm][BF ₄]	20	10.2	52	91
CER/[HEAIm][Cl]	34	9.7	68	82
CER/[PHMG][TS]	40	9.2	83	78

t_i : induction period; W_{\max} : maximal rate of reaction ($W = d\alpha/dt$); t_{\max} : time to maximal rate of reaction; α_c : maximal conversion of $-\text{O}-\text{C}\equiv\text{N}$ groups

In addition, the maximal rate of reaction, W_{\max} , increased by 10-20 % and the time to maximal rate of reaction, t_{\max} , decreased by 7-42 % (**Table 3-2**). Therefore, the introduction of

ILs into the DCBE reaction medium significantly accelerated the conversion of $-O-C\equiv N$ groups from the early stages of CER network formation. It should be noticed that conversion of $-O-C\equiv N$ groups reached the value of $\alpha_c \sim 0.98$ for all the CER networks synthesized after the complete curing schedule. Further, for all CER-based systems, the reaction rate increased dramatically in the kinetic-controlled stage (linear part of conversion vs. time curve in **Figure 3-3a**) until it reached a maximum W_{max} (**Figure 3-3b**). After reaching the gel point, the reaction rate decreased drastically as the polymerization process became diffusion-limited. For all the CER/IL networks, the reaction was faster compared to neat CER (completion after about 360 min).

3.3.2. CER/IL curing mechanisms

The curing mechanisms of CER/IL composites were studied on model reactions starting from DCBE/IL mixtures with a 50/50 wt.% composition. The spectrum of CER/[OMIm][BF₄] showed only characteristic absorbance bands of both individual components (see **Figure 3-4**, curve **3**) that evidenced the chemical inertness of [OMIm][BF₄] towards DCBE. In a previous work [31], we have already proposed the mechanism of DCBE polymerization in the presence of [OMIm][BF₄] *via* the formation of a $[CN]^{\delta+}-[OMIm]^{\delta-}$ complex as a key intermediate (**Figure 3-5**).

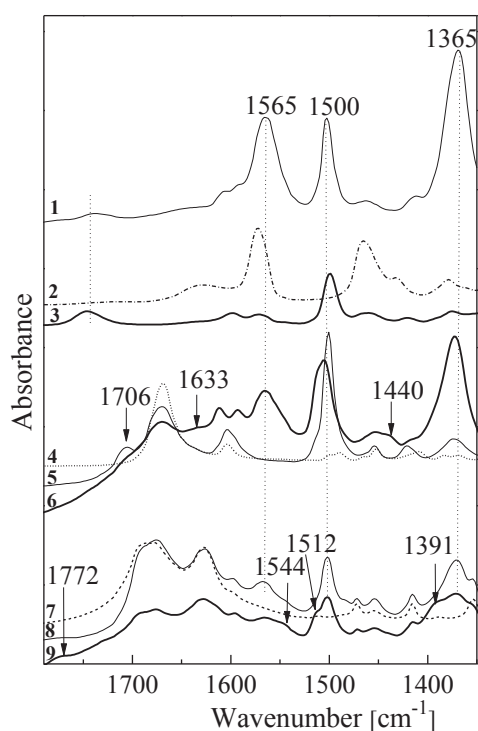


Figure 3-4: FTIR spectra in 1780-1350 cm^{-1} region for: (1) neat CER, (2) [OMIm][BF₄], (3) CER/[OMIm][BF₄] 50/50 wt.%, (4) [HEAIm][Cl], (5) DCBE/[HEAIm][Cl] 50/50 wt.% before curing, (6) CER/[HEAIm][Cl] 50/50 wt.% after curing, (7) [PHMG][TS], (8) DCBE/[PHMG][TS] 50/50 wt.% before curing, (9) CER/[PHMG][TS] 50/50 wt.% after curing. The spectra were shifted vertically for the sake of clarity.

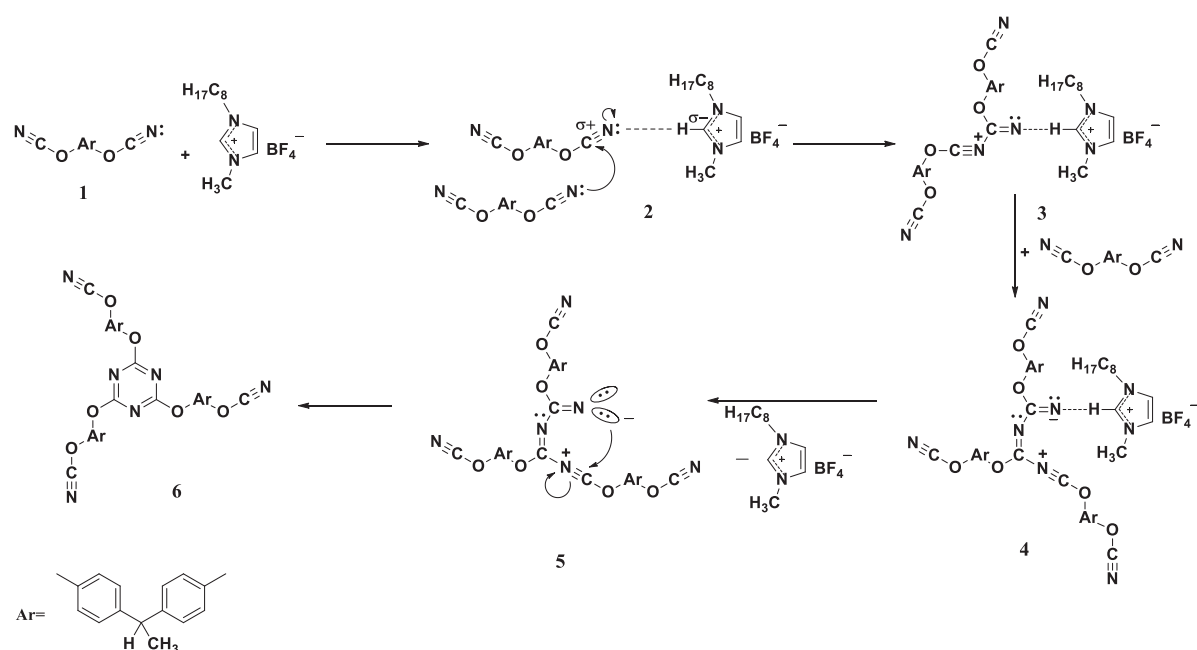


Figure 3-5: Proposed mechanism for [OMIm][BF₄]-catalyzed DCBE polycyclotrimerization.

One could suppose the same mechanism for DCBE polymerization in the presence of [HEAIm][Cl]. However, in the latter case, the competition between the catalytic complex formation and the covalent bonding through the reaction of cyanate groups of DCBE with –OH and >NH groups of [HEAIm][Cl] should be considered. Thus, a three-step mechanism was proposed for the formation of cyanurate cycles from DCBE polymerization being catalyzed by [HEAIm][Cl] (**Figure 3-6**). Our hypothesis was based on the well-known mechanisms of polycyclotrimerization of CERs in the presence of hydroxy [1, 32-35] and amino [36, 37] compounds. First, during the mixing procedure, the –OCN groups of DCBE could react with hydroxyl groups of [HEAIm][Cl] with formation of imidocarbonate O–C(=NH)–O fragment (**Figure 3-6**, compound **2**), which further reacted with a second DCBE molecule with formation of a stabilized dimer (**Figure 3-6**, compound **3**). A third DCBE molecule reacted with the dimer **3**, thus giving rise to the intermediate **4**, which was further transformed into the triazine ring. This transformation could be potentially followed by two mechanisms: either [HEAIm][Cl] release leading to product **5** (cyanurate cycle) or [HEAIm][Cl] incorporation directly into the cyanurate network (**Figure 3-6**, compound **6**) with release of ROH (monocyanate of bisphenol A). According to Grigat and Putter [36] as well as our previous works [33-35], the more acidic phenol compared to alcohol was released, and thus, a substituted triazine ring should be obtained with the release of a monophenol derived from DCBE. Moreover, we presumed that

[HEAIm][Cl] could also increase the polarization of the C=N bond in the imidocarbonate (Figure 3-6, compound 2), thus making the carbon atom of this functional group more electrophilic. This was confirmed by FTIR through the appearance of a shoulder at 1440 cm^{-1} attributed to N–C=O asymmetric vibrations along with a band at 1706 cm^{-1} , which could be related to C=O stretching vibrations in the urea linkage of imidazolidinone (Figure 3-6, compound 4'; see Figure 3-4, curve 6) [38]. The formation of compound 4' from 2 might be possible upon releasing of monophenol derivative through the formation of iminoxazolidine 3', which could also be accompanied by its partial isomerization into compound 4'. Furthermore, the reaction between the secondary >NH groups of [HEAIm][Cl], which were less reactive than –OH groups, was possible as well. The occurrence of structure 3' was confirmed by FTIR with the appearance of a shoulder at 1633 cm^{-1} assigned to the N–H in the isourea linkage [39] (see Figure 3-4, curve 6), which seemed to be formed together with the cyanurate-based compounds (Figure 3-6, compounds 5 and 6). Accordingly, hybrid chemical structures with additional network junctions could be produced for the CER/[HEAIm][Cl] system.

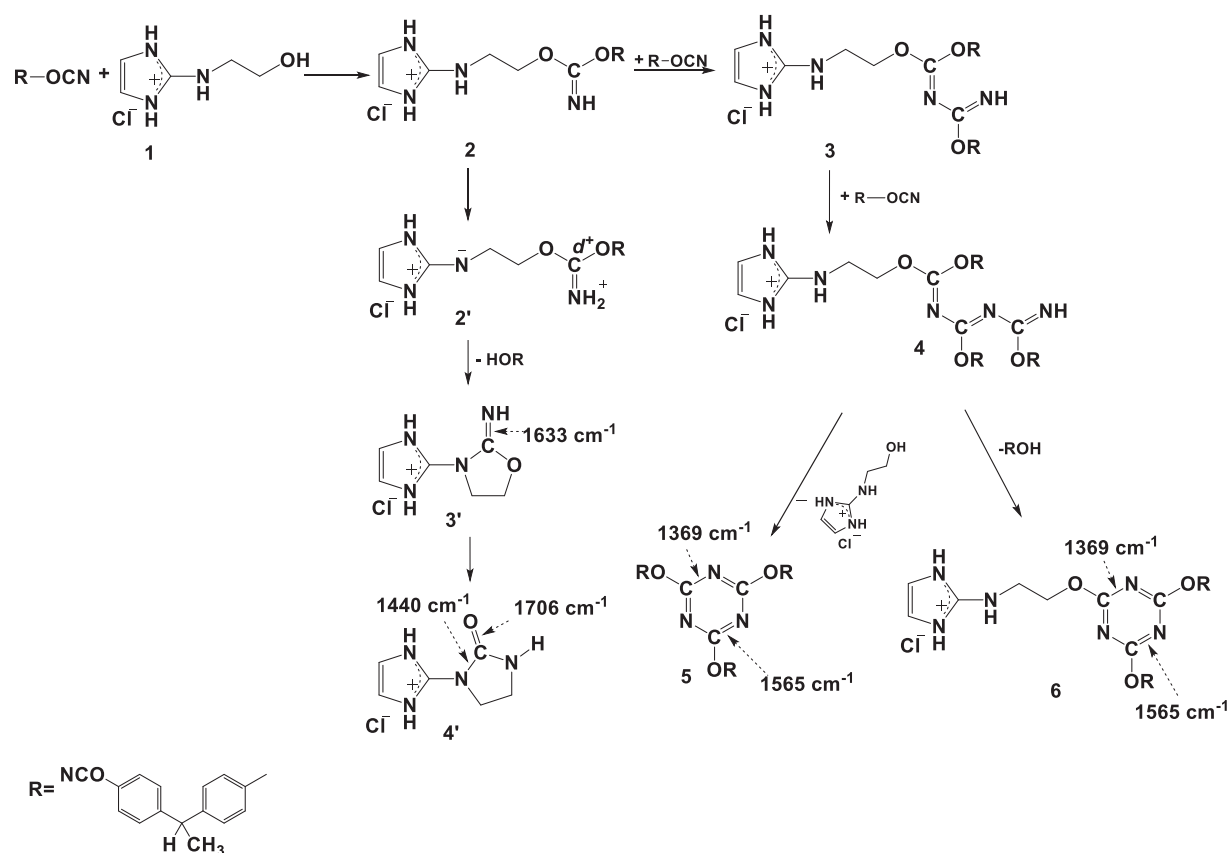


Figure 3-6: Proposed mechanism for [HEAIm][Cl]-catalyzed DCBE polycyclotrimerization.

The proposed mechanism of DCBE polycyclotrimerization process in the presence of [PHMG][TS] was also based on the reactivity of secondary amino groups towards cyanate groups, as represented schematically in **Figure 3-7**. The new strong absorption FTIR bands around 1565 and 1369 cm^{-1} could be attributed to the C=N–C and O–C–N stretching vibrations in cyanurate groups. Two routes of grafting of [PHMG][TS] polymer chains onto the CER network structure were possible. Meanwhile, the existence of a new group conjugated to a triazine ring was proved by the FTIR bands at around 1544 cm^{-1} ($\nu_{\text{C=N}}$) [40] and 1512 cm^{-1} attributed to aromatic ring stretching vibrations (**Figure 3-7**, compound **3'**; see **Figure 3-4**, curve 9). The absorption band at 1391 cm^{-1} could be assigned to the stretching vibrations $\nu_{\text{N-C}}$ [41] associated with groups bridging the triazine rings (**Figure 3-7**, compound **4**). All these observations confirmed the [PHMG][TS] incorporation into the polycyanurate network structure.

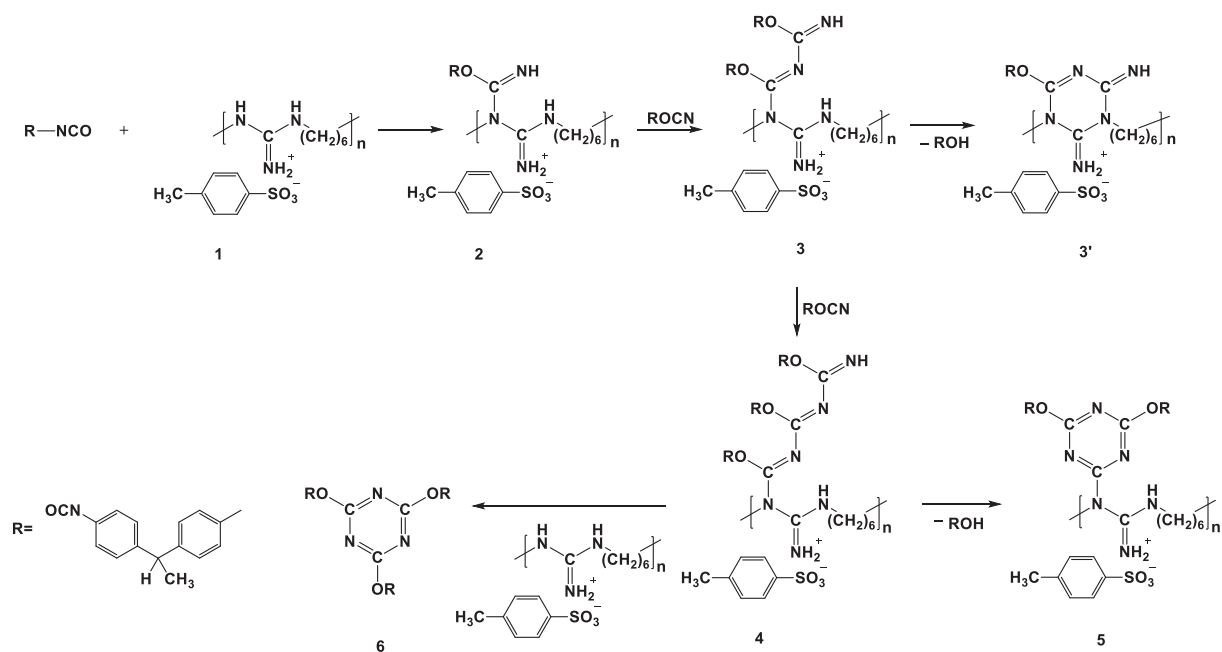


Figure 3-7: Proposed mechanism for [PHMG][TS]-catalyzed DCBE polycyclotrimerization.

Additionally, a band at 1772 cm^{-1} attributed to C=O stretching vibrations appeared in the FTIR spectra of both initial DCBE/[PHMG][TS] mixture and CER/[PHMG][TS] after complete curing (see **Figure 3-4**, curves **8** and **9**). We could suppose that the reaction of cyanate groups from DCBE and CER with traces of water [42] or phenolic impurity could occur to generate an imidocarbonate intermediate (**Figure 3-8**).

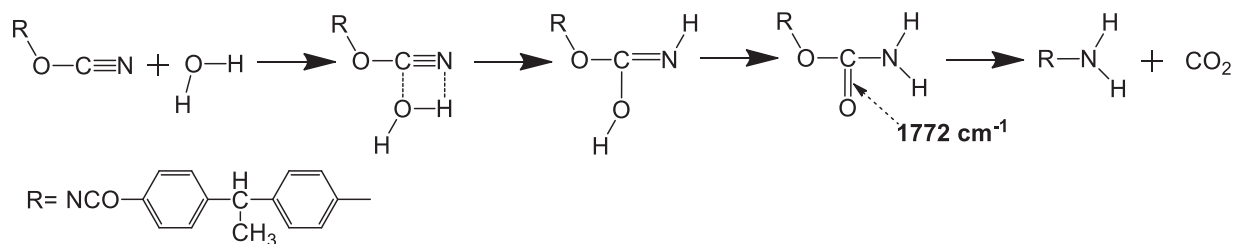


Figure 3-8: Chemical reaction between cyanate groups of DCBE and traces of water or phenol impurity accompanying the DCBE monomer.

3.3.3. Thermal stability of CER-based networks by TGA

The thermal stability of CER/IL networks as well as individual components (*i.e.*, neat CER and ILs) was investigated by TGA (**Figure 3-9**, **Table 3-3**). It is noteworthy that all CER/ILs networks exhibited high thermal stability, similarly to pure CER, as no visible mass loss was observed at temperatures below 420 °C. For all the CER-based networks, the main degradation stage occurred in a temperature range from $T_{d \text{ onset}} \approx 420\text{-}427$ °C to $T_{d \text{ end}} \approx 450\text{-}460$ °C, depending on IL structure. One could also observe some weak degradation stage in a temperature range of $T \approx 500\text{-}640$ °C for all the samples under investigation, which could be attributed to CER mass loss due to the elimination of alkenes and hydrogen, leaving a carbonaceous char containing residual oxygen and nitrogen [43, 44].

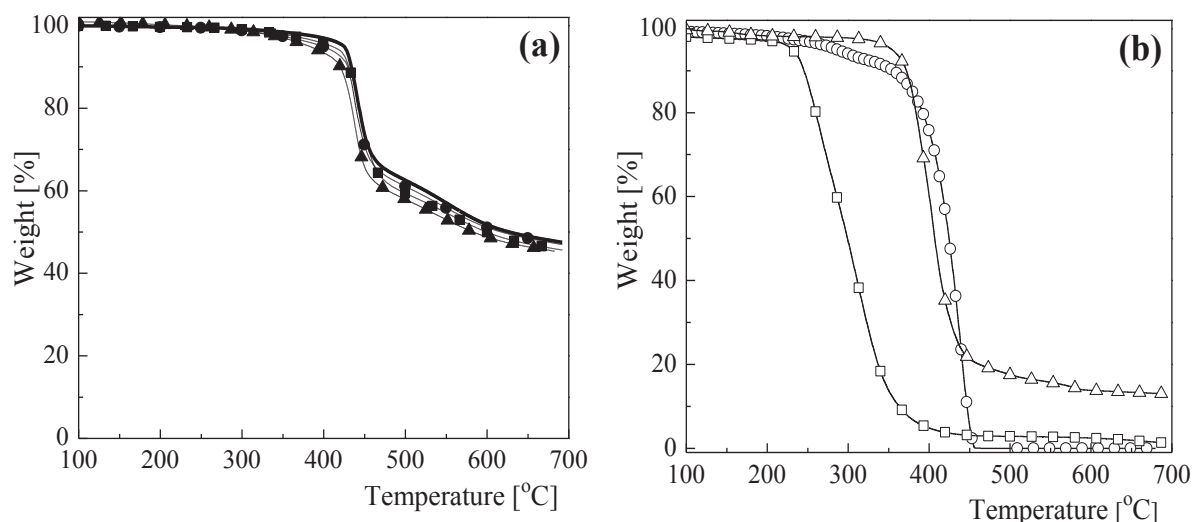


Figure 3-9: TGA curves for CER-based networks (a) and pure ILs (b): neat CER (-), CER/[OMIm][BF₄] (-●-), CER/[HEAIm][Cl] (-■-), CER/[PHMG][TS] (-▲-), [OMIm][BF₄] (-○-), [HEAIm][Cl] (-□-), and [PHMG][TS] (-Δ-).

Table 3-3: Thermal stability of CER-based networks and pure ILs as investigated by TGA

Sample	$T_{d \text{ onset}}^a$ [°C]	$T_{d \text{ max}}^b$ [°C]	Δm^c [%]	Char residue at 680 °C [%]
Neat CER	427	441	33.7	47.5
CER / [OMIm][BF ₄]	425	443	33.1	46.7
CER / [HEAIm][Cl]	424	443	35.1	45.7
CER / [PHMG][TS]	420	438	34.3	45.4
[OMIm][BF ₄]	396	439	91.3	0.0
[HEAIm][Cl]	240	295	94.2	1.3
[PHMG][TS]	372	403	78.1	13.0

^a $T_{d \text{ onset}}$: onset temperature for intensive degradation stage considered; ^b $T_{d \text{ max}}$: temperature of maximum degradation rate for intensive stage considered; ^c Δm : mass loss for intensive degradation stage considered

The thermal stability of CER/[OMIm][BF₄] and CER/[HEAIm][Cl] was quite similar to that of neat CER (see **Figure 3-9**, **Table 3-3**). This meant that using 1.0 wt.% of corresponding ILs did not change significantly the chemical structure and cross-linking density of the CER network. We considered that one such behaviour resulted from the fact that [OMIm][BF₄] had no chemical bonds with the CER network (cf. **Figure 3-5**). [HEAIm][Cl] had a covalent grafting with the cyanurate network but the molecular mass of the IL molecules was too small ($M = 164$ g/mol, see **Table 3-1**), and above all, an amount of 1.0 wt.% was too low to significantly change the chemical structure and notably the cross-linking structure of the CER matrix. Interestingly, despite a thermal stability of pure [HEAIm][Cl] substantially lower than that of other ILs and neat CER (**Figure 3-9b**, **Table 3-3**), the careful analysis of the TGA curve of the CER/[HEAIm][Cl] network did not show the corresponding mass loss (*i.e.* 1.0 wt.%) of the IL in the temperature range in which the main degradation of pure IL occurred. Therefore, the highly crosslinked CER network might prevent the IL from regular thermal degradation, probably due to its chemical incorporation into the CER matrix (see **Figure 3-6**). On the contrary, the CER/[PHMG][TS] network was characterized by a lower thermal stability compared to the other analogues (cf. **Table 3-3**). Obviously enough, one such behaviour might arise from the formation of a CER network with lower cross-linking density and structural regularity, due to the chemical incorporation of relatively long linear polymer fragments of [PHMG][TS] ($M_n = 12,520$ g/mol, see **Table 3-1**) into the CER matrix.

3.3.4. Viscoelastic properties of CER-based networks by DMTA

Figure 3-10 shows the temperature dependence of storage modulus (E') and loss factor ($\tan\delta$) for neat CER and CER/IL networks. All the samples were characterized by high α relaxation temperature values ($T_\alpha > 240$ °C, **Table 3-4**), as typically found for thermostable cross-linked polymers, due to high temperature resistance of cross-links and high cross-linking density of polymer networks [1-6, 32-35]. Unpredictably, a significant effect of the low IL content (*i.e.* 1.0 wt.%) on the viscoelastic properties of all CER/IL networks was found compared to those of pure CER (**Figure 3-10**, **Table 3-4**).

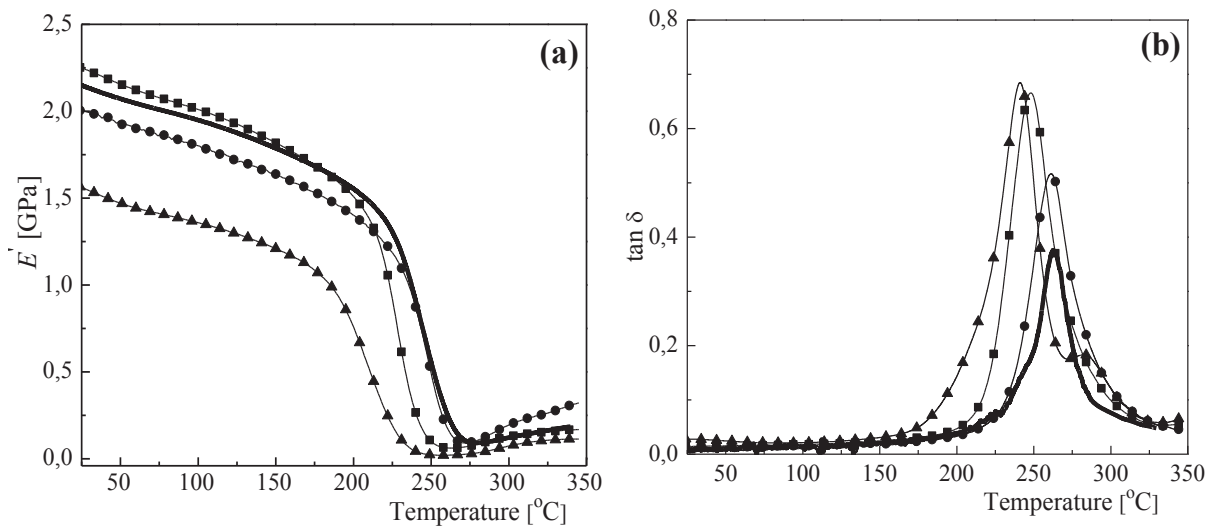


Figure 3-10: Plot of E' (a) and $\tan\delta$ (b) as a function of temperature at 1 Hz for: CER (-), CER/[OMIm][BF₄] (-●-), CER/[HEAIm][Cl] (-■-), and CER/[PHMG][TS] (-▲-).

Table 3-4: Viscoelastic properties of CER-based networks as investigated by DMTA.

Network	T_α^a [°C]	$\tan\delta_{\max}$	ΔT^b [°C]	ΔE_a^c [kJ/mol]	E' [GPa]			$T_{pc(\text{onset})}^d$ [°C]
					20 °C	200 °C	250 °C	
CER	263	0.38	33	292	2.2	1.6	0.60	288
CER/[OMIm][BF ₄]	262	0.52	40	286	2.1	1.4	0.56	277
CER/[HEAIm][Cl]	248	0.67	40	255	2.3	1.5	0.10	268
CER/[PHMG][TS]	242	0.68	42	196	1.6	0.8	0.02	260

^a T_α : α relaxation temperature; ^b ΔT : temperature width at $\frac{1}{2} \tan\delta_{\max}$ height; ^c ΔE_a : apparent activation energy of α relaxation; ^d $T_{pc(\text{onset})}$: onset of temperature of CER post-curing as determined from $E' = f(T)$

As expected, the lowest changes were observed for the CER/[OMIm][BF₄] network. This was probably due to the fact that the IL was not chemically embedded into the CER network structure. Nevertheless, a slight decrease in T_α and E' values as well as an increase in $\tan\delta_{\max}$ and ΔT values were evidenced, thus demonstrating a higher mobility of the kinetic segments between the cross-links of the CER matrix. On the contrary, the chemical incorporation of [HEAIm][Cl] and especially [PHMG][TS] into the CER matrix resulted in a substantial decrease in the values of T_α as well as a significant rise in values of $\tan\delta_{\max}$ and ΔT compared to those for neat CER. Again, these facts evidenced the increase in mobility of the kinetic segments within the CER matrix, due to the reduced cross-linking density of the polycyanurate network in the CER/IL samples. Such changes turned out to be more drastic for the CER/[PHMG][TS] network, due to the chemical incorporation of polymeric chains from the IL into the CER network compared to the grafting of small molecules of [HEAIm][Cl] into the corresponding CER matrix. For the CER/[PHMG][TS] network, a dramatic decrease in E' values was observed in the whole glassy region up to 235 °C (**Figure 3-10a**, **Table 3-4**), which confirmed the aforementioned conclusion on the formation of a CER matrix with more structural defects compared to all other analogues.

Furthermore, the changes in values of apparent activation energy of α relaxation (ΔE_a) calculated for all the samples (**Table 3-4**) confirmed the aforementioned observations. First of all, the temperature dependence of frequency, *i.e.* plots of $\log f$ vs. $(1000/T)$ (**Figure 3-11**), displayed a steep linearity in the region close to 1 Hz ($f = 1.0\text{-}20.0$ Hz), which is typical of the α relaxation. For higher f values (at around $1 \cdot 10^3$ Hz and above), this linearity was lost. From these plots, reliable values of ΔE_a were determined. Indeed, the E_a value can be translated as the amount of energy required to activate the molecular motion and rearrangement of some molecular segments around T_α [45, 46]. The E_a value for the CER/[OMIm][BF₄] network was very close to that for pure CER ($\Delta E_a = 286$ kJ/mol and $\Delta E_a = 292$ kJ/mol, respectively), thus corroborating a similar main transition process related to similar cross-linked structures in both samples because the IL was not chemically embedded into the network. The observed decline in ΔE_a values for CER/[HEAIm][Cl] ($\Delta E_a = 255$ kJ/mol) and CER/[PHMG][TS] ($\Delta E_a = 196$ kJ/mol) was consistent with the hypothesis of the formation of hybrid CER/IL networks with lower cross-linking density and more mobile kinetic segments between junctions due to the chemical incorporation of the ILs into the CER matrix.

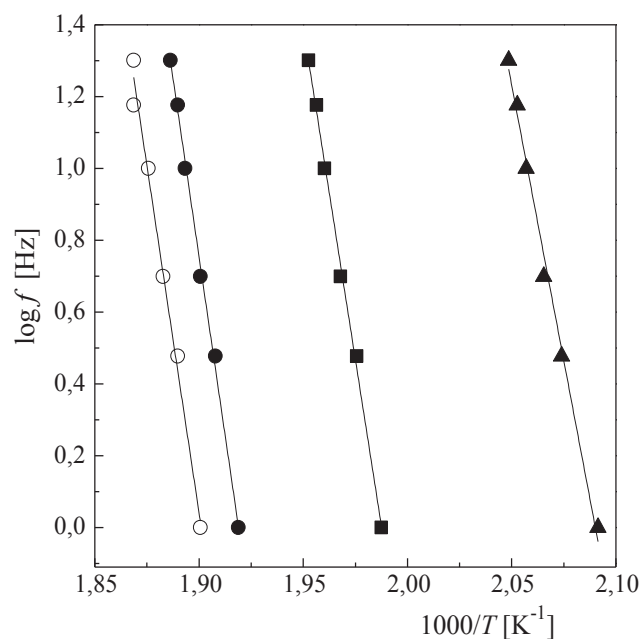


Figure 3-11: Plot of $\log f$ vs. $1000/T$ for: CER (-), CER/[OMIm][BF₄] (-●-), CER/[HEAIm][Cl] (-■-), and CER/[PHMG][TS] (-▲-).

For the CER/[PHMG][TS] network, it is noteworthy that in the $\tan \delta = f(T)$ curve, a second $\tan \delta$ peak was also observed at 284 °C, which could be explained by the post-curing process occurring in the CER matrix, while heating the sample during DMTA measurements above T_α ($T > 240$ °C) [47], due to reaction of high mobility residual $-\text{O}-\text{C}\equiv\text{N}$ groups in the hybrid CER/[PHMG][TS] network. Interestingly, a noticeable increase in the E' modulus above T_α (**Figure 3-10a**) for all the networks was also caused by a post-curing effect which occurred upon heating the samples during DMTA measurements, resulting in some increase in the final cross-linking density of CER/IL networks. As it could be seen from **Table 3-4**, the post-curing started at different temperatures ($T_{\text{pc(onset)}}$) for the different samples: one could assume that the lower the cross-linking density of the cured network, the higher the mobility of the residual $-\text{O}-\text{C}\equiv\text{N}$ groups from CER, and the lower the onset temperature of post-curing.

3.4. Conclusions

This paper thoroughly discussed the kinetic peculiarities of DCBE polycyclotrimerization in the presence of very small amounts (*i.e.* 1.0 wt.%) of ionic liquids with contrasted reactivity, *i.e.* an aprotic IL ([OMIm][BF₄]), a protic IL ([HEAIm][Cl]), and a protic polymeric IL

([PHMG][TS]). Further, the relationships between the structure of the densely cross-linked CER/IL networks and their thermal and viscoelastic properties were compared to those associated with neat CER. A strong catalytic effect of all ILs used on DCBE polycyclotrimerization leading to CER network formation was found, and the IL catalytic activity could be ranked as follows: aprotic [OMIm][BF₄] > protic [HEAIm][Cl] > protic polymeric [PHMG][TS]. Plausible mechanisms for all the DCBE/IL systems were proposed to explain the acceleration effect of the ILs.

One such acceleration effect was significantly higher in the presence of [OMIm][BF₄], due to its chemical inertness towards DCBE monomer. In the case of [HEAIm][Cl] and [PHMG][TS], the chemical grafting of the ILs to CER might occur. The polymer segment mobility and activation energy (E_a) for α relaxation were studied using DMTA for neat CER and CER/ILs networks. All the samples exhibited a high T_α (*i.e.*, 242-262 °C at 1.0 Hz). It was found that the physical incorporation of [OMIm][BF₄] into the CER network had no significant influence on T_α value compared to that of neat CER. On the contrary, the chemical incorporation of both [HEAIm][Cl] and [PHMG][TS] resulted in the significant decrease of T_α values for corresponding CER/IL networks caused by the formation of hybrid chemical structures with lower structural regularity than that of neat CER. Nevertheless, TGA results revealed that the catalytic amounts of ILs had no major influence on the thermal stability of CER-based networks compared to pure CER.

Accordingly, catalytic amounts of ILs used for the synthesis of CER thermosetting materials do not impair their main thermal characteristics, thus keeping their applicability as suitable matrices for aerospace composites or microelectronic devices.

3.5. References

1. Hamerton I.: Chemistry and technology of cyanate ester resins. Chapman & Hall, Glasgow (1994).
2. Fainleib A.: Thermostable polycyanurates: synthesis, modification, structure and properties. Nova Science Publishers, New York (2010).
3. Goertzen W. K., Kessler M. R.: Thermal and mechanical evaluation of cyanate ester composites with low-temperature processability. *Composites Part A: Applied Science and Manufacturing*, **38**, 779-784 (2007).
4. Fang T., Shimp D. A.: Polycyanate esters: Science and applications. *Progress in Polymer Science*, **20**, 61-118, (1995).
5. Fainleib A., Bardash L., Boiteux G., Grigoryeva O.: Thermosetting cyanate ester resins filled with CNTs. In “*Advances in progressive thermoplastic and thermosetting polymers, perspectives and applications*” (Ye. Mamunya, and M. Iurzenko, editors), Tehnopress editura, Iasi, Romania, Chapter 10, 379-424 (2012).
6. Grande D., Grigoryeva O., Fainleib A., Gusakova K., Lorthioir C.: Porous thermosets via hydrolytic degradation of poly(ϵ -caprolactone) fragments in cyanurate-based hybrid networks. *European Polymer Journal*, **44**, 3588-3598 (2008).
7. Throckmorton J., Palmese G.: Acceleration of cyanate ester trimerization by dicyanamide RTILs. *Polymer*, **91**, 7-13 (2016).
8. Handy S. T.: Room temperature ionic liquids: Different classes and physical properties. *Current Organic Chemistry*, **9**, 959-988 (2005).
9. Pârvolescu V. I., Hardacre C.: Catalysis in ionic liquids. *Chemical Reviews*, **107**, 2615-2665 (2007).
10. Wasserscheid P., Welton T.: *Ionic liquids in synthesis*. VCH-Wiley, Weinheim (2002).
11. Zhou J., Cheng L., Wu D.: Ring-opening polymerization of ethylene carbonate using ionic liquids as catalysts. *e-Polymers*, **11**, 883-891 (2011).
12. Kaoukabi A., Guillen F., Qayouh H., Bouyahya A., Balieu S., Belachemi L., Gouhier G., Lahcini M.: The use of ionic liquids as an organocatalyst for controlled ring-opening polymerization of ϵ -caprolactone. *Industrial Crops Products*, **72**, 16-23 (2015).
13. Abdolmaleki A., Mohamadi Z.: Acidic ionic liquids catalyst in homo and graft polymerization of ϵ -caprolactone. *Colloid and Polymer Science*, **291**, 1999-2005 (2013).
14. Ding S., Radosz M., Shen Y.: Ionic liquid catalyst for biphasic atom transfer radical polymerization of methyl methacrylate. *Macromolecules*, **38**, 5921-5928 (2005).
15. Kanno S.: Challenges for unique application of ionic liquids as a novel initiator of radical polymerization. *Molecular Crystals and Liquid Crystals*, **603**, 1-3 (2014).
16. Yang F., Yang J., Zheng K., Stansbury J. W., Nie J.: Electro-induced cationic polymerization of vinyl ethers by using ionic liquid 1-butyl-3-methylimidazolium tetrafluoroborate as initiator. *Macromolecular Chemistry and Physics*, **216**, 380-385 (2015).
17. Wu Y., Han L., Zhang X., Mao J., Gong L., Guo W., Gu K., Li S.: Cationic polymerization of isobutyl vinyl ether in an imidazole-based ionic liquid: characteristics and mechanism. *Polymer Chemistry*, **6**, 2560-2568 (2015).
18. Livi S., Duchet-Rumeau J., Gérard J. F., Pham T. N.: Polymers and ionic liquids: a successful wedding. *Macromolecular Chemistry and Physics*, **216**, 359-368 (2015).
19. Vashchuk A., Fainleib A., Starostenko O., Grande D.: Application of ionic liquids in thermosetting polymers: epoxy and cyanate ester resins. *eXPRESS Polymer Letters*, **12**, 898-917 (2018).
20. Fainleib A., Vashchuk A., Starostenko O., Grigoryeva O., Rogalsky S., Nguyen T. T. T., Grande D.: Nanoporous polymer films of cyanate ester resins designed by using ionic liquids as porogens. *Nanoscale Research Letters*, **12**, p.1-9 (2017).

21. Vashchuk A., Rios de Anda A., Starostenko O., Grigoryeva O., Sotta P., Rogalsky S., Smertenko P., Fainleib A., Grande D.: Structure-Property relationships in nanocomposites based on cyanate ester resins and 1-heptyl pyridinium tetrafluoroborate ionic liquid. *Polymer*, **148**, 14-26 (2018)
22. Dzyuba S. V., Bartsch R. A.: Efficient synthesis of 1-alkyl(aralkyl)-3-methyl(ethyl)imidazolium halides: Precursors for room-temperature ionic liquids. *Journal of Heterocyclic Chemistry*, **38**, 265-268 (2001).
23. Ennis E., Handy T. S.: Facile route to C₂-substituted imidazolium ionic liquids. *Molecules*, **14**, 2235-2245 (2009).
24. Denk M. K., Ye X.: Alkylation of ethylenethiourea with alcohols: a convenient synthesis of S-alkyl-isothioureas without toxic alkylating agents. *Tetrahedron Letters*, **46**, 7597-7599 (2005).
25. Van Krevelen D. W.: Properties of polymers: their correlation with chemical structure: their numerical estimation and prediction from additive group contributions. Elsevier, Amsterdam (2009).
26. Vogel H.: Das temperaturabhängigkeit gesetz der viskosität von flüssigkeiten. *Physikalische Zeitschrift*, **22**, 645-646 (1921).
27. Fulcher G. S.: Analysis of recent measurements of the viscosity of glasses. *Journal of the American Ceramic Society*, **8**, 789-794 (1925).
28. Tammann G., Hesse W.: Die abhängigkeit der viskosität von der temperatur bei unterkühlten flüssigkeiten. *Zeitschrift für anorganische und allgemeine Chemie*, **156**, 245-257 (1926).
29. Williams M. L., Landel R. F., Ferry J. D.: The temperature dependence of relaxation mechanisms in amorphous polymers and other glass-forming liquids. *Journal of the American Chemical Society*, **77**, 3701-3707 (1955).
30. Li G., Lee-Sullivan P., Thring R. W.: Determination of activation energy for glass transition of an epoxy adhesive using dynamic mechanical analysis. *Journal of Thermal Analysis and Calorimetry*, **60**, 377-390 (2000).
31. Fainleib A., Grigoryeva O., Starostenko O., Vashchuk A., Rogalsky S., Grande D.: Acceleration effect of ionic liquids on polycyclotrimerization of dicyanate esters. *eXPRESS Polymer Letters*, **10**, 722-729 (2016).
32. Bershtein V. A., David L., Egorov V. M., Fainleib A. M., Grigorieva O., Bey I., Yakushev P. N.: Structural/compositional nanoheterogeneity and glass transition plurality in amorphous polycyanurate-poly(tetramethylene glycol) hybrid networks. *Journal of Polymer Science Part B: Polymer Physics*, **43**, 3261-3272 (2005).
33. Fainleib A., Grigoryeva O., Hourston D.: Synthesis of inhomogeneous modified polycyanurates by reactive blending of bisphenol A dicyanate ester and polyoxypropylene glycol. *Macromolecular Symposia*, **164**, 429-442 (2001).
34. Fainleib A., Hourston D., Grigoryeva O., Shantalii T., Sergeeva L.: Structure development in aromatic polycyanurate networks modified with hydroxyl-terminated polyethers. *Polymer*, **42**, 8361-8372 (2001).
35. Fainleib A. M., Grigoryeva O. P., Hourston D. J.: Structure-Properties relationships for bisphenol A polycyanurate network modified with polyoxytetramethylene glycol. *International Journal of Polymeric Materials*, **51**, 57-75 (2001).
36. Grigat E., Putter R.: Chemie der Cyansaureester. IV. Umsetzung von Cyansaureestern mit imino- bzw. iminogruppenhaltigen substanzen. *Chemische Berichte*, **11**, 3027-3035 (1964).
37. Bauer J., Bauer M.: Curing of cyanates with primary amines. *Macromolecular Chemistry and Physics*, **202**, 2213-2220 (2001).
38. Nyquist R. A., Putzig C. L., Clark T. D.: Infrared study of 1,3-dimethyl-2-imidazolidinone in various solvents. *Vibrational Spectroscopy*, **12**, 81-91 (1996).

39. Piasek Z., Urbanski T.: The infra-red absorption spectrum and structure of urea. *Bulletin de l'Académie Polonaise des Sciences*, **10**, 113-120 (1962).
40. Arshad M. N., Bibi A., Mahmood T., Asiri A. M., Ayub K.: Synthesis, crystal structures and spectroscopic properties of triazine-based hydrazone derivatives; A comparative experimental-theoretical study. *Molecules*, **20**, 5851-5874 (2015).
41. Guo R., Sanders D. F., Smith Z. P., Freeman B. D., Paul D. R., McGrath J. E.: Synthesis and characterization of thermally rearranged (TR) polymers: effect of glass transition temperature of aromatic poly(hydroxyimide) precursors on TR process and gas permeation properties. *Journal of Materials Chemistry A*, **1**, 6063-6072 (2013).
42. Kimura H., Ohtsuka K., Matsumoto A.: Curing reaction of bisphenol-A based benzoxazine with cyanate ester resin and the properties of the cured thermosetting resin. *eXPRESS Polymer Letters*, **5**, 1113-1122 (2011).
43. Korshak V. V., Gribkova P. N., Dmitrenko A. V., Puchin A. G., Pankratov V. A., Vinogradova S. V.: Thermal and thermal-oxidative degradation of polycyanates. *Polymer Science U.S.S.R.*, **16**, 15-23 (1974).
44. Ramirez M. L., Walters R., Savitski E. P., Lyon R. E.: Thermal decomposition of cyanate ester resins. *Polymer Degradation and Stability*, **78**, 73-82 (2002).
45. Ward I. M., Hadley D. W.: *An introduction to the mechanical properties of solid polymers*. Wiley, New York (1993).
46. Lafia O. A., Imrana M. M. A., Abdullah M. K.: Glass transition activation energy, glass-forming ability and thermal stability of $\text{Se}_{90}\text{In}_{10-x}\text{Sn}_x$ ($x = 2, 4, 6$ and 8) chalcogenide glasses. *Physica B: Condensed Matter*, **395**, 69-75 (2007).
47. Bershtein V., Fainleib A., Yakushev P.: Polycyanurate-based hybrid networks and nanocomposites: structure-glass transition dynamics-dynamic heterogeneity-properties relationships. In *"Thermostable polycyanurates. Synthesis, modification, structure and properties"*. Nova Science Publishers, New York, 2010. Chapter 7, p. 195-246.

CHAPTER 4

Structure-Property Relationships in Nanocomposites Based on Cyanate Ester Resins and 1-Heptyl Pyridinium Tetrafluoroborate Ionic Liquid

Abstract: Novel thermosetting systems based on cyanate ester resins (CERs) have been created through the polycyclotrimerization reaction of dicyanate ester of bisphenol E (DCBE) in the presence of different amounts of 1-heptyl pyridinium tetrafluoroborate [HPyr][BF₄] Ionic Liquid (IL). A significant accelerating effect on the curing kinetics of DCBE was found by FTIR analysis. The reaction mechanism for the [HPyr][BF₄]-catalyzed polycyclotrimerization of DCBE was newly proposed *via* the formation of a [CN]^{δ+}-[HPyr]^{δ-} complex as a key intermediate. Structure-properties relationships for the thermostable CER/IL networks were investigated by using DSC, DMTA, dielectric spectroscopy, tensile testing, quasi-dc measurements (*I-V* characteristics), and TGA. All the nanocomposites showed excellent thermal stability up to 300 °C, indicating the formation of a densely crosslinked network even at high IL content (40 wt.%), and they could be used at high temperatures above their *T*_g without significant thermal degradation. Nanoscale phase separation led to the creation of ionic channels within the CER matrix to ensure photosensitivity properties.

A. Vashchuk, A. Rios de Anda, O. Starostenko, O. Grygoryeva, P. Sotta, S. Rogalsky, P. Smertenko, A. Fainleib, D. Grande: Structure-property relationships in nanocomposites based on cyanate ester resins and 1-heptyl pyridinium tetrafluoroborate ionic liquid. *Polymer*, **148**, 14-26 (2018).

4.1. Introduction

Cyanate Ester Resins (CERs) constitute a family of high performance materials that offer advantages as composite matrices because of their high thermal stability ($T_g > 350$ °C approaching their thermal decomposition temperature) and radiation resistance [1-3]. As compared to other thermosets like epoxy, bismaleimide, and polyimide resins, CER homopolymers present relatively lower dielectric constant (ϵ) and $\tan\delta$ values [4, 5], lower water absorption at saturation and relatively higher toughness [6]. Since all highly cross-linked thermosets tend to be brittle, the use of CERs is limited, and improving their toughness without sacrificing their thermo-mechanical properties is sought. Increasing toughness can be achieved by encapsulating a second phase [7], dispersing inorganic fillers [8-10] or modifying the structure *via* copolymerization reaction [11-12]. The use of conventional plasticizers gives films with poor mechanical stability and limits the performance of related devices [13]. Accordingly, using the unusual properties and designable nature of Ionic liquids (ILs) seems very promising for producing CER materials with controlled structure and properties.

ILs are salts with poorly coordinated ions, and they constitute solvents being liquid below 100 °C, or even at room temperature [14]. At least one ion has a delocalized charge and one component is organic, which prevents the formation of a stable crystal lattice; thereby their properties can be easily tuned by altering the combination of cations and anions [15]. Many ILs have even been developed for specific synthetic problems and have been termed «designer solvents» [16-18]. Due to their unique properties, such as excellent thermal stability, ionic conductivity, relatively low viscosity and low vapour pressure [19-20], ILs represent an alternative to conventional solvents, while avoiding their toxicity and volatility; moreover, they are increasingly used in polymer chemistry as multifunctional agents [21-27].

Recently, novel thermostable nanoporous CER materials have been generated by polycyclotrimerization of dicyanate ester of bisphenol E in the presence of varying amounts (from 20 to 40 wt.%) of 1-heptyl pyridinium tetrafluoroborate ([HPyr][BF₄]), followed by its quantitative extraction after complete CER network synthesis [28]. Thus, our investigations have shown that nanopores with an average pore diameter centered around 45-60 nm may be formed. Interestingly, [HPyr][BF₄] IL has segregated into nanosized phases during the *in-situ* CER network formation. Therefore, CER/IL-based materials may be classified as nanocomposites.

In the present chapter, the effects of [HPyr][BF₄] on the formation peculiarities and properties of CER/[HPyr][BF₄] nanocomposites have been investigated in view of the scarcity on this type of IL-based networks. It is expected that the polymerization of dicyanate esters in the presence of [HPyr][BF₄] may provide the formation of highly thermostable polycyanurate-based nanocomposites, which will afford novel high performance electrolytes and/or separator membranes. To the best of our knowledge, it is the first trial to investigate the influence of [HPyr][BF₄] on the CER curing process and to examine the thermal behavior and viscoelastic properties, as well as the photosensitivity of related nanocomposite materials. The novelty of the present study firstly consists in investigating the catalytic effect of high amounts of a pyridinium-based ionic liquid on the curing kinetics of dicyanate ester of bisphenol E (DCBE), *i.e.* a CER precursor. Secondly, the reaction mechanism for the [HPyr][BF₄]-catalyzed polycyclotrimerization of DCBE is newly proposed. Thirdly, it has also been shown for the first time that the high compatibility of CER matrix with [HPyr][BF₄] due to complex formation allowed for obtaining photosensitive densely crosslinked polymer nanocomposites having excellent mechanical and thermal properties, even at high IL content (up to 40 wt.%).

4.2. Experimental part

4.2.1. Materials

1,1'-bis(4-cyanatophenyl) ethane (dicyanate ester of bisphenol E, DCBE), under the trade name Primaset™ LECy, was kindly supplied by Lonza (Bazel, Switzerland) and used without further purification.

1-heptyl pyridinium tetrafluoroborate, [HPyr][BF₄], was synthesized as described elsewhere [28]. Its purity was confirmed by ¹H NMR spectroscopy [28] and melting point was measured by DSC ($T_m \approx -59$ °C).

4.2.2. Preparation of CER/[HPyr][BF₄] nanocomposites

DCBE was mixed with [HPyr][BF₄] in a given ratio (*i.e.*, the content of [HPyr][BF₄] was varied from 20 to 40 wt.%). A pale yellow transparent solution was obtained even with 40 wt.% IL, thus indicating the macroscopic homogeneity of the mixture. The solution was then degassed in an ultrasound bath at 60 °C for 30 min. The mixture was then poured into a PTFE-

coated mold and cured over the temperature range from 25 to 250 °C with a heating rate of 0.5°C min⁻¹. Attempts were made to produce film by 50 wt.% [HPyr][BF₄], but for one such IL content, exudation on the surface occurred after curing. The polycyclotrimerization of DCBE monomer results in the formation of three-dimensional CER networks (**Figure 4-1**).

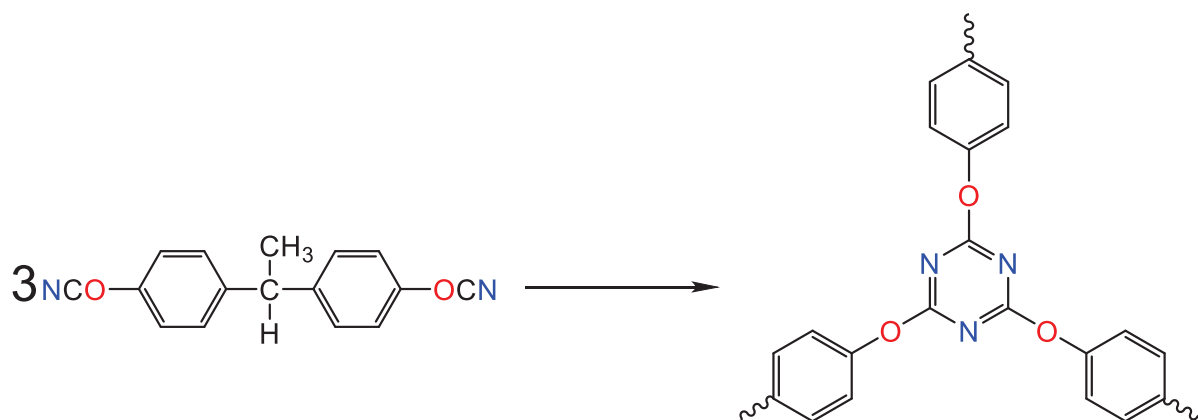


Figure 4-1: Reaction scheme associated with polycyclotrimerization of DCBE.

Nanocomposites were obtained as films with thicknesses of 100 and 900 μm. The following codes were applied to the samples studied: CER₀, CER₁, CER₂₀, CER₃₀, CER₄₀, where the subscripts indicated the [HPyr][BF₄] mass content.

4.2.3. Instrumentation

Kinetic peculiarities of the DCBE polymerization reaction were studied by using Fourier transform infrared (FTIR) spectroscopy in the range of 4000–600 cm⁻¹ using a Bruker Tensor 37 spectrometer. For each spectrum, 32 consecutive scans with a resolution of 4 cm⁻¹ were averaged; all spectra were recorded at room temperature. A given DCBE/[HPyr][BF₄] mixture was deposited on NaCl glass to create a very thin film (a few μm) of the material, and the measurements were performed each 10-30 min of isothermal curing procedure at 150 °C for 6 h. The stretching band of benzene ring at 1501 cm⁻¹ was used as an internal standard.

The conversion of cyanate groups α_c after heating at 150 °C for 6 h was calculated from **Equation 4-1**, as follows:

$$\alpha_c = \left(1 - \frac{I_{(t)2228}/I_{(0)2228}}{I_{(t)1501}/I_{(0)1501}}\right) \times 100 \quad (4-1)$$

where $I_{(t)2228}$ is the intensity of absorption band of –OCN with maxima at 2278 cm^{-1} at time t , $I_{(t)1501}$ is the intensity of benzene ring band at time t , and $I_{(0)}$ is the intensity of absorption bands of the corresponding groups in initial DCBE monomer.

Differential Scanning Calorimetry (DSC) analyses were performed on a TA Q2000 calorimeter under nitrogen atmosphere with a heating rate of 20 °C min^{-1} from 20 to 300 °C. The equipment was regularly calibrated using an Indium standard. About 10 mg of samples were sealed in hermetic aluminum pans and heated. In order to standardize the effects of previous thermal history, the T_g value was determined as the mid-point temperature between the glassy and rubbery asymptotes using the first heating scan.

The densities ρ of all CER films (average value of three measurements) were determined employing the Archimedes principle using isooctane ($\rho = 0.689 \text{ g cm}^{-3}$) as the immersion liquid. The experiments were conducted at room temperature ($T = 25 \text{ °C}$).

Dynamic Mechanical Thermal Analyses (DMTA) were performed on a TA Instruments Q800 analyzer operating with 0.05 % of strain amplitude and a frequency of 1 Hz. The samples were heated from -150 °C to 320 °C at a heating rate of 3 °C/min. The software *IgorPro* was used to analyze the E'' plot data allowing for the identification and study of the secondary and main molecular relaxations as a function of temperature. Such identifications were conducted by fitting the experimental data by purely mathematical Gaussian curves with no physical parameters.

Tensile tests were conducted on four formulations according to the ISO 527-4 norm on an Instron 5965 Universal testing machine equipped with a load cell of 100 N. Samples were cut into dog-bone shapes with a cutting mold giving a specific length of 18 mm and a width of 2 mm. Seven samples per formulation were tested with a crosshead speed of 1 mm/min (corresponding to $\dot{\epsilon} = 3.33 \text{ Hz}$ under a controlled temperature of 21 °C. The Young modulus E for each sample was calculated as the slope of the σ vs. ϵ plot between 0.25 % and 0.5 % of deformation ϵ .

Broadband dielectric measurements were recorded on a Novocontrol Alpha Analyzer equipped with a Quatro Temperature control system. 100 μm -thick samples were cut in disks of diameter 2 cm and were placed in between two upper and lower gold-plated electrodes of 2 and 4 cm in diameter respectively. The electric field voltage was fixed at 3V. The samples were analyzed from -150 $^{\circ}\text{C}$ to 300 $^{\circ}\text{C}$ with 5 $^{\circ}\text{C}$ steps with 41 frequencies ranging from 0.01 Hz to 10^6 Hz for each step. The software WinFit from Novocontrol was used to analyze the 3-D plot data for identifying and quantifying secondary and main molecular relaxations as a function of temperature and frequency.

Quasi-dc measurements of current-voltage (I - V) characteristics were performed by a standard automated tester 14 TKS-100 (Russia). Voltage step-by-step sweeps were applied to 900 μm -thick samples with a 250 ms duration for each step and 90 ms measurement time, respectively. A halogen lamp with a 10 mW cm^{-2} power irradiation was used to obtain the current-voltage characteristics under light conditions. The experiment was conducted at room temperature. The I - V curves were processed by a differential approach based on the determination of dimensionless differential slope α [29, 30], according to **Equation 4-2**:

$$\alpha(V) = \frac{d(\log I)}{d(\log V)} = \frac{dI}{dV} \times \frac{V}{I} \quad (4-2)$$

where dI/dV is the differential conductivity, and $V/I = R$ is the static resistance.

The thermal stability of composites was determined using a Setaram SETSYS evolution 1750 thermobalance, with a platinum pan under 20 mL min^{-1} nitrogen flow at a heating rate of $10 \text{ }^{\circ}\text{C min}^{-1}$ from 20 $^{\circ}\text{C}$ to 700 $^{\circ}\text{C}$. The initial mass of the samples was equal to about 10 mg in all the cases.

Solubility parameters (δ) of DCBE and [HPyr][BF₄] were calculated according to Fedor's Group Substitution Method [31]:

$$\delta = (\Delta E_{\text{coh}}/\Delta V)^{1/2} \quad (4-3)$$

where ΔE_{coh} stands for the total contribution of the structural groups to cohesive energy (E_{coh}) and ΔV is the fragmental molar volume constant.

4.3. Results and discussion

4.3.1. Kinetic peculiarities and proposed mechanism for [HPyr][BF₄]-catalyzed polycyclotrimerization of DCBE

The peculiarities of DCBE polycyclotrimerization in the absence and in the presence of [HPyr][BF₄] were studied using FTIR. In **Figure 4-2**, the FTIR spectra for pure DCBE (**Figure 4-2a**) and all the CER/[HPyr][BF₄] samples studied (**Figure 4-2b-d**) at their isothermal heating (150 °C for 6 h) are shown. For neat CER₀, after some induction time for ~60 min, the gradual decrease in the intensity of the bands of cyanate (–OCN) groups at 2266–2235 cm⁻¹ was observed (**Figure 4-2a**), and the appearance of bands at 1563 and 1366 cm⁻¹ corresponding, respectively, to C=N–C groups and N–C–O groups of cyanurate cycles, was evidenced (**Figure 4-3**). Interestingly, for all the CER/[HPyr][BF₄] samples, *i.e.* for CER₁ (**Figure 4-2b**), CER₂₀ (**Figure 4-2c**) and CER₄₀ (**Figure 4-2d**), after a shorter induction time, the intensity of the bands at 2266–2235 cm⁻¹ decreased quite steeply, and the bands at 1563 and 1366 cm⁻¹ (**Figure 4-3**) clearly appeared, thus evidencing the formation of polycyanurate crosslinked structures.

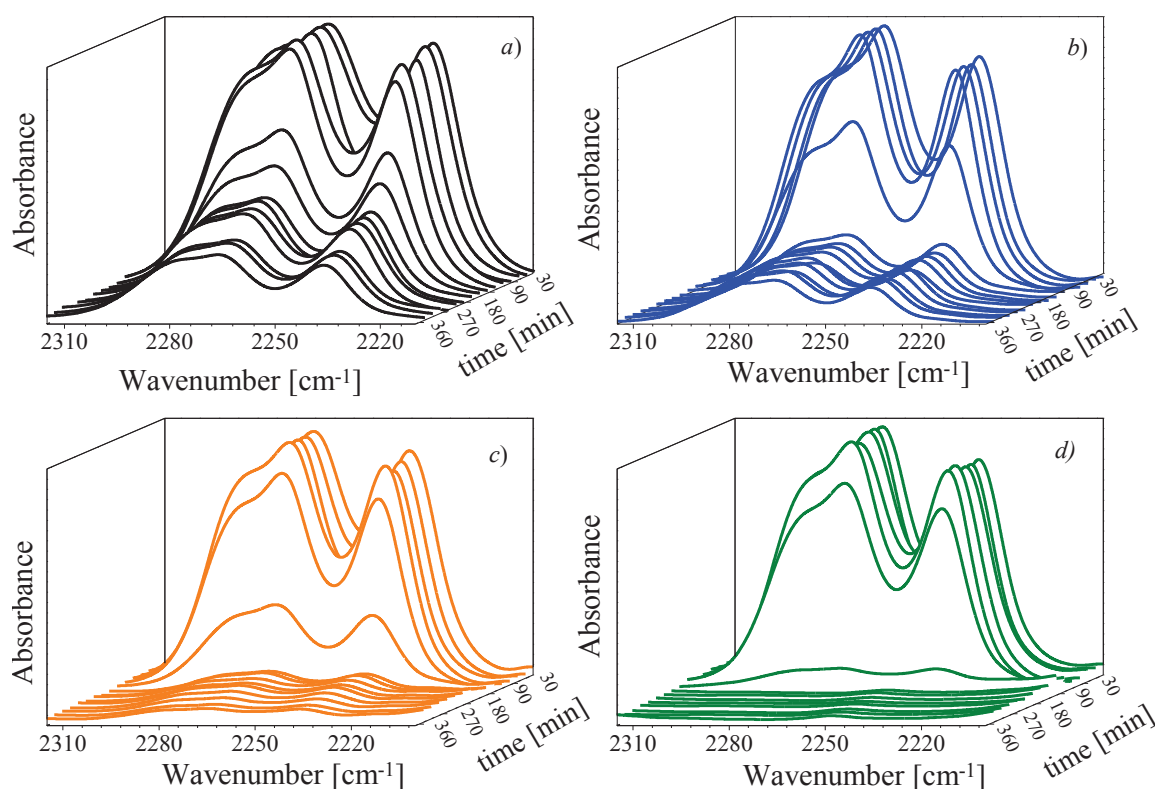


Figure 4-2: FTIR spectra in the spectral zone of 2310-2200 cm⁻¹ obtained at isothermal curing ($T = 150\text{ }^{\circ}\text{C}$ for 6 h) of pure DCBE (a) and DCBE/[HPyr][BF₄] samples: CER₁ (b), CER₂₀ (c), and CER₄₀ (d).

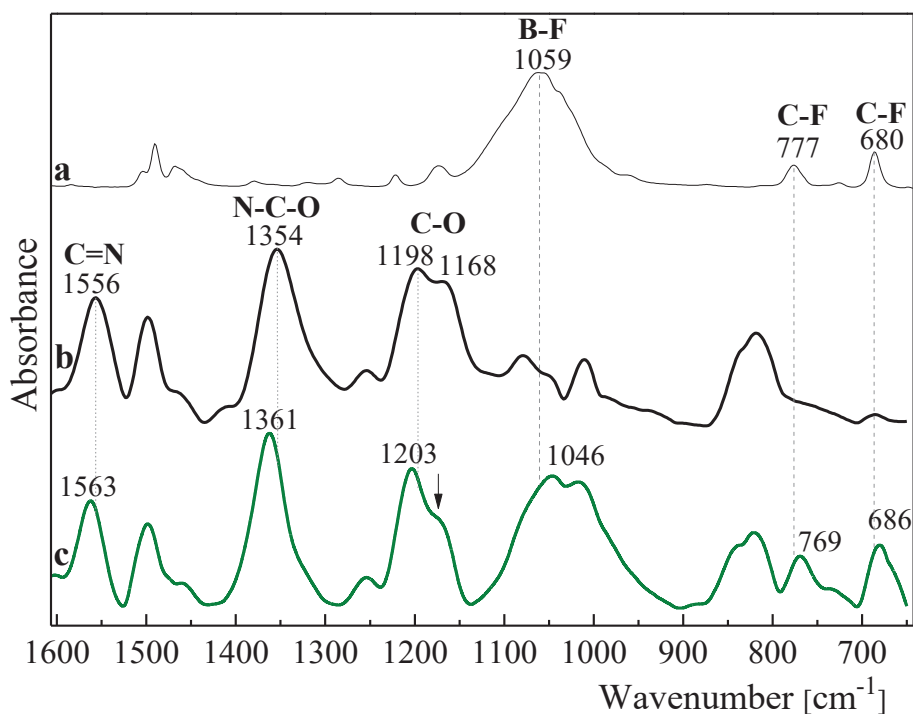


Figure 4-3: FTIR spectra in the spectral zone of 1600-650 cm^{-1} for pure [HPyr][BF₄] (a), CER₀ (b), and CER₄₀ (c).

The conversion values (α_c) of O–C≡N groups associated with the different [HPyr][BF₄] contents was calculated using FTIR data. **Figure 4a** illustrates the fractional conversion (α_c) of –OCN groups calculated according to **Equation 4-1**. It is clearly seen that polycyclotrimerization of DCBE is characterized by the presence of some induction time for pure DCBE as well as for the all compositions studied depending on the IL content. Unpredictably, the introduction of the smallest content of IL (1.0 wt.%) led to the largest decrease in the induction time, *i.e.* from ~60 min (for neat DCBE) to ~30 min, as well as to a significant enhancement of both the fractional conversion, α_c , and the reaction rate values (cf. **Figure 4-4b**) as compared to neat CER₀. One could conclude that the presence of even 1.0 wt.% of [HPyr][BF₄] significantly accelerated the conversion of –OCN groups from DCBE to lead to CER₁ network formation. Surprisingly, increasing the IL content up to 20 and 40 wt.% resulted in some increase in the induction time compared to CER₁ sample, probably due to a dilution effect. Indeed, it was possible that during the sample curing the propagation step became diffusion-controlled, instead of being chemically controlled. However, similarly to the CER₁ sample, the strong increase in α_c (**Figure 4-4a**) and reaction rate values (**Figure 4-4b**) were observed for CER₂₀ and CER₄₀ samples compared to neat CER₀. Furthermore, some other logical dependence could also be clearly seen, *i.e.* the higher content

of [HPyr][BF₄], the higher values of reaction rate and maximal fractional conversion, a_c . It is noteworthy that after reaching the gel point, the reaction became diffusion-limited, and the presence of ionic liquid [HPyr][BF₄] obviously facilitated the species diffusion and further reaction of -OCN groups of growing CER network. Accordingly, only the highest content of IL (40 wt.%) permitted to achieve full conversion (~ 100 %) (**Figure 4-4a**).

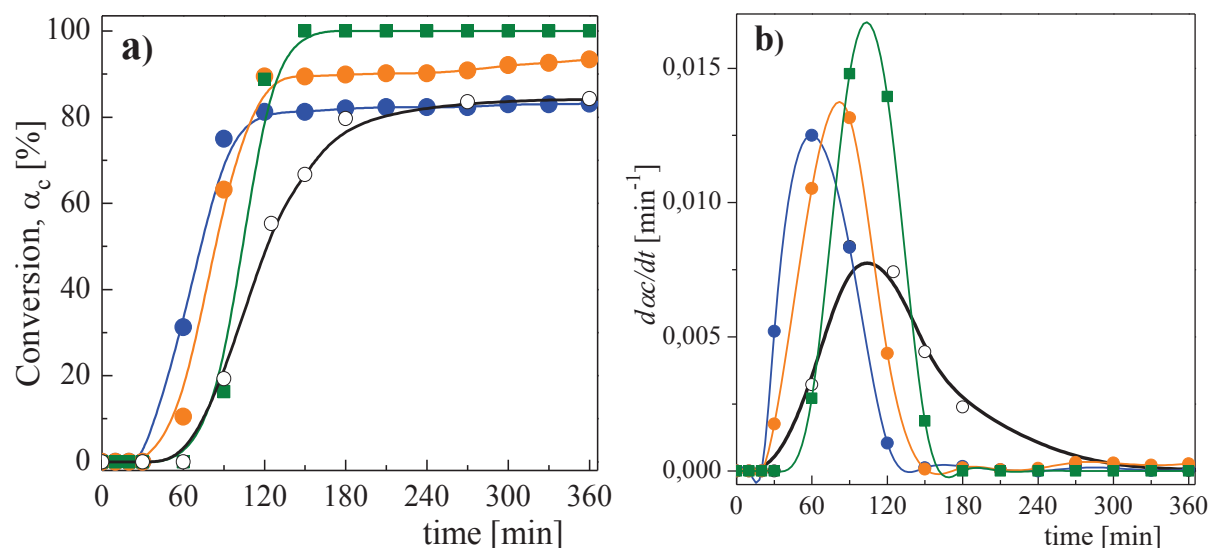


Figure 4-4: Kinetic plots of (a) -OCN groups fractional conversion, a_c , and (b) reaction rate, $d\alpha_c/dt$, versus curing time: CER₀ (○), CER₁ (●), CER₂₀ (●), CER₄₀ (■)

It could be concluded that a significant acceleration of -OCN conversion during DCBE polycyclotrimerization as well as increasing values of reaction rate and maximal fractional conversion resulted from the effect of [HPyr][BF₄]. The polycyclotrimerization reaction is known to be promoted by heat and a range of catalysts including Lewis acids, such as TiCl₄ [32]. The catalytic effect of aprotic ionic liquid 1-octyl-3-methylimidazolium tetrafluoroborate on the polycyclotrimerization reaction of DCBE has recently been reported [33]. The proposed possible mechanism included the stabilization of pseudo-nitrilium ions due to the formation of a complex with acidic C2-H hydrogen of imidazolium cation. It should be noted that imidazolium ionic liquids were found to act as Lewis acid catalysts in the Diels-Alder reaction of cyclopentadiene with crotonaldehyde and methacrolein [34] or with methyl acrylate [35]. In latter case, it was demonstrated that the rate enhancement was due to an explicit hydrogen bond between the cation of the ionic liquids and the carbonyl group of the methyl acrylate [35].

In the present investigation, the DCBE polycyclotrimerization reaction was also found to be accelerated by another aprotic ionic liquid, *i.e.* 1-heptyl pyridinium tetrafluoroborate, [HPyr][BF₄]. The ability of pyridinium-based ionic liquids to act as Lewis acid catalysts in the Diels-Alder reaction has also been reported [36]. Indeed, the pyridinium cation contains weakly acidic hydrogens in 2 and 6 positions which could play a role of hydrogen bond donors stabilizing pseudo-nitrillium ions (**Figure 4-5**).

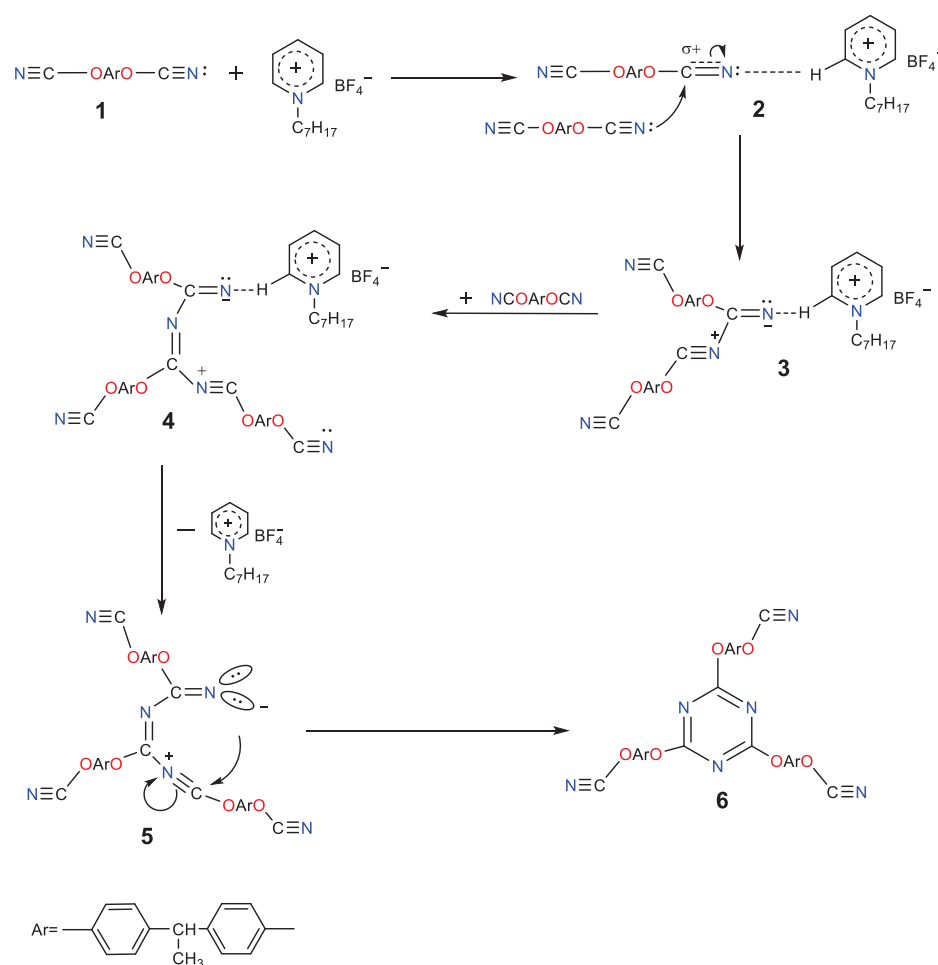


Figure 4-5: Proposed mechanism for [HPyr][BF₄]-catalyzed polycyclotrimerization of DCBE.

Interestingly, FTIR investigations showed a shift of 5-8 cm⁻¹ toward higher frequencies for the bands of CER₄₀ attributed to the triazine ring compared to neat CER₀ (cf. **Figure 4-3**). On the contrary, the bands corresponding to [BF₄]⁻ were shifted by 6-13 cm⁻¹ to lower frequencies, thus indicating that B-F and C-F were more stretched. At the same time, the vibration bands of the pyridine ring appeared at approximately the same frequencies and implied that [HPyr]⁺ did not have a strong influence on the IL-CER matrix interactions. The

latter may be explained by the formation of intermolecular hydrogen bonds between BF_4^- anion and acidic $\text{C-H}^{2/6}$ groups of the 1-alkylpyridinium cation [37] thus preventing their physicochemical interaction with polymer. The noticeable shift of B-F band absorption may indicate the interaction of tetrafluoroborate anions with electrophilic centers of triazine rings located at carbon atoms (**Figure 4-6**). Such interactions may also cause the observed shift of C=N, C-O, and N-C-O stretching bands (**Figure 4-3**).

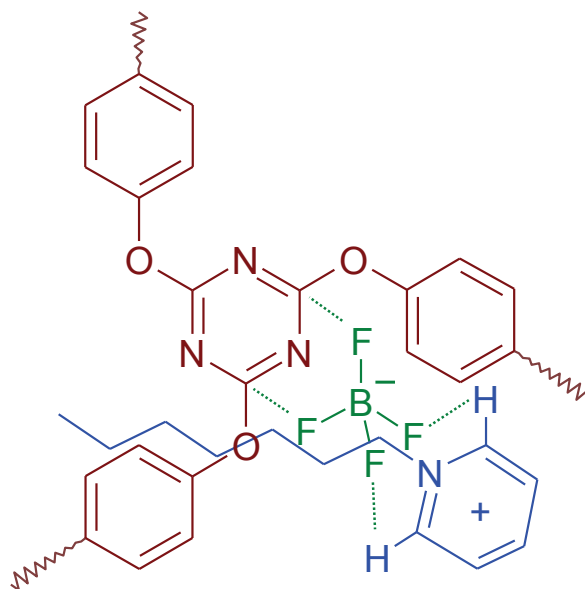


Figure 4-6: Scheme for complex formation in CER/[HPyr][BF_4] networks.

4.3.2. Molecular mobility and viscoelastic properties of CER/[HPyr][BF_4] nanocomposites

4.3.2.1. DSC investigation

Figure 4-7 shows the DSC thermograms obtained for the CER-based samples under investigation, and the corresponding thermal characteristics are summarized in **Table 4-1**. It should be stressed that, since these materials were highly crosslinked, it was difficult to characterize their T_g , and thus rapid heating rates had to be applied. This could be seen itself in **Figure 4-7** for the CER₄₀ sample. For this sample after the step-like transition, an overshoot (*i.e.* the baseline was not reached) was observed. This phenomenon was certainly due to a rapid change in volume of the sample provoked when reaching the glass transition. Further, it could be seen that there was no residual curing reaction, implying that the samples were fully cured. Then, it should be mentioned that the presence of a single T_g value for the CER/[HPyr][BF_4]

nanocomposites would suggest a homogeneous dispersion of the IL within the CER matrix. CER₀ showed a T_g value around 235 °C, and using 40 wt.% [HPyr][BF₄] reduced the T_g value to 66 °C (**Table 4-1**). Such a dramatic decrease resulted from the increase in the polymer chain mobility, due to the IL acting as a plasticizing effect. A broadening of glass transitions with increasing plasticizer contents was observed (**Table 4-1**), which was attributed to the heterogeneity of the composite systems. The values of glass transition temperatures for CER/[HPyr][BF₄] networks were higher than that measured by DSC for the CER/Dicyanamide IL system described in the literature, where a nearly 100°C decrease in T_g at 10 wt.% IL loading was obtained [38]. It is noteworthy that a decrease in the value of T_g contributes to easier movements of polymer chains, and as a result, an increase in the conductivity is expected. In addition, for CER/[HPyr][BF₄] networks, a significant shift of the glass transition temperature onset ($T_{g \text{ onset}}$) toward lower values was observed in all the compositions (cf. **Table 4-1**) compared to the individual CER₀. One such decrease was also associated with a plasticizing effect of [HPyr][BF₄].

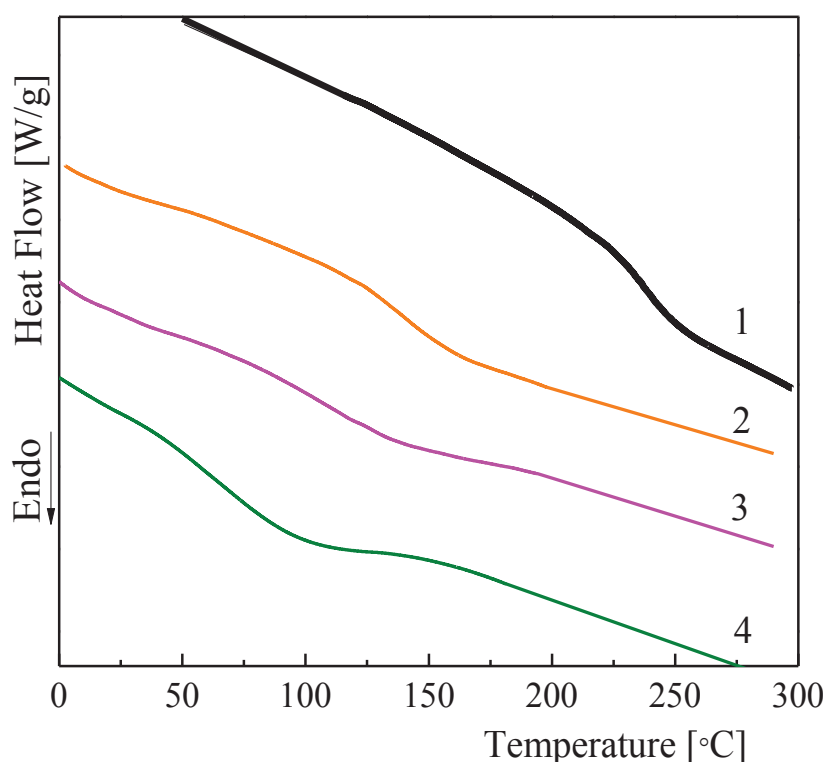


Figure 4-7: DSC thermograms for CER/[HPyr][BF₄] networks: CER₀ (1), CER₂₀ (2), CER₃₀ (3), CER₄₀ (4).

Table 4-1: Thermal and mechanical characteristics for CER/[HPyr][BF₄] nanocomposites

Samples	DSC			DMTA							Tensile	
	T_g^1	$T_{g\text{onset}}^2$	ΔT_g^3	$T_{\alpha(\tan\delta)}^4$	$T_{\alpha(E')}^5$	E' ⁶ [MPa] at		E'_R ⁷	ρ	G_R ⁸	E^9	σ
	[°C]	[°C]	[°C]	[°C]	[°C]	-140°C	T_{α}	[MPa]	[g/cm ³]	[MPa]	[MPa]	[M
CER ₀	235	216	36	293	277	4442	922	30	1.259	17	2050 ± 244	±
CER ₂₀	135	116	41	217	160	4846	1196	11	1.268	16	3074 ± 12	±
CER ₃₀	106	75	57	151	98	4950	1714	9	1.253	13	2259 ± 142	±
CER ₄₀	66	37	57	111	57	5005	2097	7	1.247	12	1796 ± 90	=

¹ T_g : midpoint temperature of the heat capacity jump; ² $T_{g\text{onset}}$: value associated with the intercept of tangent to midpoint of the sp baseline; ³ $\Delta T_g = T_{g\text{end}} - T_{g\text{onset}}$: width of glass transition range, where $T_{g\text{end}}$ stands for the temperature value associated with the specific heat increment with the «rubbery» baseline; ⁴ $T_{\alpha(\tan\delta)}$: glass transition temperature determined from $\tan\delta$; ⁵ $T_{\alpha(E')}$: glass E' data; ⁶ E' : storage modulus; ⁷ E'_R : storage modulus at the rubbery plateau; ⁸ G_R : calculated theoretical storage modulus at the ¹⁰ σ_S : Yield stress value; ¹¹ ϵ_R : elongation at break; ¹² $T_{d\ 5\%}$: temperature values for a 5% mass loss; ¹³ $T_{d\ \text{max}}$: temperature value of

It could be plausible that, in the case of CERs, the network swelled in the presence of IL and the forces of attraction between the polymer chains exceeded the forces of attraction between the IL molecules and the chain components. There was an exchange of secondary bond interactions, thus leading to an increase in the free volume of the network, and potentially a softening due to the fewer chain-chain interactions and an increasing plasticizing effect. The effect of [HPyr][BF₄] on the CER network described as a plasticizer is the separation of the polymer chains by a molecule that does not form covalent bonds with the chains [28], but simply serves as a space occupier. Thus, such materials are potentially crosslinked polymers that may contain [HPyr][BF₄] as well as low molecular weight reaction products between cross-links (**Figure 4-8**). To obtain a numerical estimation of the degree of interaction between [HPyr][BF₄] and DCBE, the values of solubility parameters were calculated. It was determined that $\delta_{[\text{HPyr}][\text{BF}_4]}$ was equal to $18.7 \text{ (J/cm}^3)^{1/2}$ for [HPyr][BF₄] and δ_{DCBE} was equal to $24.5 \text{ (J/cm}^3)^{1/2}$ for DCBE. It is known that the higher the difference between the solubility parameter values, the higher the degree of phase separation. Based on this assertion, the [HPyr][BF₄] could then be recovered from CER/IL nanocomposites by ethanol extraction to design nanoporous frameworks with controlled morphology and porosity [28].

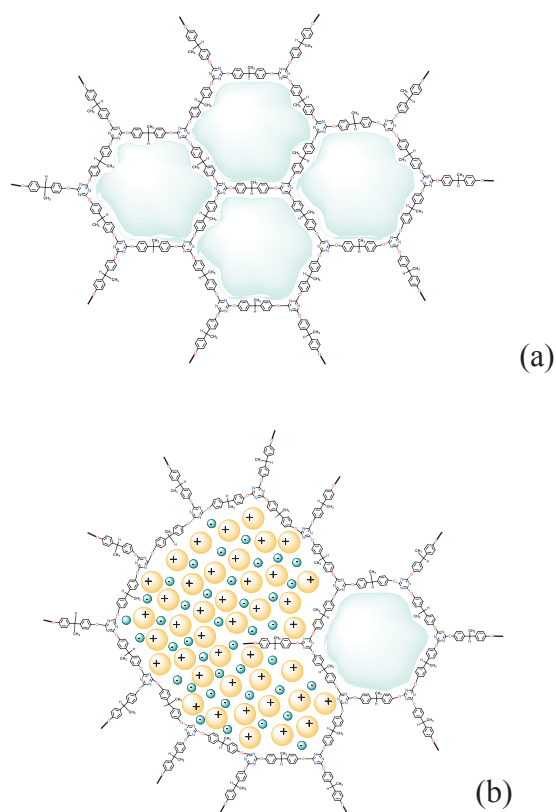


Figure 4-8: Scheme of CER matrix (a) and agglomerated IL in the CER matrix (b).

Therefore, the main effect of [HPyr][BF₄] was the reduction of interchain interactions, such as entanglements and secondary bonding.

4.3.2.2. Dynamic Mechanical Thermal Analysis

The effect of [HPyr][BF₄] on the viscoelastic properties of CER/[HPyr][BF₄] composite networks was then evaluated by DMTA. Figure 4-9 shows the variation in storage modulus (E') and $\tan\delta$ as a function of temperature for the CER networks with different [HPyr][BF₄] contents. The E' value is closely related to the load-bearing capacity of a material, which is an important parameter reflecting its stiffness. It is noticeable that the incorporation of [HPyr][BF₄] led to an increase in E' compared to the CER₀ network in the temperature range below the glass transition (**Table 4-1**), which could be explained by an improvement of stiffness due to complex formation between [BF₄]⁻ and C atoms of the CER matrix. Then, with increasing temperature, this complex was destroyed, and the presence of detached [HPyr][BF₄] led to reduced T_α values. All systems also displayed E' value at T_α higher than that of neat CER₀ (from 0.9 to 2.1 GPa for CER₄₀), *i.e.* CER₄₀ showed about 44% improvement compared to CER₀ which was considered to be significant. This behavior may be attributed to the presence of an aromatic ring in the [HPyr][BF₄] structure, which imparts a higher stiffness to the CER chains. According to rubber elasticity theory, the value of storage modulus above T_α may be related to the crosslink density. The theoretical storage modulus at the rubbery plateau G_R was calculated from **Equation 4-4** [53,54].

$$G_R = \frac{2\rho RT}{3M_C} \quad (4-4)$$

where ρ is the density, R is the ideal gas constant (8.314 J mol⁻¹ K⁻¹), T is the temperature (usually $T_\alpha + 50^\circ\text{C}$) and M_C is the molar mass between crosslinks, which for these materials was considered to be 212 g/mol. For both the experimental E_R' and the theoretical G_R moduli at the rubbery plateau, it was firstly observed that their values were comparable and had the same order of magnitude (see **Table 4-1**). In the case of “classical” elastomeric crosslinked polymers, where the distance between crosslinks is of at least 50 monomeric units, the modulus at the rubbery state is of *ca.* 0.1 to 1 MPa [53]. Our theoretical and experimental values (of *ca.* 20-30 MPa) correspond to a polymer at the rubbery state where the distance between crosslinks is typically that of one monomeric unit, thus confirming the proposed network chemical structure. Therefore, it could be concluded that **Equation 4-4** is not only limited to “classical” elastomers,

but it may also be extended to denser crosslinked materials, as long as the storage modulus is carefully taken in the elastomeric regime [53,54].

It is then seen that when the concentration of [HPyr][BF₄] increased, the values of such moduli decreased. This effect was more pronounced in the systems modified with 40 wt.% [HPyr][BF₄] which then could be explained by the presence of long alkyl chains in the pyridinium-based IL that did not react with the CER network [28].

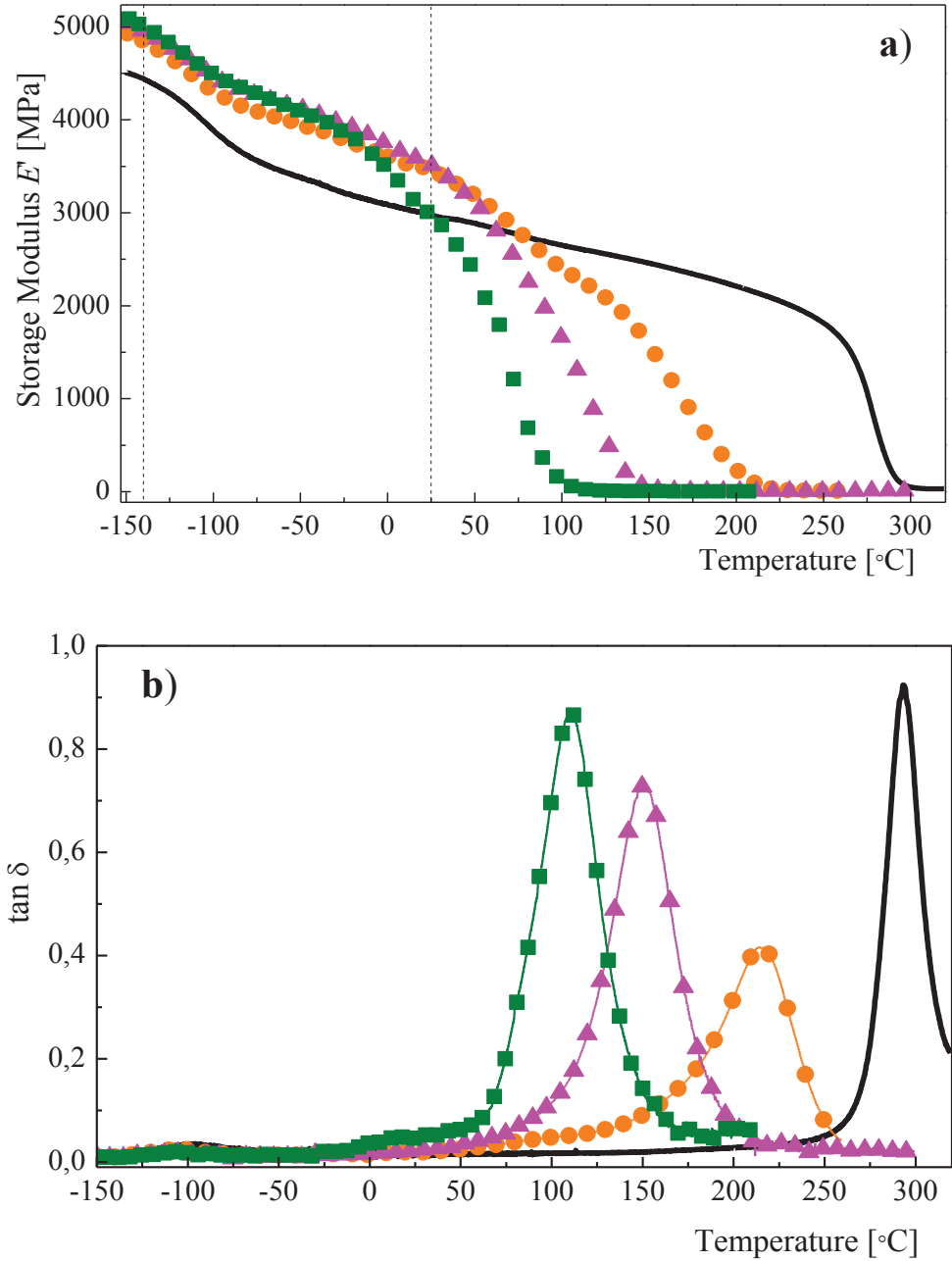


Figure 4-9: Dependence of storage modulus E' (a) and loss factor $\tan \delta$ (b) on temperature at 1 Hz for CER and CER/[HPyr][BF₄] networks: CER₀ (-), CER₂₀ (o), CER₃₀ (▲), CER₄₀ (■).

It is well known that the $T_{\alpha(\tan\delta)}$ values are widely considered to be equivalent to the calorimetric T_g in literature. It is important to mention that the data obtained from DSC were much lower (typically 50-60% lower, see **Table 4-1**) than $T_{\alpha(\tan\delta)}$ evaluated from the $\tan\delta$ peak of DMTA curves as they approached $T_{\alpha(E')}$ and $T_{\alpha(E'')}$. The main reason for this is that DSC characterizes the enthalpy change induced by local segmental motion, which is reliable to define T_g , whereas this change is relatively small in the case of highly crosslinked materials. Therefore, it is difficult to detect the change step in DSC, while in DMTA, the dynamic modulus variation, which is more sensitive, is used to identify this transition temperature. This makes DMTA a preferred technique for measuring T_g 's of highly filled materials, such as composites.

Furthermore, it was clear that the $\tan\delta$ peak was shifted towards lower temperatures when the [HPyr][BF₄] content was increased (**Figure 4-9**). Moreover, the $T_{\alpha(\tan\delta)}$ peak became broader with the addition of [HPyr][BF₄], because of an increase in the molecular dynamic heterogeneity in the system induced by the IL presence. On the other hand, no peak doubling could be observed, thus indicating good compatibility between [HPyr][BF₄] and the CER matrix. This was confirmed in **Figure 4-10** in which CER₂₀ had a considerably smaller loss modulus E'' in the transition region compared to CER₀. This molecular miscibility diminished when the [HPyr][BF₄] concentration increased. For CER₃₀ and CER₄₀, E'' tended to increase towards the values for pure CER. This can be explained by the ILs leading to the formation of ionic aggregates in which IL ions were close together (**Figure 4-8**), and the chain mobility could be increased resulting in a decrease in the rubbery modulus.

The loss modulus (E'') can be considered to be more sensitive to molecular motions in polymer chains than E' for stiff polymers. Therefore, the E'' curve was deconvoluted by the contribution of single relaxation processes, which when summed through a fit yielded the experimental curve. This deconvolution showed four distinct peaks, with the observed following features (**Figure 4-10**): (i) the one at higher temperature was due to the α -relaxation, while the other ones at lower temperatures were identified as β - and γ -relaxation; (ii) the intensity of the low-temperature sub- T_{α} process was much lower than that of the α -relaxation. All materials exhibited a broad transition interval of temperatures, with a maximum near -100 °C associated with the γ -relaxation of CER, which could be ascribed to the motion of the phenylene groups present in the links between the planar six-member three-arm cyanurate structures [39-42]. The secondary transition, appearing as a shoulder around -50 °C in the CER materials, was a shifted β -relaxation, attributed to the motions of chain fragments between

network junctions [39-42]. Two further molecular relaxations of low intensity between the β and α relaxations were also detected. These relaxations were named β' and β'' . These relaxations appeared to be well separated from β and α processes. A discussion concerning their origin was further developed. In the frame of in this work, it was interesting to enlighten their origin and their associated molecular dynamics, as these relaxations are usually not reported in such polymers.

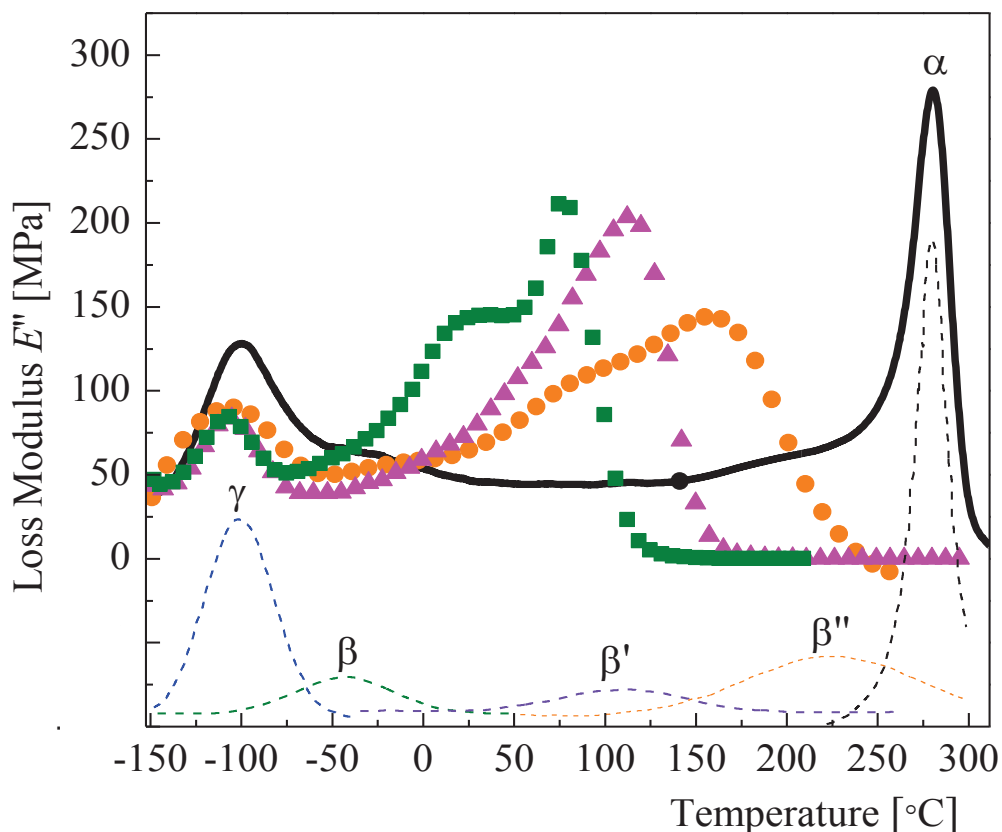


Figure 4-10: Dependence of E'' on temperature at 1 Hz for CER and CER/[HPyr][BF₄] networks: CER₀ (-), CER₂₀ (●), CER₃₀ (▲), CER₄₀ (■). The four observed molecular relaxations in CER₀ were mathematically deconvoluted and are highlighted (blister lines).

4.3.2.3. Broadband dielectric spectroscopy

Figure 4-11 shows a 3-D plot of the loss permittivity ϵ'' as a function of temperature and frequency obtained for neat CER₀. In this spectrum, it is noteworthy that the same molecular relaxations observed by DMTA were also detected by Broadband Dielectric Spectroscopy (BDS). It is important to mention that the so-called β' and β'' processes are well separated from β and α relaxations, as observed above by DMTA.

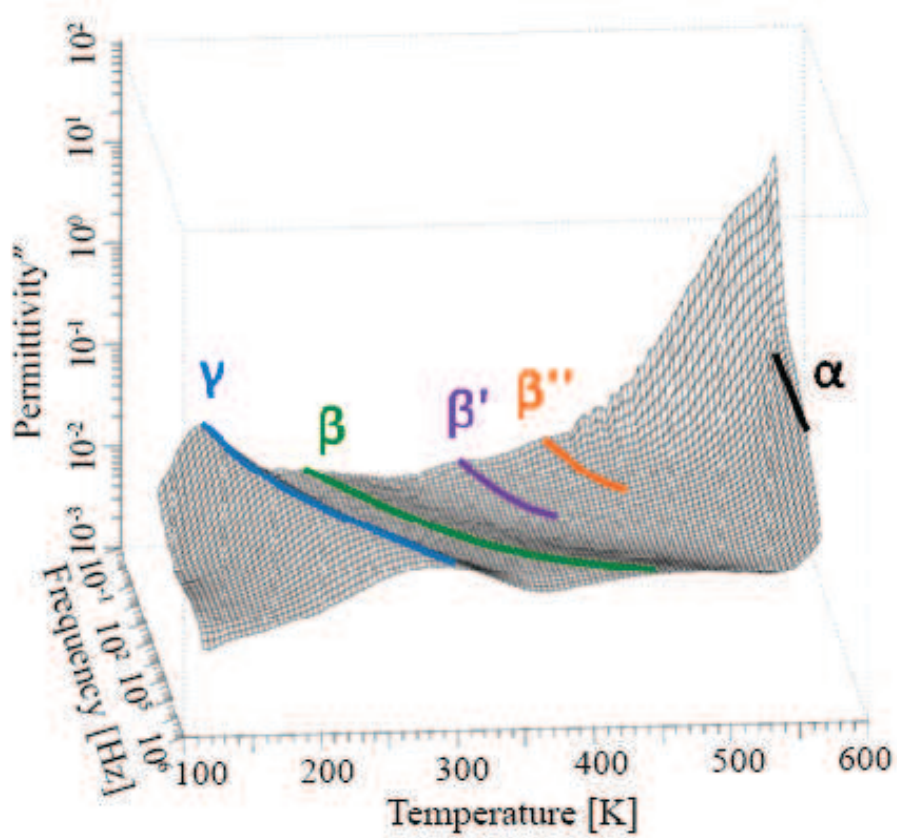


Figure 4-11: 3D spectrum of loss dielectric permittivity as a function of frequency and temperature obtained by BDS measurements for neat CER₀ with highlighted molecular relaxations.

The complex permittivity ε^* data for the identified relaxations was fitted on the frequency-time domain with a Havriliak-Negami model [43-46] (**Equation 4-5**):

$$\varepsilon^* = \varepsilon' + i\varepsilon'' = \varepsilon_\infty + \frac{\Delta\varepsilon}{(1 + (i\omega\tau)^m)^n} \quad (4-5)$$

The use of this model to fit the α relaxation was found to be pertinent. Indeed, the m and n parameters ($0 < m \text{ \& } n \leq 1$) describing respectively the broadening and the symmetry of a relaxation were found to differ from the unity. This would mean that the relaxation had a broad range of relaxation times τ and that it was asymmetrical, thus confirming the behavior of a main molecular relaxation. On the other hand, it was observed that the n asymmetry exponent on the Havriliak-Negami model was equal to unity for the γ , β , β' , and β'' relaxations, while the exponent m remained different from 1. This would mean that these relaxations had also a broad range of relaxation times τ but that they were symmetrical. This behavior would correspond to

that of local secondary relaxations. Hence, the Cole-Cole model was used to better fit such relaxations [43-46] (**Equation 4-6**):

$$\varepsilon^* = \varepsilon' + i\varepsilon'' = \varepsilon_\infty + \frac{\Delta\varepsilon}{(1 + (i\omega\tau)^m)} \quad (4-6)$$

From these fits, the n and m parameters as a function of the frequency as well as the mean relaxation time τ for each relaxation as a function of temperature were obtained. **Figure 4-12** shows the inverse of the n and m parameters as a function of the frequency for each relaxation, *i.e.* their amplitudes. As stated above, it was seen that all of the molecular relaxations, with exception of the α relaxation, were symmetrical.

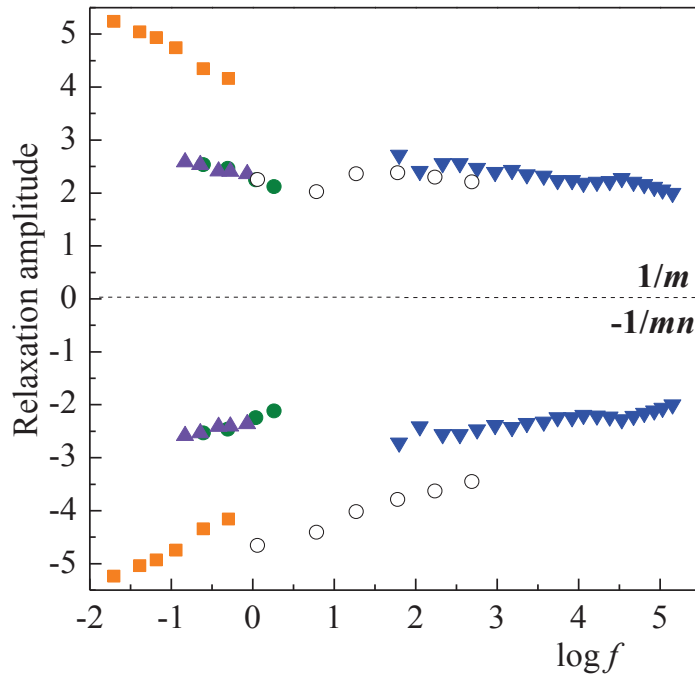


Figure 4-12: Molecular relaxation amplitude for the observed molecular relaxations obtained from BDS measurements for neat CER₀: γ (\blacktriangledown), β (\bullet), β' (\blacktriangle), β'' (\blacksquare), α (\circ).

The relaxation times were then transformed into frequencies f according to $f = 1/2\pi\tau$, so that we were able to plot the relaxation map for each molecular relaxation, which is displayed in **Figure 4-13**.

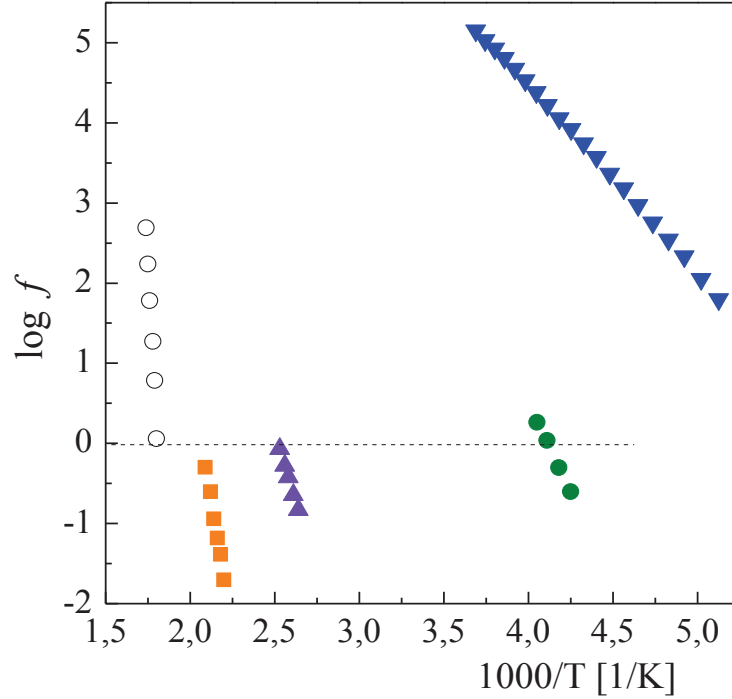


Figure 4-13: Molecular relaxation cartography for the observed molecular relaxations obtained from BDS measurements for neat CER₀: γ (\blacktriangledown), β (\bullet), β' (\blacktriangle), β'' (\blacksquare), α (\circ).

Considering that the γ , β , β' , and β'' relaxations were symmetrical, their activation energy and the f_0 factor were calculated according to an Arrhenius equation [46, 47] (**Equation 4-7**):

$$f(T) = f_0 \exp\left[-\frac{E_a}{RT}\right] \quad (4-7)$$

where T corresponds to the temperature associated with a given frequency, and R is the ideal gas constant ($8.314 \text{ J mol}^{-1} \cdot \text{K}^{-1}$). Concerning the α relaxation, it was observed in **Figure 4-10** that its trend was more asymptotic than linear, plus that it was asymmetrical. This behavior corresponded to that of a main glassy molecular relaxation and thus in order to obtain its activation energy, the Vogel-Fulcher-Tamman equation was used [46, 48-53] (**Equation 4-8**):

$$f(T) = f_0 \exp\left[-\frac{E_a}{R(T - T_{VFT})}\right] \quad (4-8)$$

In the latter relationship, the main relaxations were considered to tend to an asymptotic temperature T_{VFT} at high frequencies that was fairly equal to $T_g - 50 \text{ }^\circ\text{C}$.

The calculated activation energy E_a and f_0 factor values for all relaxations are summarized in **Table 4-2**. Concerning the secondary γ and β as well as the main α relaxations, the calculated energies corresponded to those expected for such types of molecular motions. However, in the case of the β' and β'' relaxations, the E_a values calculated with the Arrhenius equation seemed to be too high for localized motions. E_a values for these relaxations were then calculated with the VFT equation as if they were main relaxations (**Table 4-2**). The obtained values were in good agreement with those of very strong localized molecular motions as well as for weak main relaxation processes. Moreover, the f_0 values gave also a good indication of the nature of molecular processes [43]. In the case of secondary relaxations, *i.e.* Arrhenian motions, f_0 varied from 10^{12} to 10^{17} Hz. Higher values denote a main relaxation behavior. It was herein observed (**Table 4-2**) that the γ relaxation had a f_0 value corresponding to that of a secondary relaxation. For the β'' relaxation, a f_0 value higher than 10^{17} Hz (by nine orders of magnitude) was calculated. Such a large value is non-physical and thus confirmed that this relaxations seemed to behave as a VFT process (*i.e.* main relaxation). In the case of the β and β' relaxations, they presented f_0 values of 10^{17} Hz. This would mean that they had an intermediary behavior between a secondary and a main relaxation. However, as mentioned above, the activation energy of the β' relaxation did not correspond to that of a secondary relaxation, meaning that it behaved as a mild main process.

Table 4-2: Calculated activation energy E_a for each of the observed molecular relaxations of CER samples

Molecular relaxation	E_a (kJ/mol) – Arrhenius	f_0 (Hz) – Arrhenius	E_a (kJ/mol) – VFT
γ	45	6.6×10^{13}	-
β	82	3.9×10^{17}	-
β'	135	6.7×10^{17}	89
β''	205	6.1×10^{26}	105
α	-	-	274

4.3.2.4. Discussion on β' and β'' relaxations

It is known that secondary transitions may have a significant influence on the mechanical properties of polymers, namely their toughness [46, 53, 55]. It is thus important to study the effect of additives such as plasticizers on these relaxations as well. The variation of T_γ , T_β , $T_{\beta'}$, and $T_{\beta''}$ with the content of IL is shown in **Figure 4-14**.

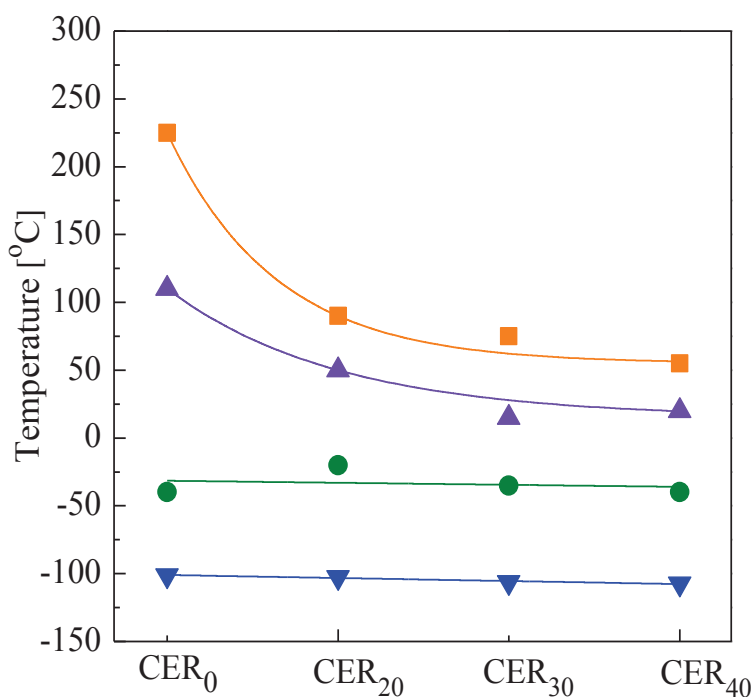


Figure 4-14: Secondary transition temperatures of CER/[HPyr][BF₄] networks as determined by DMTA: T_γ (▼), T_β (●), $T_{\beta'}$ (▲), $T_{\beta''}$ (■).

The results observed in **Figure 4-14** suggested that T_γ and T_β did not seem to be influenced by the IL presence. However, as it was observed for T_α , both $T_{\beta'}$ and $T_{\beta''}$ were sensitive to chemical composition and decreased when [HPyr][BF₄] content increased. A hypothesis to explain such a plasticizing effect due to the IL presence on $T_{\beta'}$ and $T_{\beta''}$ would be that these relaxations are not secondary but main molecular motions. Moreover, it would seem that the β relaxation is indeed a secondary relaxation, From BDS measurements, it was observed that these relaxations were very steep (**Figure 4-13**). It might be possible that they exhibited a VFT behavior at high frequencies but unfortunately this could not be verified as the relaxations motions at high frequencies were masked within the loss permittivity ϵ'' of the samples (**Figure 4-11**).

The origin of these relaxations may come from the curing technique used in this study. Previous works conducted in our team on CER samples have used an isothermal step-by-step curing process. In an earlier study, the same γ , β , and α relaxations observed herein were also identified [42]. In the present work, as mentioned in the Experimental part, the samples were cured with a temperature ramp. As these systems were extremely reactive, it might be possible that polymerized non-crosslinked chains were present within the materials structure. The chemical nature of the so-called non-crosslinked chains was identical to that associated with the crosslinked polymer, and thus the molecular motions giving place to the main molecular relaxation would be similar. However, as these «free» chains are not constrained in the network, these movements could be activated at lower energies and temperatures, thus giving birth to supplementary main relaxations within the materials. This hypothesis could be verified by studying the CERs containing ILs by BDS. Indeed, the amplitude and the asymmetry of the molecular relaxations for these formulations could be compared to those of pure CER. However, samples containing ILs would become electrically conductive within the spectrometer, hiding the observation of the molecular relaxations.

4.3.2.5. Tensile testing

As it could be seen from **Table 4-1**, the IL presence surprisingly seemed to reinforce CERs mechanically at 25 °C, namely an increase in Young's modulus E was observed for CER₂₀ and CER₃₀. However, for the CER₄₀ sample, its Young's modulus decreased to the level of pure CER. This trend was identical to that observed by DMTA at 25 °C (dashed line in **Figure 4-9a**). These results could be explained by the fact that for CER samples containing ILs their glass transition temperature was greatly reduced. In the case of CER₂₀ and CER₃₀, the onset of their glass transitions occurred at *ca.* 20-30 °C, meaning that the network had begun to become mobile. In the case of the CER₄₀ material, the glass transition process at 25 °C already started, which meant that a part of the network was already mobile and thus plasticized. Tensile tests confirmed the results obtained by DMTA. Furthermore, the yield stress σ_y and the elongation at break ϵ_R were also obtained by tensile tests (**Table 4-1**). It is noteworthy that the yield stress followed the same trend as that of Young's and storage moduli, somehow confirming the probable influence of [HPyr][BF₄] on CER mechanical behavior. However, it would seem that the [HPyr][BF₄] content had no apparent influence on the value of elongation at break.

4.3.3. Photosensitivity of CER/[HPyr][BF₄] nanocomposites

Figure 4-15a,b presents the results of I - V characteristics at room temperature for the CER/[HPyr][BF₄] networks as a function of the [HPyr][BF₄] amount. It is noteworthy that both In/CER/Ag and In/CER/IL/Ag structures have photosensitivity. The current values of CER₃₀ found in darkness were similar to that of CER₀, obviously because of the rigid network which made the mobility of the ions difficult. At the same time the difference between dark and light currents was noticeable. Contrariwise, the CER₄₀ materials had higher current even in the dark condition.

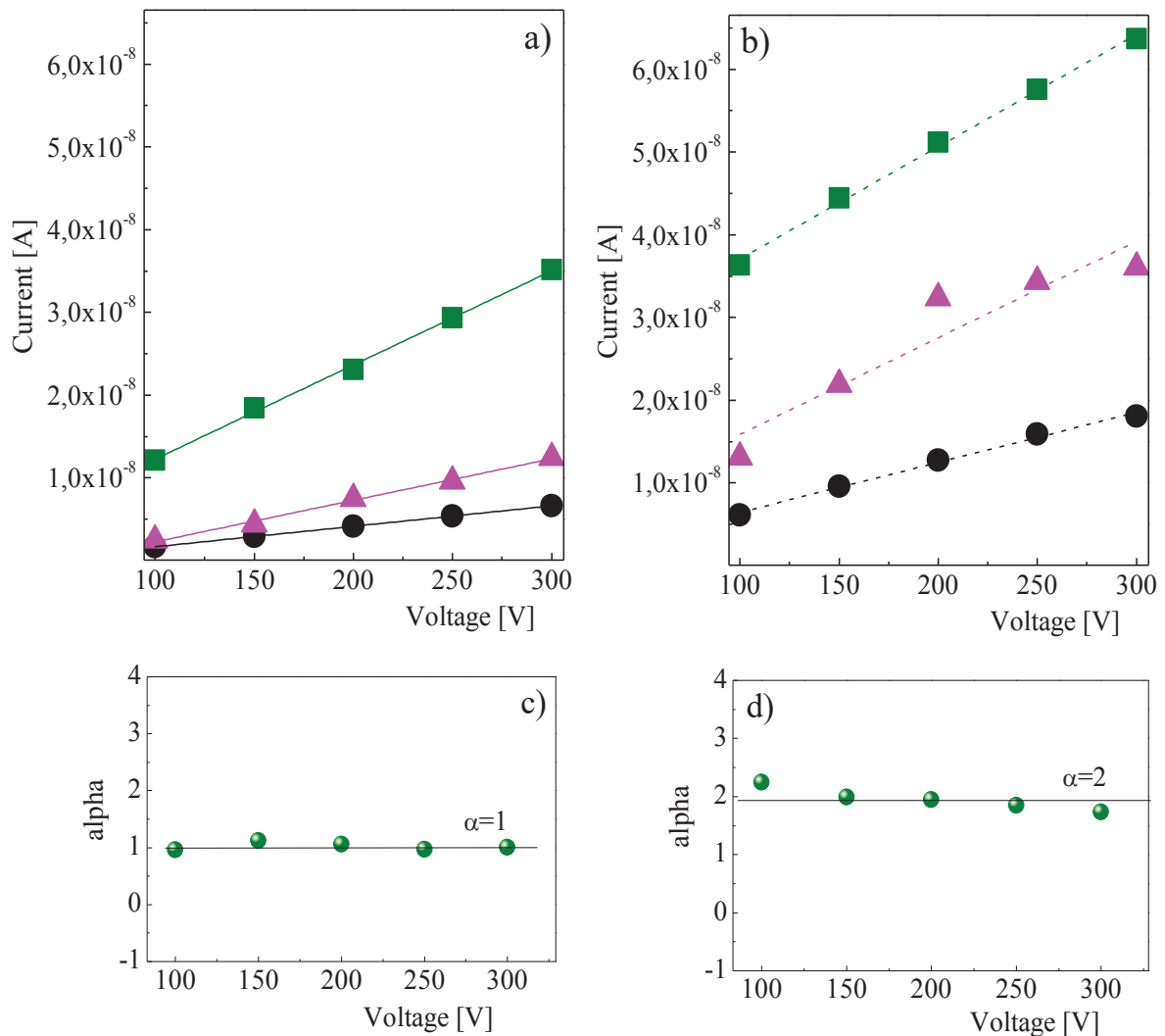


Figure 4-15: Current-voltage characteristics of In/CER/Ag structure for 900 μ m-thick samples at room temperature: in darkness (a) and under white light (b): CER (●), CER₃₀ (▲) and CER₄₀ (■) and differential slope of CER₄₀ in darkness (c) and under white light (d).

A differential approach based on I - V characteristic approximation was introduced in order to recognize mechanisms of injection and recombination and to determine physical parameters of structures (see Experimental part). It was found that the «dark» plot with a differential slope $\alpha = 1$ (cf. **Figure 4-15c**) corresponded to Ohmic conductivity, and the «illuminated» plot with $\alpha = 2$ (cf. **Figure 4-15d**) fitted with a monomolecular mechanism of recombination. This meant that in the first case the structure had not barriers which could create additional resistivity for charge carriers, whereas in the second case there were structures with deep traps.

4.3.4. Thermal stability of CER/[HPyr][BF₄] nanocomposites

The effect of [HPyr][BF₄] on the thermal stability of CER networks is illustrated in **Figure 4-16** as a function of IL content in the system. All CER-based films showed good thermal stability, although the materials had not been purified or treated in any way after polycyclotrimerization.

The CER₀ network displayed high thermal stability (**Table 4-1**). Its degradation began with hydrocarbon chain scission and cross-linking junctions at temperatures above 415 °C, followed by a sharp thermal decomposition on decyclization of the triazine ring at 450 °C that released volatile cyanate-ester decomposition products. Moreover, the CER₀ exhibited a second decomposition stage between 500-650 °C that was attributed to mass loss with the elimination of alkenes and hydrogen, leaving a carbonaceous char containing residual oxygen and nitrogen [56].

As one could see, there was only one degradation stage for CER/IL composites, thus confirming the good dispersion of [HPyr][BF₄] within the CER matrix. Despite the higher thermal stability of pure IL, the introduction of [HPyr][BF₄] into the CER matrix lowered the onset of thermal decomposition of the nanocomposites, probably due to the formation of networks with lower crosslink density compared to CER₀. However, it was also shown that the high compatibility between CER matrix and IL allowed for obtaining densely crosslinked polymer materials having a good thermal stability up to 300 °C even at high [HPyr][BF₄] content (up to 40 wt.%). The char yield after pyrolysis empirically related to the char-forming tendency decreased with the [HPyr][BF₄] content.

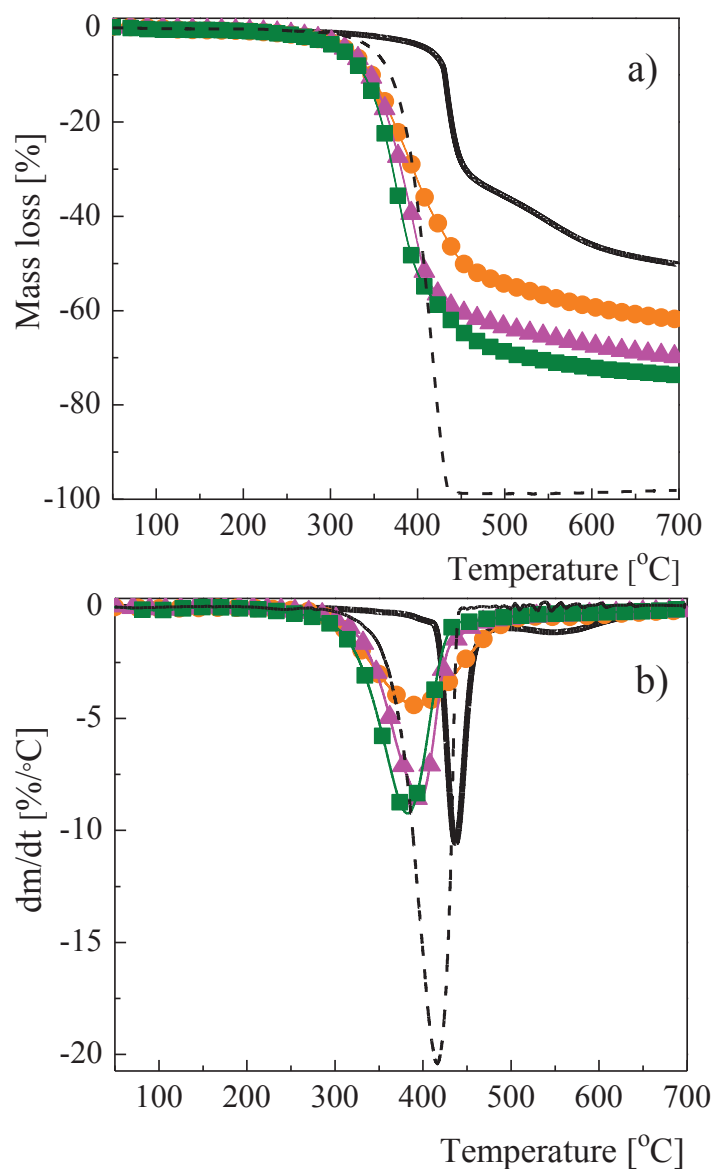


Figure 4-16: Evolution of mass loss as a function of temperature, *i.e.* a) TGA and b) DTG data, of CER networks modified with [HPyr][BF₄]: CER₀ (—), CER₂₀ (●), CER₃₀ (▲), CER₄₀ (■), [HPyr][BF₄] (---).

4.4. Conclusions

In this study, we investigated new highly filled nanocomposites containing physically inserted [HPyr][BF₄] within the CER network. The kinetics of the thermal curing process in the IL presence was studied by FTIR analysis, and the following conclusions could be underlined: (i) even 40 wt.% of IL accelerated the curing process, (ii) with an IL content increasing in the curing system, a higher total conversion was observed. A plausible mechanism based on the

formation of a $[\text{CN}]^{\delta+}-[\text{HPyr}]^{\delta-}$ complex was firstly proposed to account for the acceleration effect of the ionic liquid on the curing process associated with CERs. Hence, during the synthesis of CER/[HPyr][BF₄] nanocomposites, the IL acted both as a catalyst and a structure-directing agent increasing free volume. The materials obtained were mechanically strong and tough enough to produce self-standing thin films. It was found that CER-[HPyr][BF₄] complex formation had an impact on the viscoelastic properties of CER matrix by increasing the storage modulus in the glassy region. Interestingly, T_{γ} and T_{β} seemed not to be influenced by the [HPyr][BF₄] presence, while T_{α} , $T_{\beta'}$ and $T_{\beta''}$ were sensitive to chemical composition. From the BDS results, β' and β'' relaxations were not secondary but main molecular motions. Furthermore, the effect of the IL on the CER/IL tensile strength was elucidated. The incorporation of IL into the CER matrix decreased the packing density of polymer chain and increased free volume, while leading to better toughness. Moreover, nanoscale phase separation led to the creation of ionic channels within the CER matrix to ensure photosensitivity properties. All systems had excellent thermal stability up to 300 °C, indicating the formation of a densely crosslinked network even with a content of ionic liquid up to 40 wt.%. In general, the nanocomposite materials obtained could be used at high temperatures above their T_g (66-135 °C) without significant thermal degradation. These results are promising and open new perspectives in the field of power industry where the ionic liquid can be used as ionic channels for lithium salts to ensure suitable conduction properties.

4.5. References

1. Hamerton I.: Chemistry and technology of cyanate ester resins. Chapman & Hall, Glasgow (1994).
2. Fainleib A.: Thermostable polycyanurates: synthesis, modification, structure and properties. Nova Science Publishers, New York (2010).
3. Nair C. P. R., Mathew D., Ninan K. N.: Cyanate ester resins, recent developments. *Advances in Polymer Science*, **155**, 1-99 (2001).
4. Zheng L., Liang G., Gu A., Yuan L., Guan Q.: Unique pure barium titanate foams with three-dimensional interconnecting pore channels and their high-k cyanate ester resin composites at very low barium titanate loading. *Journal of Materials Chemistry C*, **4**, 10654-10663 (2016).
5. Gu J., Xu S., Tang Y., Lv Z., Liang C., Meng X.: Fabrication of novel wave-transparent HMPBO fibre/BADCy laminated composites. *RSC Advances*, **5**, 37768-37773 (2015).
6. Ganguli S., Dean D., Jordan K., Price G., Vaia R.: Mechanical properties of intercalated cyanate ester – layered silicate nanocomposites. *Polymer*, **44**, 1315-1319 (2003).
7. Guan Q., Yuan L., Zhang Y., Gu A., Liang G.: Improving the mechanical, thermal, dielectric and flame retardancy properties of cyanate ester with the encapsulated epoxy resin-penetrated aligned carbon nanotube bundle. *Composites Part B: Engineering*, **123**, 81-91 (2017).
8. Rao P. S., Renji K., Bhat M. R.: Molecular dynamics simulations on the effects of carbon nanotubes on mechanical properties of bisphenol E cyanate ester validating experimental results. *Journal of Reinforced Plastics and Composites*, **36**, 186-195 (2016).
9. Toldy A., Niedermann P., Szebényi G., Szolnoki B.: Mechanical properties of reactively flame retarded cyanate ester/epoxy resin blends and their carbon fibre reinforced composites. *eXPRESS Polymer Letters*, **10**, 1016-1025 (2016).
10. Gu X., Zhang Z., Yuan L., Liang G., Gu A.: Developing high performance cyanate ester resin with significantly reduced post-curing temperature while improved toughness, rigidity, thermal and dielectric properties based on manganese-Schiff base hybridized graphene oxide. *Chemical Engineering Journal*, **298**, 214-224 (2016).
11. Gu J., Dong W., Tang Y., Guo Y., Tang L., Kong J., Tadakamalla S., Wang B., Guo Z.: Ultralow dielectric, fluoride-containing cyanate ester resins with improved mechanical properties and high thermal and dimensional stabilities. *Journal of Materials Chemistry C*, **5**, 6929-6936 (2017).
12. Zhou C., Gu A., Liang G., Yuan L.: Novel toughened cyanate ester resin with good dielectric properties and thermal stability by copolymerizing with hyperbranched polysiloxane and epoxy resin. *Polymers for Advanced Technologies*, **22**, 710-717 (2011).
13. Appetecchi G. B., Croce F., Scrosati B.: Kinetics and stability of the lithium electrode in poly(methylmethacrylate)-based gel electrolytes. *Electrochimica Acta*, **40**, 991-997 (1995).
14. Walden P.: Molecular weights and electrical conductivity of several fused salts. *Bulletin de l'Académie impériale des sciences de St.-Petersbourg*, **8**, 405-422 (1914).
15. Torimoto T., Tsuda T., Okazaki K. I., Kuwubata S.: New frontiers in materials science opened by ionic liquids. *Advanced Materials*, **22**, 1196-1221 (2010).
16. George A., Brandt A., Tran K., Zahari S. M. S. N. S., Klein-Marcuschamer D., Sun N., Sathitsuksanoh N., Shi J., Stavila V., R. Parthasarathi, Singh S., Holmes B. M., Welton T., Simmons B. A., Hallett J. P.: Design of low-cost ionic liquids for lignocellulosic biomass pretreatment. *Green Chemistry*, **17**, 1728-1734 (2015).
17. Araque J. C., Hettige J. J., Margulis C. J.: Modern room temperature ionic liquids, a simple guide to understanding their structure and how it may relate to dynamics. *The Journal of Physical Chemistry B*, **119**, 12727-12740 (2015).
18. Amde M., Liu J. F., Pang L.: Environmental application, fate, effects, and concerns of ionic liquids: A review. *Environmental Science & Technology*, **49**, 12611-12627 (2015).

19. Hayes R., Warr G. G., Atkin R.: Structure and nanostructure in ionic liquids. *Chemical Reviews*, **115**, 6357-6426 (2015).
20. Young J. A., Zhang C., Devasurendra A. M., Tillekeratne L. M. V., Anderson J. L., Kirchhoff J. R.: Conductive polymeric ionic liquids for electroanalysis and solid-phase microextraction. *Analytica Chimica Acta*, **910**, 45-52 (2016).
21. Kohno Y., Saita S., Men Y. J., Yuan J. Y., Ohno H.: Thermoresponsive polyelectrolytes derived from ionic liquids. *Polymer Chemistry*, **6**, 2163-2178 (2015).
22. Shaplov A. S., Marcilla R., Mecerreyes D.: Recent advances in innovative polymer electrolytes based on poly(ionic liquid)s. *Electrochimica Acta*, **175**, 18-34 (2015).
23. Zhang S. G., Dokko K., Watanabe M.: Porous ionic liquids: synthesis and application. *Chemical Science*, **6**, 3684-3691 (2015).
24. Tsurumaki A., Tajima S., Iwata T., Scrosati B., Ohno H.: Antistatic effects of ionic liquids for polyether-based polyurethanes. *Electrochimica Acta*, **175**, 13-17 (2015).
25. Mendecki L., Chen X. R., Callan N., Thompson D. F., Schazmann B., Granados-Focil S., Radu A.: Simple, robust, and plasticizer-free iodide-selective sensor based on copolymerized triazole-based ionic liquid. *Analytical Chemistry*, **88**, 4311-4317 (2016).
26. Mannan H. A., Mohshim D. F., Mukhtar H., Murugesan T., Man Z., Bustam M. A.: Synthesis, characterization, and CO₂ separation performance of polyether sulfone/[EMIM][Tf₂N] ionic liquid-polymeric membranes (ILPMs). *Journal of Industrial and Engineering Chemistry*, **54**, 98-106 (2017).
27. Tibbits A. C., Yan Y. S. S., Kloxin C. J.: Covalent incorporation of ionic liquid into ion-conductive networks via thiolene photopolymerization. *Macromolecular Rapid Communications*, **38**, 1-7 (2017).
28. Fainleib A., Vashchuk A., Starostenko O., Grigoryeva O., Rogalsky S., Nguyen T. T. T., Grande D.: Nanoporous polymer films of cyanate ester resins designed by using ionic liquids as porogens. *Nanoscale Research Letters*, **12**, 126/1-126/9 (2017).
29. Smertenko P., Fenenko L., Brehmer L., Schrader S.: Differential approach to the study of integral characteristics in polymer films. *Advances in Colloid and Interface Science*, **116**, 255-261 (2005).
30. Ciach R., Dotsenko Yu. P., Naumov V. V., Shmyryeva A. N., Smertenko P. S.: Injection technique for study of solar cells test structures. *Solar Energy Materials and Solar Cells*, **76**, 613-624 (2003).
31. Van Krevelen D.W.: Properties of polymers: their correlation with chemical structure: their numerical estimation and prediction from additive group contributions. Elsevier, Amsterdam (2009).
32. Cunningham I. D., Brownhill A., Hamerton I., Howlin B.: Kinetics and mechanism of the titanium tetrachloride-catalysed cyclotrimerisation of aryl cyanates. *Journal of the Chemical Society, Perkin Transactions 2*, **9**, 1937-1943 (1994).
33. Fainleib A., Grigoryeva O., Starostenko O., Vashchuk A., Rogalsky S., Grande D.: Acceleration effect of ionic liquids on polycyclotrimerization of dicyanate esters, *eXPRESS Polymer Letters*, **10**, 722-729 (2016).
34. Howarth J., Hanlon K., Fayne D., McCormac P.: Moisture stable dialkylimidazolium salts as heterogeneous and homogeneous Lewis acids in the Diels-Alder reaction. *Tetrahedron Letters*, **38**, 3097-3100 (1997).
35. Aggarwal A., Lancaster N. L., Sethi A. R., Welton T.: The role of hydrogen bonding in controlling the selectivity of Diels-Alder reactions in room-temperature ionic liquids. *Green Chemistry*, **4**, 517-520 (2002).
36. Hiao Y.: Study of organic reactions in pyridinium-based ionic liquids, PhD Dissertation. New Jersey Institute of Technology, Department of Chemistry and Environmental Science (2006).

37. Sun H., Qiao B., Zhang D., Liu C.: Structure of 1-butylpyridinium tetrafluoroborate ionic liquid: quantum chemistry and molecular dynamic stimulation studies. *The Journal of Physical Chemistry A*, **114**, 3990-3996 (2010).
38. Throckmorton J., Palmese G.: Acceleration of cyanate ester trimerization by dicyanamide RTILs. *Polymer*, **91**, 7-13 (2016).
39. Georjon O., Schwach G., Gérard J-F., Galy J.: Molecular mobility in polycyanurate networks investigated by viscoelastic measurements and molecular simulations. *Polymer Engineering & Science*, **37**, 1606-1620 (1997).
40. Fitz B. D., Mijovic J.: Molecular dynamics in cyanate ester resin networks and model cyanurate compounds. *Macromolecules*, **33**, 887-899 (2000).
41. Balta Calleja F. J., Privalko E. G., Sukhorukov D. I., Fainleib A. M., Sergeeva L. M., Shantali T. A., Shtompel V. I., Monleon Pradas M., Gallego Ferrer G., Privalko V. P.: Structure–property relationships for cyanurate-containing, full interpenetrating polymer networks. *Polymer*, **41**, 4699-4707 (2000).
42. Fainleib A., Grigoryeva O., Garda M. R., Saiter J. M., Lauprêtre F., Lorthioir C., Grande D.: Synthesis and characterization of polycyanurate networks modified by oligo(ϵ -caprolactone) as precursors of porous thermosets. *Journal of Applied Polymer Science*, **106**, 3929-3938 (2007).
43. McCrum N. G., Read B. E., Williams G.: *Anelastic and dielectric effects in polymer solids*. Dover, New York (1991).
44. Havriliak S., Negami S. A.: Complex plane representation of dielectric and mechanical relaxation processes in some polymers. *Polymer*, **8**, 161-210 (1967).
45. Rios de Anda A., Fillot L. A., Rossi S., Long D., Sotta P.: Influence of the sorption of polar and non-polar solvents on the glass transition temperature of polyamide 6, 6 amorphous phase. *Polymer Engineering & Science*, **51**, 2129-2135 (2011).
46. Rios de Anda A., Fillot L. A., Long D., Sotta P.: Influence of the amorphous phase molecular mobility on impact and tensile properties of polyamide 6,6. *Journal of Applied Polymer Science*, **133**, 43457/1-43457/9 (2016).
47. Laidler K. J.: *A glossary of terms used in chemical kinetics, including reaction dynamics*. *Pure and Applied Chemistry*, **68**, 149-192 (1996).
48. Vogel H.: *Die temperaturabhängigkeit gesetzer viskosität von flüssigkeiten*. *Physikalische Zeitschrift*, **22**, 645-646 (1921).
49. Fulcher G. S.: Analysis of recent measurements of the viscosity of glasses. *Journal of the American Ceramic Society*, **8**, 339-355 (1925).
50. Tammann G., Hesse W.: *Die abhängigkeit der viskosität von der temperatur bei unterkühlten flüssigkeiten*. *Zeitschrift für anorganische und allgemeine Chemie*, **156**, 245-257 (1926).
51. Williams M. L., Landel R. F., Ferry J. D.: The temperature dependence of relaxation mechanisms in amorphous polymers and other glass-forming liquids. *Journal of the American Chemical Society*, **77**, 3701-3707 (1955).
52. Bartolomeo P., Chailan J. F., Vernet J. L.: On the use of WLF equation to study resin curing by dielectric spectroscopy, *Polymer*, **42**, 4385-4392 (2001).
53. Halary J-L., Lauprêtre F.: *De la macromoleculle au matériau polymère*. Belin, Paris (2006).
54. Ehrenstein G.W. : *Fasserverbund-Kunststoffe*, Carl Hanser Verlag, Munich (2006).
55. Halary J-L., Lauprêtre F., Monnerie L.: *Mécanique des matériaux polymères*. Belin, Paris (2008).
56. Ramirez M. L., Walters R., Savitski E. P., Richard E.: *Thermal decomposition of cyanate ester resins*. Lyon technical report documentation (2001).

CHAPTER 5

Nanoporous Polymer Films of Cyanate Ester Resins Designed by Using Ionic Liquids as Porogens

Abstract: Novel nanoporous film materials of thermostable Cyanate Ester Resins (CERs) were generated by polycyclotrimerization of dicyanate ester of bisphenol E in the presence of varying amounts (from 20 to 40 wt. %) of an ionic liquid (IL), *i.e.* 1-heptylpyridinium tetrafluoroborate, followed by its quantitative extraction after complete CER network formation. The completion of CER formation and IL extraction was assessed using gel fraction content determination, FTIR, ¹H NMR, and energy dispersive X-ray spectroscopy (EDX). SEM and DSC-based thermoporometry analyses demonstrated the formation of nanoporous structures after IL removal from CER networks, thus showing the effective role of IL as a porogen. Pore sizes varied from ~20 to ~180 nm with an average pore diameter of around 45-60 nm depending on the initial IL content. The thermal stability of nanoporous CER-based films was investigated by thermogravimetric analysis.

A. Fainleib, A.Vashchuk, O. Starostenko, O. Grigoryeva, S. Rogalsky, T-Th-T. Nguyen, D. Grande: Nanoporous polymer films of cyanate ester resins designed by using ionic liquids. *Nanoscale Research Letters*. **12**, 1-9. (2017).

5.1. Introduction

High crosslink density Cyanate Ester Resins (CERs) – also known as polycyanurates (PCNs) – are commonly used in aerospace applications and electronic devices as high temperature polymer matrices [1-3]. The specific interest in these high performance polymers arises from their unique combination of intrinsic properties, including thermal, fire, radiation and chemical resistance, high tensile moduli (3.1-3.4 GPa) and glass transition temperatures ($T_g > 220$ °C), low dielectric constants ($\epsilon \sim 2.6-3.2$), high adhesion to conductor metals and composites as well as low water/moisture uptake [1, 2].

Ionic liquids (ILs) are organic salts that typically consist of bulky, asymmetric organic cations and inorganic symmetric anions. Room-temperature ILs are defined as salts with melting points below or equal to room temperature [4, 5]. ILs have attracted widespread interest in polymer science due to their versatile properties, such as negligible saturated vapor pressure, wide liquid-state temperature range, non-flammability, incombustibility, high electrical conductivity, and good stability to oxidation [6-10]. They have progressively been used as solvents and catalysts for polymerization reactions [10] as well as additives in the design of polymer materials [11]. Their peculiar structure enables easy separation, recovery, and recycling of the catalyst from the reaction mixtures. In the case of membrane processes, ILs are being used in the design and modification of advanced materials that enable performance levels not typical of conventional materials [12]. Another application of ILs consists of their use as effective and reusable porogens in vinylic networks [13]. When ILs are used as porogenic solvents, during the *in-situ* formation of polymer networks, chemically-induced phase separation occurs. To act as efficient porogens, ILs have to possess: (i) high-boiling temperature to avoid any premature evaporation, (ii) high thermal stability to remain unchanged up to the complete curing of the polymer networks, and (iii) easy extractability to be readily removed from the cured networks, thus affording porous thermosetting materials.

Porous polymeric materials have a large variety of applications in many areas as highly selective membranes, selective adsorbents and filters, porous electrodes for fuel cells, sensors or insulators, etc [14]. Pioneering reports on the design of porous CERs were published by Hedrick and co-workers in the late 1990's [15-17]. Since 2008 two of our research groups have jointly developed various original approaches to nanoporous CER-based thermosetting films [18-23]. Two strategies relied on the use of oligo(ϵ -caprolactone) chains as porogens, which were removed from the synthesized CER networks by either extraction [18] or selective

hydrolysis [19]. Alternatively, other pore generation methods involved: (i) the use of high-boiling temperature liquids, *i.e.* phthalates, as porogens [20, 21], (ii) the synthesis of CER networks with different degrees of cyanate group conversion, followed by the extraction of unreacted dicyanate monomer [22], and (iii) the irradiation of CER films by α -particles, followed by an alkaline etching to reveal the tracks created after bombing [23].

Recently, we have investigated the catalytic effect of ILs on the curing process of CERs and an acceleration effect has clearly been highlighted in the polycyclotrimerization of dicyanate ester of bisphenol E in the presence of a specific ionic liquid [24]. To the best of our knowledge, ILs have not been used as porogens to generate porous CER thermosets so far. In the present work, novel nanoporous CER-based thermosetting films are engineered by using a room-temperature ionic liquid, namely 1-heptylpyridinium tetrafluoroborate ([HPyr][BF₄]), as a porogen, and the effect of porogen content on the structure and properties of resulting porous CERs is examined.

5.2. Experimental

5.2.1. Materials

1,1'-bis(4-cyanatophenyl) ethane (dicyanate ester of bisphenol E, DCBE), under the trade name Primaset™ LECy was kindly supplied by Lonza (Basel, Switzerland) and was used as received. The following chemicals were used for the synthesis of the 1-heptylpyridinium tetrafluoroborate, [HPyr][BF₄]: pyridine, 1-chloroheptane, ethyl acetate, hexane, tetrafluoroboric acid (48 wt.% in H₂O), methylene chloride, and sodium sulfate. The chemicals were provided by Fluka and were used as received.

5.2.2. Ionic liquid synthesis

1-Heptylpyridinium tetrafluoroborate [HPyr][BF₄] was synthesized using the following method. A mixture of dry pyridine:1-chloroheptane with a molar ratio 1.0:1.1 was heated at 140 °C for 20 h under stirring. A white solid product, *i.e.* 1-heptylpyridinium chloride, was obtained after cooling the reaction mixture to room temperature. It was purified by recrystallization from ethyl acetate:hexane mixture (1:1 vol/vol). 1-heptylpyridinium chloride (50 g, 0.23 mol) was dissolved in 300 mL of water and 30 mL of tetrafluoroboric acid was

added to the solution. The water immiscible layer of the ionic liquid [HPyr][BF₄] formed was extracted with methylene chloride (3 × 150 mL), washed with water and dried over sodium sulfate. The solvent was distilled off, and the resulting ionic liquid was dried under a reduced pressure of 1 mbar at 80 °C for 12 h. The synthetic route to the ionic liquid [HPyr][BF₄] is depicted in **Figure 5-1**.

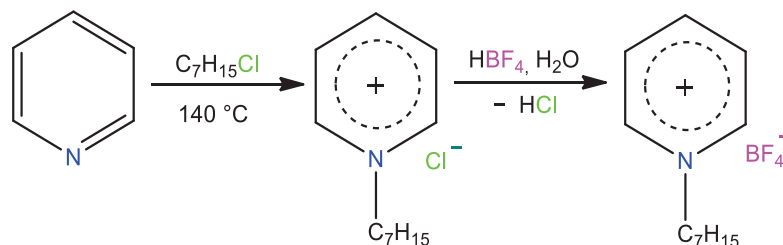


Figure 5-1: Synthetic route to ionic liquid [HPyr][BF₄].

5.2.3. Preparation of CER-based films

DCBE was mixed with [HPyr][BF₄] in a given ratio (the content of [HPyr][BF₄] was equal to 20, 30, and 40 wt. %) and the homogeneous mixtures were subjected to an ultrasonic bath at 60 °C for 30 min. These solutions were then poured into a PTFE-coated mold and cured over the temperature range from 25 to 250 °C with a heating rate of 0.5 °C/min. The polycyclotrimerization of DCBE resulted in the formation of a CER network (see **Figure 5-2**).

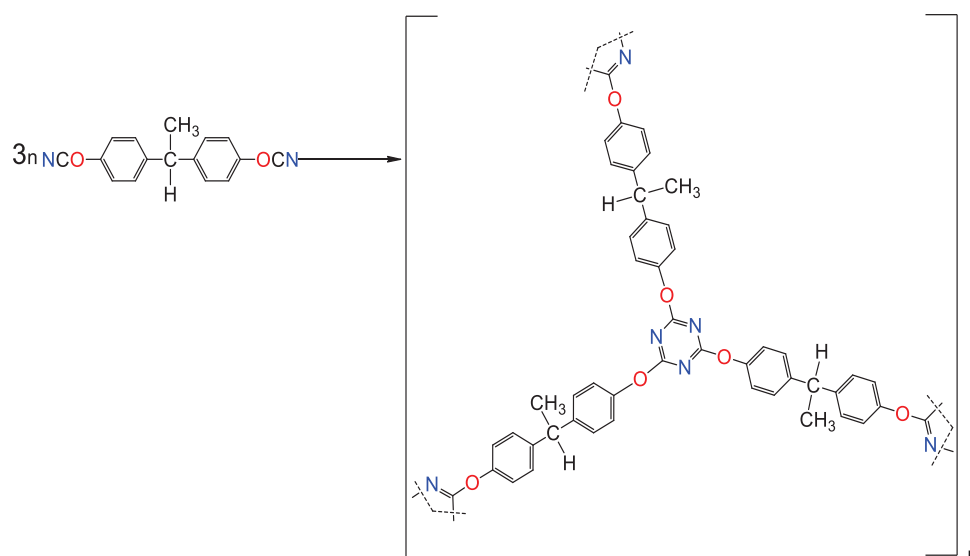


Figure 5-2: Scheme of CER network formation.

For generation of porous structure the films obtained with a thickness around 100 μm were subjected to extraction with ethanol in a Soxhlet apparatus for 16 h. After extraction, the samples were dried up to a constant weight at 25 $^{\circ}\text{C}$. The following codes were applied to the samples under investigation: CER_{ext}, CER_{20ext}, CER_{30ext}, CER_{40ext}, respectively for the extracted CER sample synthesized without IL and for extracted CER samples synthesized in the presence of IL, where the subscripts indicate the initial content of [HPyr][BF₄]. The code CER₄₀ was applied to the non-extracted sample with a [HPyr][BF₄] content of 40 wt. %: it was used as a reference sample for the sake of comparison.

5.3.4. Physico-chemical techniques

Gel fraction contents of the CER-based networks were determined after Soxhlet extraction and drying up to constant weight. The experimental values of gel fraction contents, $w_{g(\text{exp})}$, were determined as the contents of insoluble part of the samples using **Equation 5-1**:

$$w_{g(\text{exp})} = \frac{m_2}{m_1} \cdot 100\% \quad (5-1)$$

where m_1 and m_2 stand for the mass of a dried sample before and after extraction, respectively.

The theoretical values of gel fraction contents were calculated with the conjecture that non-reactive [HPyr][BF₄] was completely extracted from CER films using **Equation 5-2**:

$$w_{g(\text{theor})\text{CER}} = w_{g(\text{exp})\text{CER}} - w_{g[\text{HPyr}][\text{BF}_4]} \quad (5-2)$$

where $w_{g(\text{exp})\text{CER}}$ and $w_{g[\text{HPyr}][\text{BF}_4]}$ stand for the experimental value of gel fraction content for pure CER (~100 wt. %) and the initial [HPyr][BF₄] content in the systems, respectively.

FTIR spectra were recorded on a Bruker Tensor 37 spectrometer between 4000 and 450 cm^{-1} using the Attenuated Total Reflection (ATR) mode. For each spectrum, 32 consecutive scans with a resolution of 0.6 cm^{-1} were averaged.

¹H NMR spectroscopy was conducted with a Bruker AV II spectrometer operating at a resonance frequency of 400 MHz. The spectra were recorded at room temperature using DMSO-*d*₆ as an internal standard ($\delta = 2.5$ ppm).

Scanning Electron Microscopy (SEM) analyses of the samples were performed on a MERLIN microscope from Zeiss equipped with Inlens and SE2 detectors using an accelerating voltage of 4 kV. Prior to analyses, the films were cryofractured and coated with a Pd/Au alloy (4 nm thickness) in a Cressington 208 HR sputter-coater. Energy-dispersive X-ray spectroscopy (EDX) was performed using a SSD X-Max detector of 50 mm² from Oxford Instruments (127 eV for the K α of Mn) coupled to the SEM equipment. To determine the main porosity characteristics derived from SEM data (*i.e.*, pore sizes and pore size distributions), 1000 pores for each sample were at least evaluated using the *ImageJ 1.48v* software. Pores with area inferior to 20 nm² and superior to 1.25 \times 10⁵ nm² were ignored to avoid counting of improbable values. Since pore circularity values revealed from *ImageJ* analysis varied from 0.80 to 0.90 (assuming that «0» corresponded to an infinitely elongated polygon and «1» was related to a perfect circle), pore diameters were calculated assuming circular pore shapes.

DSC-based thermoporometry was used as an independent quantitative technique for determining pore sizes and pore size distributions. The basic principles of this technique are well-known [25,26]. In this study, thermoporometry was performed using water as a penetrating liquid. From the melting thermograms of water contained in the porous films,

Equation 5-3, 5-4, 5-5 were applied to determine pore diameters (D_p), pore size distributions (dV/dR_p), and heat flow values $\Delta H(T)$ respectively:

$$D_p (nm) = 2 \cdot \left(0.68 - \frac{32.33}{T_m - T_{m0}} \right) \quad (5-3)$$

$$dV/dR (cm^3 \cdot nm^{-1} \cdot g^{-1}) = \frac{dq/dt \cdot (T_m - T_{m0})^2}{32.33 \cdot \rho \cdot v \cdot m \cdot \Delta H(T)} \quad (5-4)$$

$$\Delta H(T)(J \cdot g^{-1}) = 332 + 11.39 \cdot (T_m - T_{m0}) + 0.155 \cdot (T_m - T_{m0})^2 \quad (5-5)$$

where T_m and T_{m0} are the melting temperatures of confined and bulk water, respectively; dq/dt , ρ , v , m , and $\Delta H(T)$ are the heat flow recovered by DSC, the water density, the heating rate, the sample mass and the melting enthalpy of water, correspondingly.

Due to the hydrophobicity of CER films, we resorted to an ethanol pretreatment in order to improve their hydrophilic character and favor the water penetration into the pores. Such a pretreatment using an organic solvent miscible with water, followed by its subsequent replacement by water, ensured pore accessibility to water. In addition, it was assumed that pore filling was predominant over the bulk polymer swelling either in ethanol or water, due to the

high cross-link density of the CER network. The samples were first immersed to ethanol for 2 h, and then distilled water was gradually added to remove the ethanol. Afterwards, the samples were kept in pure distilled water for 2 weeks. After surface wiping, the melting thermograms were recorded using TA Instruments 2010 calorimeter under nitrogen atmosphere in temperature range from -50 to 5 °C at a heating rate of 1 °C/min. The typical sample mass was about 10-15 mg.

Thermogravimetric analysis (TGA) measurements were performed using a Setaram SETSYS evolution 1750 thermobalance. Samples were heated in a platinum crucible from 20 to 700 °C at a heating rate of 10 °C min⁻¹ under argon atmosphere.

5.3. Results and Discussion

The generation of nanoporous thermosetting films was accomplished through the formation of CER-based thin films derived from the *in-situ* polycyclotrimerization of DCBE in the presence of [HPyr][BF₄] with further removal of the latter (**Figure 5-3**). The gel fraction contents associated with CER samples were determined after ethanol extraction. **Figure 5-4** clearly shows that the experimental and theoretical values of the gel fraction content nearly matched, thus strongly suggesting the completion of CER formation and [HPyr][BF₄] extraction from CER-based networks, while confirming the chemical inertness of the ionic liquid towards CER. It should be noted that even a [HPyr][BF₄] content as high as 40 wt. % in the initial system did not hinder the formation of a highly crosslinked CER structure.

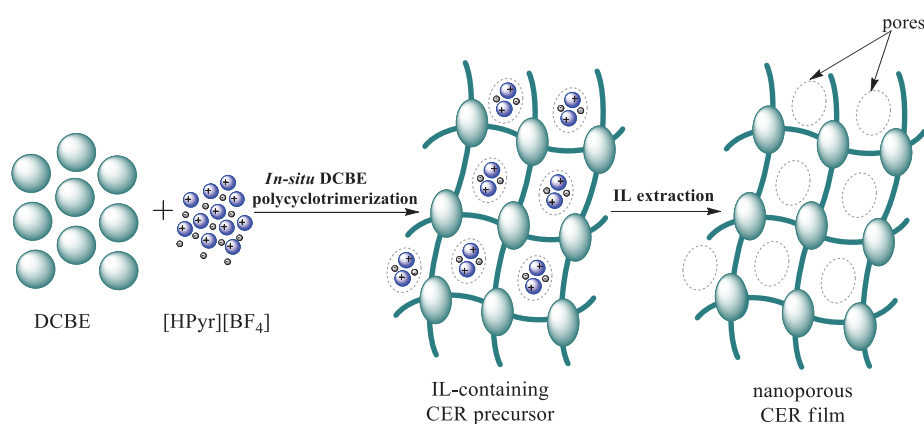


Figure 5-3: Representative scheme of CER formation in the presence of [HPyr][BF₄] and subsequent pore formation.

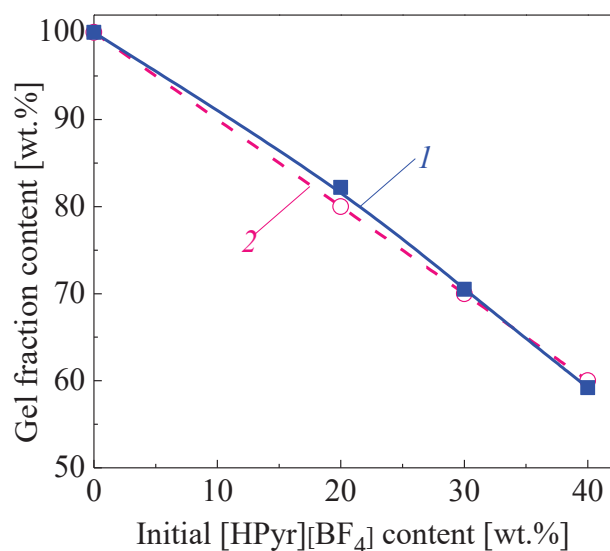


Figure 5-4: Experimental (1) and theoretical (2) values of gel fraction contents after extraction as a function of [HPyr][BF₄] content.

5.3.1. Spectroscopic analyses of network structure

In order to evaluate the effect of [HPyr][BF₄] on network structure and further confirm its chemical inertness to DCBE, FTIR analysis was performed. **Figure 5-5** displays FTIR spectra of CER_{ext}, CER_{40ext}, CER₄₀, and pure [HPyr][BF₄].

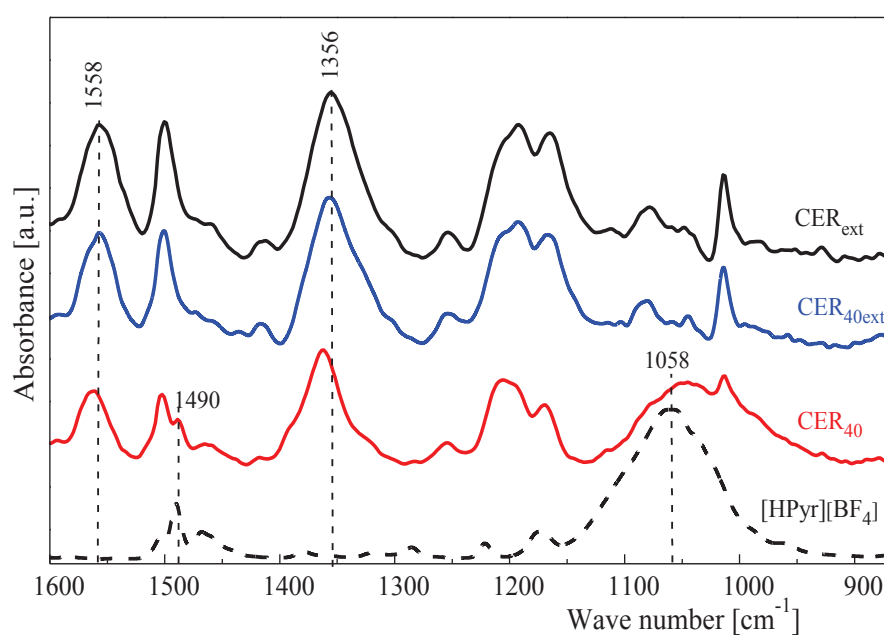


Figure 5-5: FTIR spectra of ionic liquid [HPyr][BF₄] and typical CER networks before and after extraction.

The FTIR analysis of the CER_{40ext} samples (and of the other extracted CER samples, not shown here) demonstrated the presence of C=N–C and N–C–O/N=C–O stretching absorption bands of cyanurate repeating units at 1356 cm⁻¹ and 1558 cm⁻¹, respectively, and did not indicate any stretching absorption bands of unreacted cyanate groups at 2272–2236 cm⁻¹, thus corroborating the formation of CER network. It should be pointed out that, for both the CER₄₀ and the pure [HPyr][BF₄], the band at 1490 cm⁻¹ and the broad band with maximum at 1058 cm⁻¹, corresponding to the stretching mode of pyridinium cation [27] and the asymmetric stretching of BF₄⁻ anion of the ionic liquid, respectively, were observed. Logically, after [HPyr][BF₄] extraction, such absorption bands disappeared from FTIR spectrum of the CER_{40ext} sample, while the intensities of the bands at 1558 cm⁻¹ and 1356 cm⁻¹ did not change significantly. It is noteworthy that the well-defined bands in the region of 1100–1000 cm⁻¹ in the spectra of CER_{ext} and CER_{40ext} corresponded to C–O–C bonds in the CER network structure. Consequently, FTIR analysis confirmed the chemical inertness of IL to the CER network and the efficient removal of [HPyr][BF₄] from CER matrix.

¹H NMR spectra of [HPyr][BF₄] and a typical sol fraction obtained after CER extraction are shown in **Figure 5-6**. The resonance signals at 0.84, 1.28, 1.91, 3.34 and 4.60 ppm could be assigned to the protons from -C₇H₁₅, and the presence of protons from pyridinium ring could be observed with chemical shifts equal to 8.16, 8.60, and 9.08 ppm.

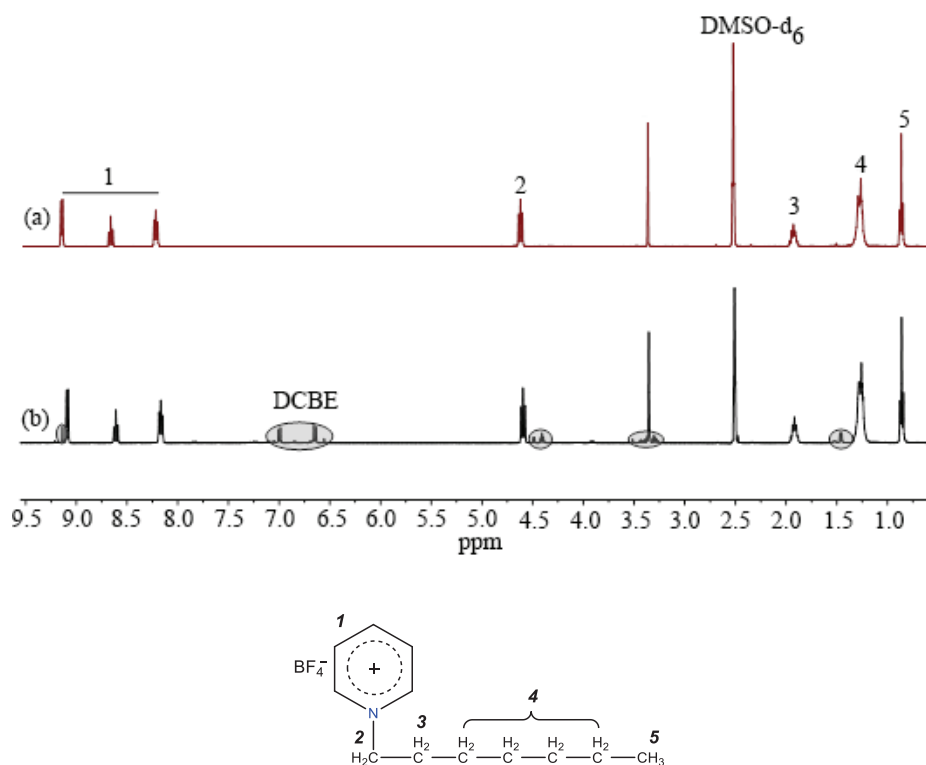


Figure 5-6: ¹H NMR spectra of [HPyr][BF₄] (a) and sol fraction after CER₄₀ extraction (b).

Obviously enough, the ^1H NMR spectrum of the sol fraction closely matched that of $[\text{HPyr}][\text{BF}_4]$, only traces of unreacted DCBE and/or soluble low molar mass cyanurate fragments non-incorporated into CER network being observed in the interval of 6.62-7.08 ppm. Once again, this spectroscopic analysis confirmed that $[\text{HPyr}][\text{BF}_4]$ was successfully removed from CER networks.

5.3.2. SEM and EDX analyses of CER-based films

Typical SEM images of CER films before extraction of $[\text{HPyr}][\text{BF}_4]$ and after extraction of the latter are presented in **Figure 5-7**. As it was expected, both CER_{ext} and CER_{40} samples (**Figure 5-7a** and **Figure 5-7c**, respectively) exhibited compact and non-porous structures, whereas $\text{CER}_{20\text{ext}}$ and $\text{CER}_{40\text{ext}}$ samples (**Figure 5-7b** and **Figure 5-7d**, respectively) displayed a nanoporous structure with pore diameters ranging from 25 to 170 nm, depending on their CER/IL composition. Pore sizes generally increased and pore size distributions widened when increasing the porogenic solvent (*i.e.* $[\text{HPyr}][\text{BF}_4]$) content (**Table 5-1**) in the IL-filled CER precursors.

The micrographs obtained were carefully analyzed using the *ImageJ* software. Most of pore area fractions ranged from 500 to 5000 nm^2 (**Figure 5-8**) that corresponded to pore diameters (D_p) from ~ 25 to 80 nm. The quantity of larger pores (with pore area higher than 5000 nm^2 , *i.e.* $D_p > 80$ nm) turned out to be negligible. The values of average pore diameters were found to be around 40, 60, and 65 nm for $\text{CER}_{20\text{ext}}$, $\text{CER}_{30\text{ext}}$, and $\text{CER}_{40\text{ext}}$, respectively (**Table 5-1**). It is noteworthy that the porosity ratio values as determined from SEM data were in excellent agreement with expected values, considering the complete removal of IL initial content. Besides SEM micrographs, **Figure 5-7** also shows corresponding EDX spectra. As expected, the absence of B and F elements of $[\text{HPyr}][\text{BF}_4]$ was observed in the porous samples studied, which confirmed the complete extraction of IL from CER/IL precursor samples. **Table 5-2** summarizes the experimental and theoretical values of element contents in the CER-based samples under study. Interestingly, both sets of values were in good agreement.

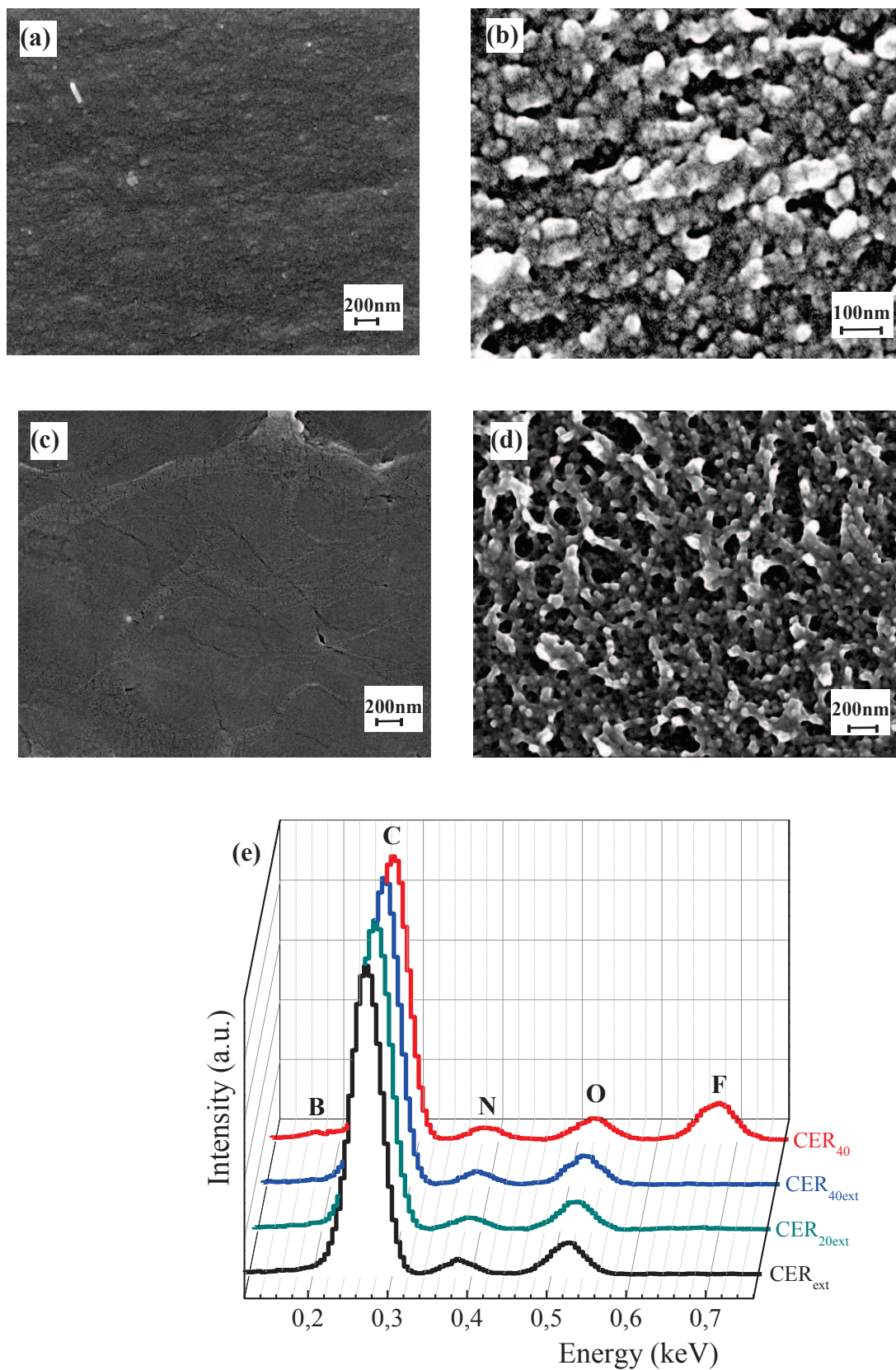


Figure 5-7: Typical SEM micrographs of CER-based samples: CER_{ext} (a), CER_{20ext} (b), CER₄₀ (c), CER_{40ext} (d), and corresponding EDX spectra (e).

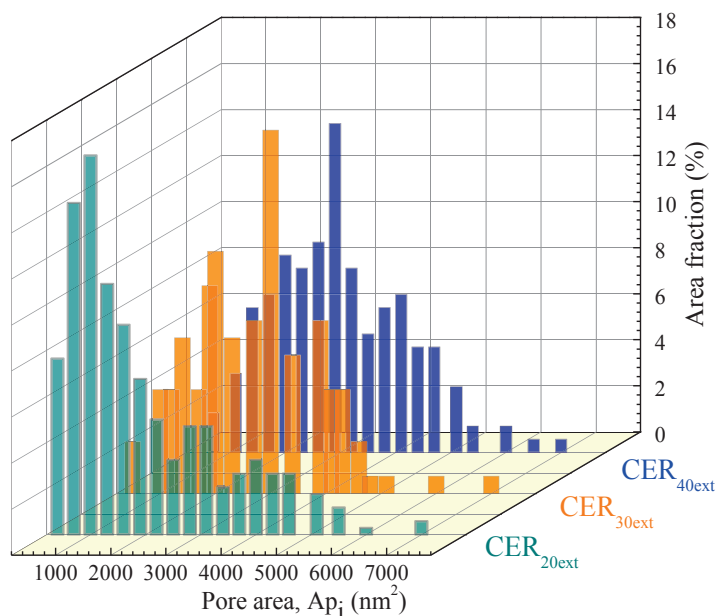


Figure 5-8: Pore area distributions derived from SEM data for the nanoporous CER samples.

Table 5-1: Main porosity characteristics for nanoporous CER-based films

Porous films	SEM			DSC-based thermoporometry		
	Average pore diameter [nm]	Pore size distribution [nm]	Porosity ratio	Average pore diameter [nm]	Pore size distribution [nm]	Total pore volume [cm ³ /g]
CER _{20ext}	40	25-100	0.18	45	20-105	0.037
CER _{30ext}	60	25-165	0.30	60	20-175	0.120
CER _{40ext}	65	25-170	0.39	60	20-180	0.124

Table 5-2: Experimental and theoretical values of element contents in typical CER samples

Samples	Element contents (wt. %)									
	Experimental (EDX)					Theoretical (calculated)				
	C	N	O	F	B	C	N	O	F	B
CER _{ext}	76.0	12.0	12.0	0	0	76.2	11.1	12.7	0	0
CER _{20ext}	75.8	12.1	12.1	0	0	76.2	11.1	12.7	0	0
CER _{30ext}	76.8	11.5	11.7	0	0	76.2	11.1	12.7	0	0
CER _{40ext}	77.3	11.7	11.0	0	0	76.2	11.1	12.7	0	0
CER ₄₀	67.1	9.0	7.1	14.4	2.4	69.3	9.0	7.7	12.1	1.8

5.3.3. Investigation of nanoporous CER-based films by DSC-based thermoporometry

The melting thermograms of water in nanoporous CER samples in the temperature region between -3 and 4 °C as well as the corresponding profiles of pore size distributions are given in **Figure 5-9a** and **5-9b**, respectively. In the thermograms of CER samples, two endothermic peaks were detected: one with a maximum, T_m , between -2 and 0 °C corresponding to the melting of water constrained within the pores of the films, and a second one with a maximum, T_{m0} , between 0 and 2 °C related to the melting of bulk water (**Figure 5-9a**). It was found that pore size distributions for the porous CER-based films under investigation were in the range of ~20-180 nm (**Figure 5-9b**), and their average pore diameters were around 45-60 nm, depending on the initial IL content in the CER precursors (**Table 5-2**). It is noteworthy that an increase in the [HPyr][BF₄] content resulted in an increase in pore diameters and a broadening of pore size distributions, along with increasing pore volumes. These results were in close agreement with those obtained from SEM analysis. Minor discrepancies between the pore characteristics determined by both techniques could be explained by a difference between real pore shapes of CER structures and circular ones used for the mathematical data processing in SEM analysis.

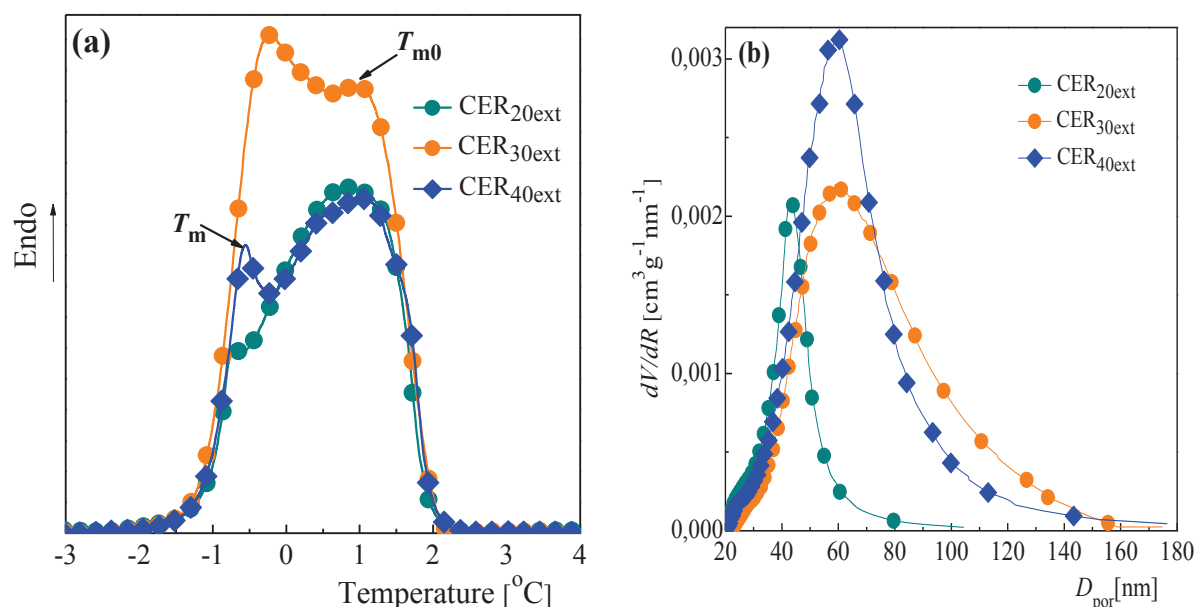


Figure 5-9: DSC melting thermograms of water confined within the pores of nanoporous CERs (a) and corresponding pore size distribution profiles (b).

5.3.4. Thermal stability of CER-based films by TGA

The influence of [HPyr][BF₄] on the thermal stability of nanoporous CER networks was investigated by TGA. Mass loss and corresponding derivative curves are presented in **Figure 5-10**, and the main corresponding data are summarized in **Table 5-3**. For the neat CER sample, the first step of the intensive mass loss was observed in the temperature range of ~ 390-490 °C, which was associated with the degradation of the skeleton of cross-linked CER network, and the second step was observed at higher temperatures with a small mass loss. For pure [HPyr][BF₄], we could observe a single degradation stage in the temperature interval ranging from ~ 350 to 438 °C with an intense mass loss value of about 94 wt. %.

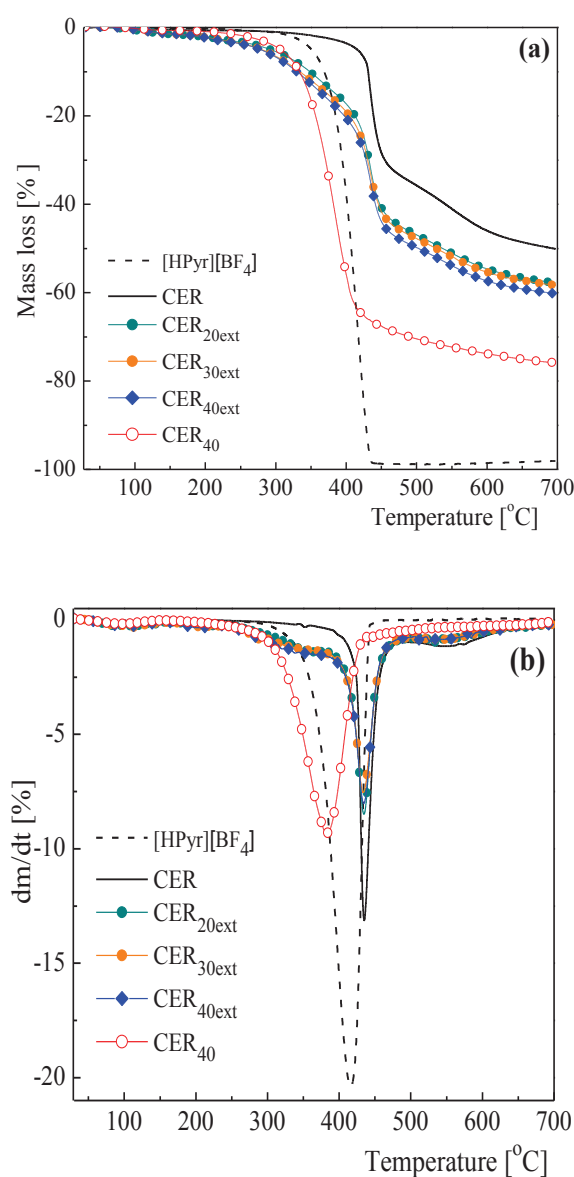


Figure 5-10: Mass loss (a) and corresponding derivative (b) curves as determined by TGA for [HPyr][BF₄] and typical CER-based films.

In contrast to pure CER, the thermal decomposition of nanoporous CER films was more complex and involved more stages, especially in the lower temperature range. A slight initial mass loss of about 2-5 wt. % below 280 °C might arise from the removal of entrapped moisture within the CER network. The first decomposition step for CER_{20ext}, CER_{30ext} and CER_{40ext} really occurred in the temperature range of 285-395 °C with a mass loss of ~14-17 wt. % corresponding to the degradation of porous and defective network regions of CER structures. Near 400 °C, the onset temperature of intensive degradation with higher mass loss (~29-30 wt. %) then occurred, which could be attributed to the destruction of triazine cycles of CER skeleton. The overall decomposition approximately led to 40-42 wt. % char residues. Surprisingly, the thermal stability of the nanoporous CER-based networks decreased compared to that of pure CER, although they had the same chemical structure: the temperature values for onset of intensive degradation (T_{d1}) and 50 % mass loss ($T_{d50\%}$) decreased respectively from 425 °C and 694 °C for the CER sample to 395 °C and 503 °C for the CER_{40ext} sample (**Table 5-3**). The higher the initial [HPyr][BF₄] content in the CER precursors, the lower the thermal stability of the nanoporous films obtained. Nevertheless, the temperatures of maximum mass loss (T_{dmax}) are nearly identical for the CER, CER_{20ext}, CER_{30ext}, and CER_{40ext} films. Interestingly, the presence of IL in the CER₄₀ sample led to a significant reduction of T_{dmax} by 50 °C, and one such film degraded in a single step. One could suppose that one such strong dilution (40 wt. % of IL) hindered the DCBE polycyclotrimerization, as the probability of the elementary reaction step might decrease, *i.e.* the reaction of three cyanate groups together to afford the formation of cyanurate rings. The existence of molecules of DCBE monomer or other intermediate oligomeric molecules, which were not incorporated into the CER network (as confirmed by ¹H NMR spectrum of the sol fraction, see **Figure 5-6**), along with IL, might drastically decrease the T_{dmax} value of CER₄₀ sample. After extraction of all the soluble fragments, the final nanoporous CER_{40ext} sample was characterized by a high T_{dmax} value comparable to that of the other nanoporous materials obtained ($T_{dmax} = 435$ °C).

Removing IL from CER precursory networks afforded nanoporous films, which degraded in two steps corresponding to the destruction of the defective CER network at lower temperatures and the degradation of the regularly crosslinked network regions with T_{dmax} equal to that of nonporous CER analogue. Consequently, applying [HPyr][BF₄] as a porogen reduced the thermal stability of resulting nanoporous films compared to that of neat CER to some extent, probably due to the formation of less regular CER structures.

Table 5-3: TGA data obtained for CER-based networks and pure [HPyr][BF₄]

Samples	T_{d1}^a [°C]	T_{dmax}^b [°C]	$T_{d50\%}^c$ [°C]	Mass loss at T_{dmax} [%]	Char residue [wt. %]
CER	425	435	694	16	50
CER _{20ext}	399	435	538	32	42
CER _{30ext}	396	434	528	33	42
CER _{40ext}	395	435	503	35	40
CER ₄₀	340	385	393	42	25
[HPyr][BF ₄]	376	416	407	67	2

^a T_{d1} : onset temperature of intensive degradation as determined by value for intersection of tangents to curve at the first inflection point; ^b T_{dmax} : temperature value of maximal degradation rate; ^c $T_{d50\%}$: temperature values for a 50 % mass loss.

5.4. Conclusions

Novel nanoporous film materials based on thermostable polycyanurates generated *in situ* by polycyclotrimerization of DCBE in the presence of ionic liquid [HPyr][BF₄] have been developed. Nanoporous CER-based films were obtained by extraction of the ionic liquid from CER networks. Complete IL removal was confirmed by determination of gel fraction contents, FTIR, ¹H NMR, and EDX spectroscopic analyses. SEM and DSC-based thermoporometry were used as complementary techniques for nanopore characterization. Depending on the IL porogen content, the average pore diameter values were found in the range of 45-60 nm with pore size distributions of ~20-180 nm. It is also noteworthy that an increase in the [HPyr][BF₄] content resulted in increasing pore diameters and broader pore size distributions. The TGA curves showed high thermal stability of the nanoporous films obtained with an onset decomposition temperature near 300 °C. It should be stressed that the synthesis of CERs in the presence of IL was carried out without using any additional solvent or specific catalyst, the ionic liquid being highly thermostable and potentially being utilized repeatedly.

5.5. References

1. Hamerton I. ed.: Chemistry and technology of cyanate ester resins. Glasgow: Chapman & Hall (1994).
2. Fainleib A. ed.: Thermostable polycyanurates. Synthesis, modification, structure and properties. New York: Nova Science Publishers (2010).
3. Hillermeier R., Seferis J. C.: Environmental effects on thermoplastic and elastomer toughened cyanate ester composite systems. *Journal of Applied Polymer Science*, **77**, 556-567 (2000).
4. Appleby D., Hussey C. L., Seddon K. R., Turp J. E.: Room-temperature ionic liquids as solvents for electronic absorption-spectroscopy of halide-complexes. *Nature*, **323**, 614-616 (1986).
5. Watanabe M., Tokuda H., Tsuzuki S., Susan M. A. B. H., Hayamizu K.: How ionic are room-temperature ionic liquids? An indicator of the physicochemical properties. *The Journal of Physical Chemistry B*, **110**, 19593-19600 (2006).
6. Welton T.: Room-temperature ionic liquids. Solvents for synthesis and catalysis. *Chemical Reviews*, **99**, 2071-2083 (1999).
7. Holbrey J. D., Seddon K. R.: Ionic liquids. *Journal of Cleaner Production*, **1**, 223-236 (1999).
8. Wassersheid P., Keim W.: Ionic liquids – new “Solutions” for transition metal catalysis. *Angewandte Chemie International Edition*, **39**, 3772-3789 (2000).
9. Wilkes J. S.: Properties of ionic liquid solvents for catalysis. *Journal of Molecular Catalysis A: Chemical*, **214**, 11-17 (2004).
10. Mecerreyes D.: Applications of ionic liquids in polymer science and technology. Berlin: Springer-Verlag (2015).
11. Livi S., Duchet-Rumeau J., Gérard J. F., Pham T. N.: Polymers and ionic liquids: a successful wedding. *Macromolecular Chemistry and Physics*, **216**, 359-368 (2015).
12. Bara J. E., Carlisle T. K., Gabriel C. J., Camper D., Finotello A., Gin D. L., Noble R. D.: Guide to CO₂ separations in imidazolium-based room-temperature ionic liquids. *Industrial & Engineering Chemistry Research*, **48**, 2739-2751 (2009).
13. Snedden P., Cooper A. I., Khimiyak Y. Z., Scott K., Winterton N.: Cross-linked polymers in ionic liquids: Ionic liquids as porogens. In: Brazel CS, Rogers D, editors. *Ionic liquids in polymer systems: solvents, additives and novel applications*. Washington, DC: ACS Symposium Series 913, 133-147 (2005).
14. Wu D., Xu F., Sun B., Fu R., He H., Matyjaszewski K.: Design and preparation of porous polymers. *Chemical Reviews*, **112**, 3959-4015 (2012).
15. Kiefer J., Hilborn J. G., Hedrick J. L., Cha H. J., Yoon D. Y., Hedrick J. C.: Microporous cyanurate networks via chemically induced phase separation. *Macromolecules*, **29**, 8546-8548 (1996).
16. Hedrick J. L., Russell T. P., Hedrick J. C., Hilborn J. G.: Microporous polycyanurate networks. *Journal of Polymer Science Part A: Polymer Chemistry*, **34**, 2879-2888 (1996).
17. Kiefer J., Hedrick J. L., Hilborn J. G.: Macroporous thermosets by chemically induced phase separation. *Advances in Polymer Science*, **147**, 161-247 (1999).
18. Grigoryeva O., Gusakova K., Fainleib A., Grande D.: Nanopore generation in hybrid polycyanurate/poly(ϵ -caprolactone) thermostable networks. *European Polymer Journal*, **47**, 1736-1745 (2011).
19. Grande D., Grigoryeva O., Fainleib A., Gusakova K., Lorthioir C.: Porous thermosets *via* hydrolytic degradation of poly(ϵ -caprolactone) fragments in cyanurate-based hybrid networks. *European Polymer Journal*, **44**, 3588-3598 (2008).

20. Grande D., Grigoryeva O., Fainleib A., Gusakova K.: Novel mesoporous high-performance films derived from polycyanurate networks containing high-boiling temperature liquids. *European Polymer Journal*, **49**, 2162-2171 (2013).
21. Gusakova K., Saiter J. M., Grigoryeva O., Gouanve F., Fainleib A., Starostenko O., Grande D.: Annealing behavior and thermal stability of nanoporous polymer films based on high-performance cyanate ester resins. *Polymer Degradation and Stability*, **120**, 402-409 (2015).
22. Fainleib A., Gusakova K., Grigoryeva O., Starostenko O., Grande D.: Synthesis, morphology, and thermal stability of nanoporous cyanate ester resins obtained upon controlled monomer conversion. *European Polymer Journal*, **73**, 94-104 (2015).
23. Fainleib O. M., Grigoryeva O. P., Gusakova K. G., Sakhno V. I., Zelinsky A. G., Grande D.: Novel nanoporous thermostable polycyanurates for track membranes. *Physics and Chemistry of Solid State*, **10**, 692-696 (2009).
24. Fainleib A., Grigoryeva O., Starostenko O., Vashchuk A., Rogalsky S., Grande D.: Acceleration effect of ionic liquids on polycyclotrimerization of dicyanate esters. *eXPRESS Polymer Letters*, **10**, 722-729 (2016).
25. Brun M., Lallemand A., Quinson J. F., Eyraud C.: A new method for the simultaneous determination of the size and shape of pores: the thermoporometry. *Thermochimica Acta*, **21**, 59-88 (1977).
26. Hay J. N., Laity P. R.: Observations of water migration during thermoporometry studies of cellulose films. *Polymer*, **41**, 6171-6180 (2000).
27. Billingham J., Breen C., Yarwood J.: *In situ* determination of Bronsted/Lewis acidity on cation-exchanged clay mineral surfaces by ATR-IR. *Clays and Clay Minerals*, **31**, 513-522 (1996).

Conclusions and Prospects

A new approach toward the synthesis of heat-resistant CERs in the presence of various types of ionic liquids (aprotic, protic or polymeric protic) with diverse functional roles (catalyst, filler, porogen, inert or reactive modifier) has been developed. The comprehensive studies on the obtained polymer materials have made it possible to draw the following conclusions.

1. For the first time, thermostable polycyanurate networks and corresponding nanoporous films were synthesized by using ionic liquids of various chemical structures as multifunctional agents, namely catalysts, reactive modifiers, fillers or porogens. The relationships between synthetic conditions, structure, and miscellaneous physical properties of the materials were established.

2. Regardless of their chemical structure, type and content in the system, all ionic liquids catalyzed the polycyclotrimerization reaction of DCBE during CER synthesis: they promoted reduction of the induction period and reaction time, accelerated the conversion of cyanate groups and provided complete conversion at lower temperatures.

3. The catalytic activity of the inert aprotic [OMIm][BF₄] and [HPyr][BF₄] resulted from the ability of formation of intermediate complexes with $-O-C\equiv N$ groups, *i.e.* $[CN]^{\delta+}[OMIm]^{\delta-}$ and $[CN]^{\delta+}[HPyr]^{\delta-}$, respectively, and the mechanisms of catalysis for DCBE polycyclotrimerization were proposed.

4. In the presence of reactive [HEAIm][Cl] or [PHMG][TS], the process of DCBE polycyclotrimerization begun with the formation of covalent bonds between $-O-C\equiv N$ groups and $-OH$ and/or $>NH$ groups of ionic liquid with subsequent stepwise transformation of intermediates, which may also be involved in catalysis. It was determined that the synthesized hybrid CER/IL networks retained a high glass transition temperature ($T_g = 242-284$ °C) and thermal stability ($T_d = 420-424$ °C).

5. Using the inert aprotic [HPyr][BF₄] as a filler during *in situ* synthesis of CER caused significant changes in physico-chemical and mechanical properties of CER/[HPyr][BF₄] composites, due to the interaction of $[BF_4]^{\delta-}$ anions with electrophilic centers of triazine rings from CERs. Depending on the IL content (20-40 wt.%) in the CERs, increasing elastic modulus in the glassy region by 10-25 %, increasing tensile strength by 34-120 %, increasing Young's modulus by 10-50 %, and retaining high thermal stability ($T_d = 330-340$ °C) were fixed.

Simultaneously, the plasticizing effect of IL was revealed, that led to decreasing in the glass transition temperature of the samples to $T_g = 111\text{-}217$ °C (depending on the IL content).

6. A straightforward and effective method for creating nanoporous CER films has been developed by complete extraction of [HPyr][BF₄] from CER/IL composites. By using [HPyr][BF₄] as a porogen, film materials with high thermal stability ($T_d = 395\text{-}399$ °C), independently of the porogen content, and regular nanoporous structure with an average pore diameter of 40-65 nm were formed. The resulting nanoporous CERs are promising for applications as heat-resistant membranes.

In our studies, we have found that ILs can be effectively used for CERs as catalytic or/and crosslinking agents, plasticizers, fillers or porogens, thus providing a new route to the design of advanced materials. Despite these successes, using ILs still remains an emerging field of research and the effect of other IL types has to be further studied. The influence of IL on the ductility, abrasion resistance, and self-repairing ability of IL-based CER materials remains to be investigated. It appears reasonable to expect *(i)* understanding of IL organization within the polymer network; *(ii)* network-IL interactions; *(iii)* suitable functionalization of the ILs for reactive modification of thermosets; *(iv)* molecular mechanisms of IL lubrication; *(v)* separation/sorption properties of IL-based thermosetting networks before and after extraction for membrane technologies; *(vi)* compatibilizing effect of ILs in the hydrophobic CERs filled with hydrophilic fillers. The prospect of ILs as electrolyte salts for engineering of highly conducting polymer electrolytes and characterizing their ion transport behaviour left out of consideration and further studies are still needed. The IL-based thermosetting materials could be good candidates for use in any application, in which high conductivity combined with high thermal stability and non-volatility are required.

Résumé

Cette thèse de doctorat aborde de nouvelles conceptions de films à base de résines d'ester de cyanate (CER) en présence de liquides ioniques (LIs) en tant qu'agents multifonctionnels: catalyseurs, agents de modification réactifs, renforts ou agents porogènes. Les liquides ioniques de structures et de concentrations variables accélèrent de manière significative la polycyclotrimérisation du dicyanate d'ester de bisphénol E, en l'absence de tout solvant organique supplémentaire ou additif. Les réseaux de polycyanurates résultants dopés avec des liquides ioniques aprotiques peuvent constituer des matériaux prometteurs pour la production de structures photosensibles. De tels systèmes nanocomposites permettent la séparation, la récupération et le recyclage aisés des LIs par simple extraction, ce qui permet finalement l'obtention de films nanoporeux thermostables. Les caractéristiques de la porosité de ces matériaux dépendent de la concentration des LIs dans les précurseurs CERs. Les LIs protoniques contenant des groupements fonctionnels $>NH$ et $-OH$, indépendamment de leur masse molaire, de la structure chimique du cation et de l'anion, sont incorporés chimiquement dans le réseau polycyanurate. Ainsi, les matériaux hybrides obtenus avec des fragments de liquides ioniques pourraient fournir d'excellents candidats pour des recherches futures sur les ionomères et les nanocomposites.

Mots-clés: résines d'ester de cyanate, liquides ioniques, catalyseur, agent multifonctionnel, matériaux nanoporeux

Abstract

This PhD thesis addresses new designs of cyanate ester resin (CER) films in the presence of ionic liquids as multifunctional agents: catalysts, reactive modifiers, fillers or porogens. It should be emphasized that ionic liquids (ILs) of varying structures and concentrations significantly accelerate the polycyclotrimerization of dicyanate ester of bisphenol E, in the absence of any additional organic solvent or additive. The resulting polycyanurate networks doped with aprotic ionic liquids can be promising materials for producing photosensitive structures. Such nanocomposite systems allow for easier separation, recovery, and recycling of ILs by mere extraction, which eventually affords thermally stable nanoporous films. The porosity features of these materials depend on the concentration of ILs in the CER precursors. Protic ILs containing functional $>NH$ and $-OH$ groups, regardless of molar mass, chemical structure of cation and anion, chemically incorporate into the polycyanurate network, thus the resulting hybrid materials with fragments of ionic liquids could provide excellent candidates for future research in ionomers and nanocomposites.

Keywords: cyanate ester resins, ionic liquids, catalyst, multifunctional agent, nanoporous materials